1969

Phase equilibria and thermodynamic studies in the system Ca0-Fe0-Fe$_2$0$_3$–Si0$_2$

Muharrem Timucin

PHASE EQUILIBRIA AND THERMODYNAMIC STUDIES IN THE SYSTEM $CaO-FeO-Fe_2O_3-SiO_2$

by

MUHARREM TIMUCIN

A DISSERTATION

Presented to the Faculty of the Graduate School of the

UNIVERSITY OF MISSOURI - ROLLA

In Partial Fulfillment of the Requirements for the Degree

DOCTOR OF PHILOSOPHY

in

METALLURGICAL ENGINEERING

1969

Advisor

H. O. McDonald

ABSTRACT

A study of phase relations and thermodynamic properties of phases in the system $CaO-FeO-Fe_2O_3-SiO_2$ was conducted at 1450°C and 1550°C. The region of stability of the different phases was determined by microscopic examination of the specimens. The thermodynamic properties of liquids were determined by analyses of quenched samples equilibrated at oxygen pressures from about 10^{-11} to 1 atm.

Isothermal phase diagrams were constructed from the data for 0, 5, 10, 20, and 30 weight percent silica sections of the $CaO-FeO-Fe_2O_3-SiO_2$ system, and the effect of temperature and increased silica additions on the oxygen solubility of the liquid oxides was measured.

Multicomponent Gibbs-Duhem integrations were used to calculate the activities of the oxide components CaO, FeO, and SiO_2 from the measured oxygen activity data on the liquid oxides. The results were discussed in terms of the formation and behavior of slags in the Basic Oxygen Furnace steelmaking process.

TABLE OF CONTENTS

TABLE OF CONTENTS (continued)

ACKNOWLEDGEMENTS

The author most gratefully acknowledges the invaluable guidance and the active interest of his advisor, Dr. Arthur E. Morris, throughout this study.

The author would also like to express his gratitude to the National Lime Association for the financial support of the research, and to UNESCO for a fellowship.

LIST OF FIGURES

LIST OF FIGURES (continued)

LIST OF FIGURES (continued)

LIST OF FIGURES (continued)

LIST OF TABLES

CHAPTER I

INTRODUCTION

The molten iron produced by the blast furnace is nearly saturated with carbon and contains such impurities as silicon, manganese, phosphorus, and sulfur in undesirable amounts which have to be removed during the subsequent steelmaking operation. Steelmaking slags, containing iron oxides, act like a sink for the oxygen of the furnace atmosphere and as a reservoir of oxygen for the underlying metal. The slag assists in the transfer of the necessary oxygen from the gas to the metal for the oxidation of these impurities. Some of the reaction products are then absorbed by the solvent slag, others go off in the gas.

Metallurgists have long realized that the chemistry of the slag is an important factor in making good steel, and have directed many research efforts toward studying the reactions taking place between the slag and the metal phases, between the slag and gas phases, and those among the slag constituents themselves. Consequently, these studies have contributed to an understanding of the activity-composition relations and thermodynamic properties of several binary and multicomponent systems formed by oxides which appear in steelmaking slags.

Owing to the past importance of the conventional Basic Open Hearth (BOH) process much of the earlier work was concentrated on liquid slags under reducing atmospheres. Only a

few studies have been made over a wide range of oxygen pressures at steelmaking temperatures. The Basic Oxygen Furnace (BOF) steelmaking process has introduced some relatively new conditions. The BOF slag is not homogeneous and its temperature varies across the furnace with time. Furthermore, because of a foaming action the removal of impurities is much faster since oxygen is transferred to the metal not only at oxygen potentials represented by those near the slag-metal interface but also at much higher potentials. Hence, it is apparent that additional knowledge on phase equilibria and thermodynamics of BOF slags, which would cover a wide range of oxygen potentials and a series of temperatures, was desirable.

A study of actual BOF slags would involve a rather complex system incorporating at least six major components, with a number of others which enter in lesser amounts. Obviously the problem of determining the phase equilibria and activity-composition relations in a six component system would be difficult. A valuable first step, however, would be to make some generalizations from experimental information in systems containing a smaller number of components, and yet which adequately approximate BOF slags. The essential components of BOF slags are lime, silica, and iron oxide; accordingly the system CaO-FeO-Fe_2O_3-SiO_2 was chosen to be the subject of the present investigation. Specifically, the aim of the present work was the following, at 1450°C and 1550°C:

1.) To determine the region of stabilities and melting relations of the solid phases that are stable in the ternary $CaO-FeO-Fe_2O_3$ system, as a function of oxygen pressure of the gas phase,
2.) To establish the effect of varying silica additions on these relations especially in the high-lime part of the system,
3.) To determine the compositions of liquid slags formed in the ternary $CaO-FeO-Fe_2O_3$, and in the low-silica portion of the quaternary $CaO-FeO-Fe_2O_3-SiO_2$ systems as a function of oxygen pressure of the gas phase, and
4.) To calculate the activity-composition relations of oxide components in the above systems with the aid of information obtained in the previous three steps.

It should be mentioned that in reality the systems of interest are the Ca-Fe-O ternary and the Ca-Fe-Si-O quaternary. The $CaO-FeO-Fe_2O_3$ and $CaO-FeO-Fe_2O_3-SiO_2$ systems are parts of those parent systems. The oxygen pressures used in this and similar previous investigations limit the present study to the $FeO-Fe_2O_3$ portion of the parent Fe-O binary. Although metallic iron precipitates as a separate phase at very low oxygen pressures the representation of compositions by the oxide components are adequate and more convenient for the purposes of this work.

The relationship of the parent Ca-Fe-O ternary to the $CaO-FeO-Fe_2O_3$ system is shown in Figure 1a. The importance of the gas phase during the equilibration of any sample in the $CaO-FeO-Fe_2O_3$ system may be illustrated by the help of that figure. At a constant temperature, the oxygen content of the condensed phases is a function of the partial pressure of oxygen in the gas phase. Since only oxygen is exchanged between the gas and the condensed phases, the ratio Fe/Ca of the latter phases remains constant during the equilibration. This constancy of Fe/Ca ratios is described by a family of straight lines, referred to as oxygen reaction lines, radiating from the O apex of the triangle in Figure 1a. Oxygen reaction lines are also drawn in Figure 1b corresponding to those in the parent ternary.

The effect of increasing silica additions was investigated at constant silica sections of the $CaO-FeO-Fe_2O_3-SiO_2$ system with 5%, 10%, 20% and 30% by weight of SiO_2. The relationship of the parent Ca-Fe-O-Si quaternary to the $CaO-FeO-Fe_2O_3-SiO_2$ system is shown in Figure 2.

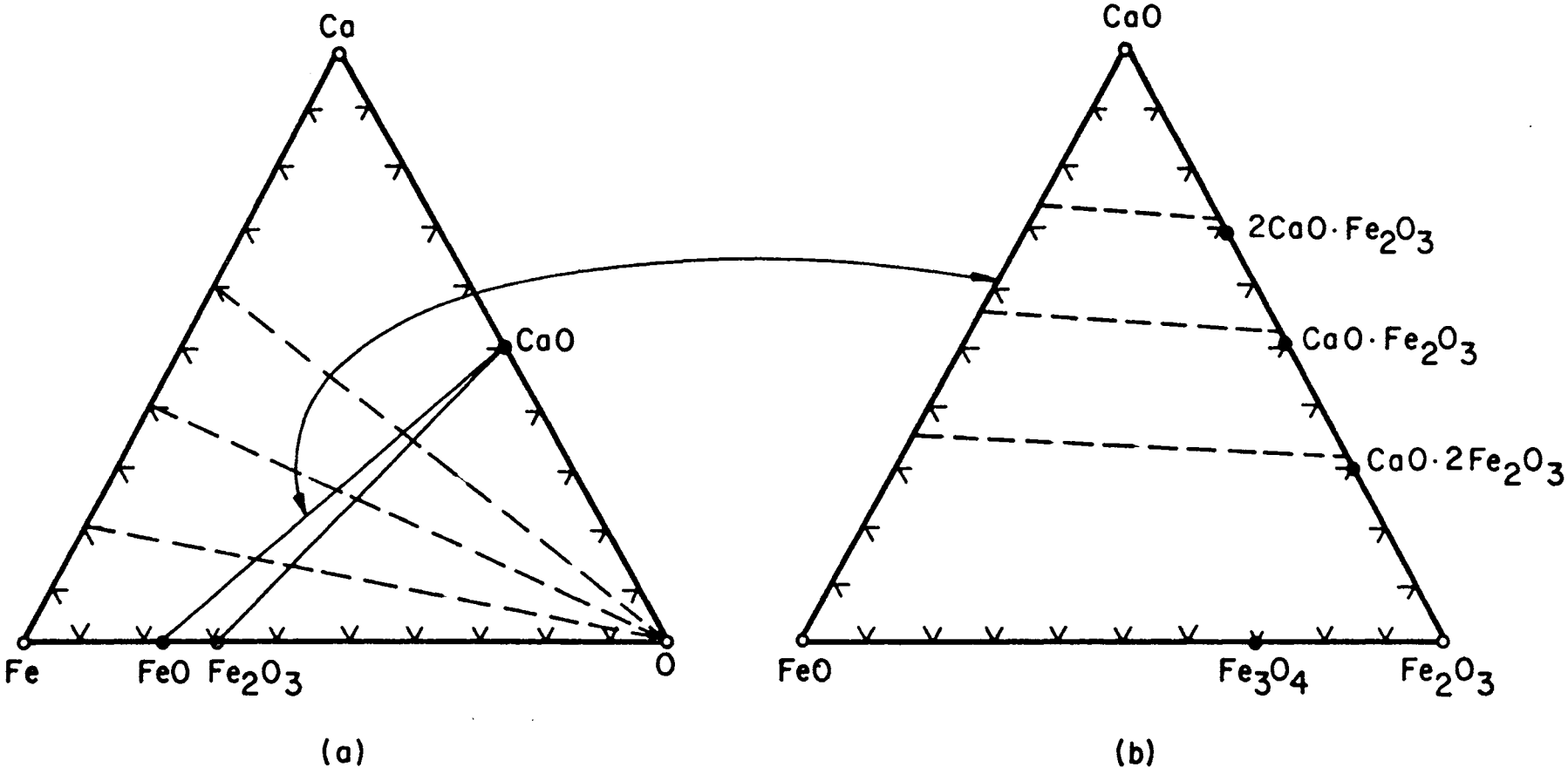

Figure 1. Schematic Diagrams Showing the Relationship Between (a) The Parent Ca-Fe-O System, and (b) The $CaO-FeO-Fe_2O_3$ System. Dashed Lines are the "Oxygen Reaction Lines" mentioned in the text.

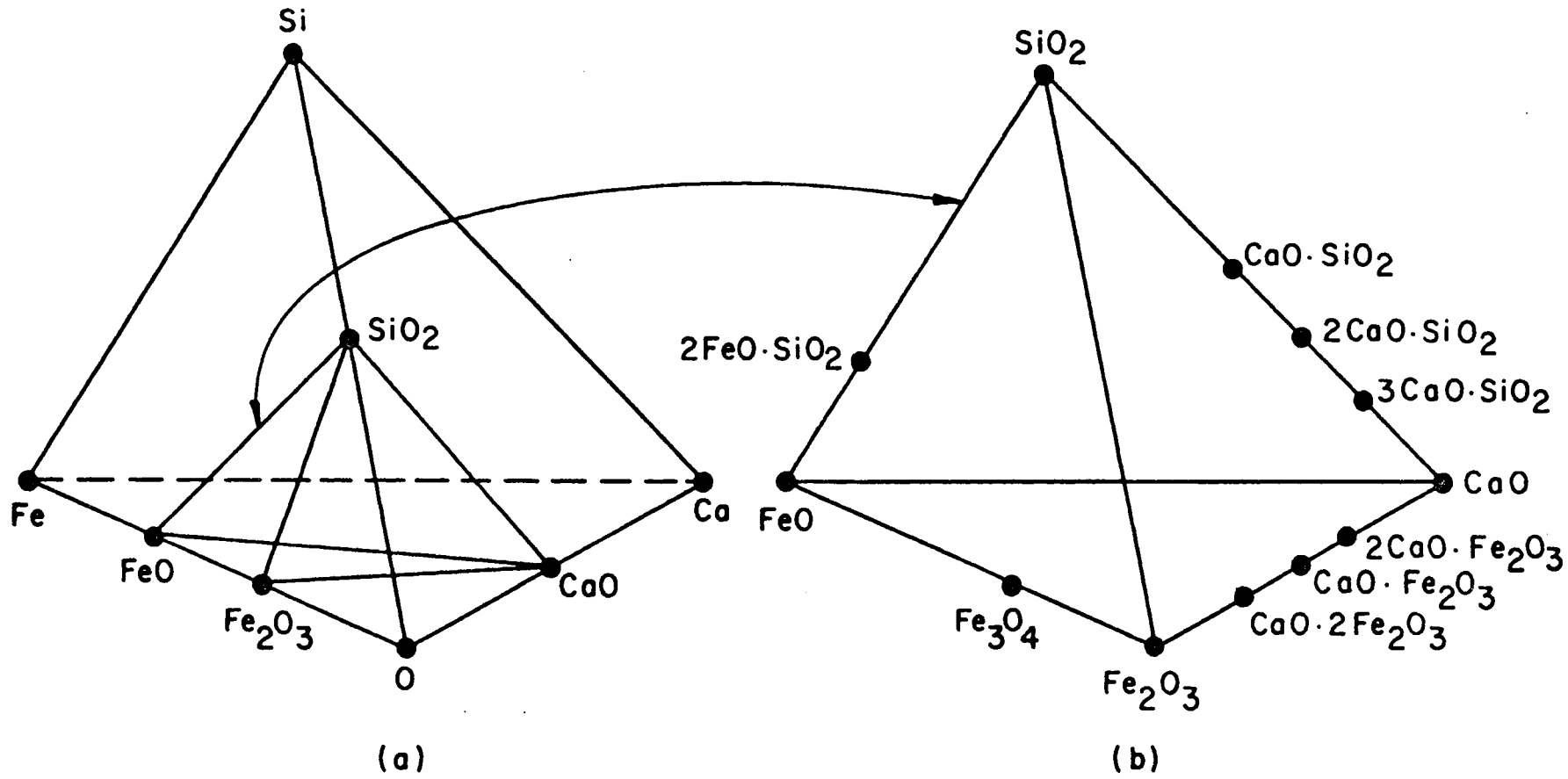

Figure 2. Schematic Diagrams Showing the Relationship Between (a) The Parent Ca-Fe-O-Si System, and (b) The $CaO-FeO-Fe_2O_3-SiO_2$ System.

CHAPTER II

REVIEW OF LITERATURE

Systems containing SiO_2, CaO, FeO and Fe_2O_3 are equally important to ceramists and geochemists as they are to metallurgists, since the region where calcium silicates are primary crystalline phases has an important bearing on such things as cement chemistry, and the higher silica parts of the system include compositions approximating these encountered in some igneous rocks. Previous phase equilibria work thus comes from workers in a variety of fields. The thermochemistry of the systems, on the other hand, has been the subject of most interest to metallurgists.

The System $FeO-Fe_2O_3$

The $FeO-Fe_2O_3$ system is a part of the main Fe-O binary. The most extensive discussion of the stability relations existing among metallic iron and its oxides is found in papers by Darken and Gurry[1,2]. They supplemented the results of earlier investigators with a large amount of new data. Their version of Fe-O phase diagram has since remained unchallenged with the exception of a few modifications on the oxygen-rich portion introduced by Phillips and Muan[3]. Muan and Osborn[4] have recently summarized all the phase equilibria and thermodynamic information in a large scale $FeO-Fe_2O_3$ diagram as reproduced in Figure 3, where the stability ranges of various condensed phases are shown as a function of temperature and total composition of the

condensed phases. A family of dash-dot curves are also included in the diagram to show the equilibrium partial pressures of oxygen of the gas phase coexisting with the condensed phases. Some of the features of this diagram that are of particular interest to this investigation are:

(a) Wustite is not stable at 50 atomic percent iron and oxygen, but contains an excess of oxygen over the stoichiometric formula with considerable variations in the Fe/O ratio. At the phase boundary where wustite is in equilibrium with iron the equilibrium oxygen pressure, for example at 1100°C, is about 10^{-13} atm., whereas the oxygen pressure at the other phase boundary corresponding to wustite-magnetite equilibrium is about 10^{-11} atm. Hence, various compositions of wustite can readily be obtained at 1100°C by varying the oxygen pressure of the gas phase between the limits

$$10^{-13} < Po_2 < 10^{-11}$$

The formula FeO will be used throughout this thesis to designate a hypothetical stoichiometric wustite, while "FeO" will stand for the nonstoichiometric compound.

(b) Fe_3O_4, magnetite, is stoichiometric up to about 800°C, however it can dissolve increasing amounts of excess oxygen above 800°C.

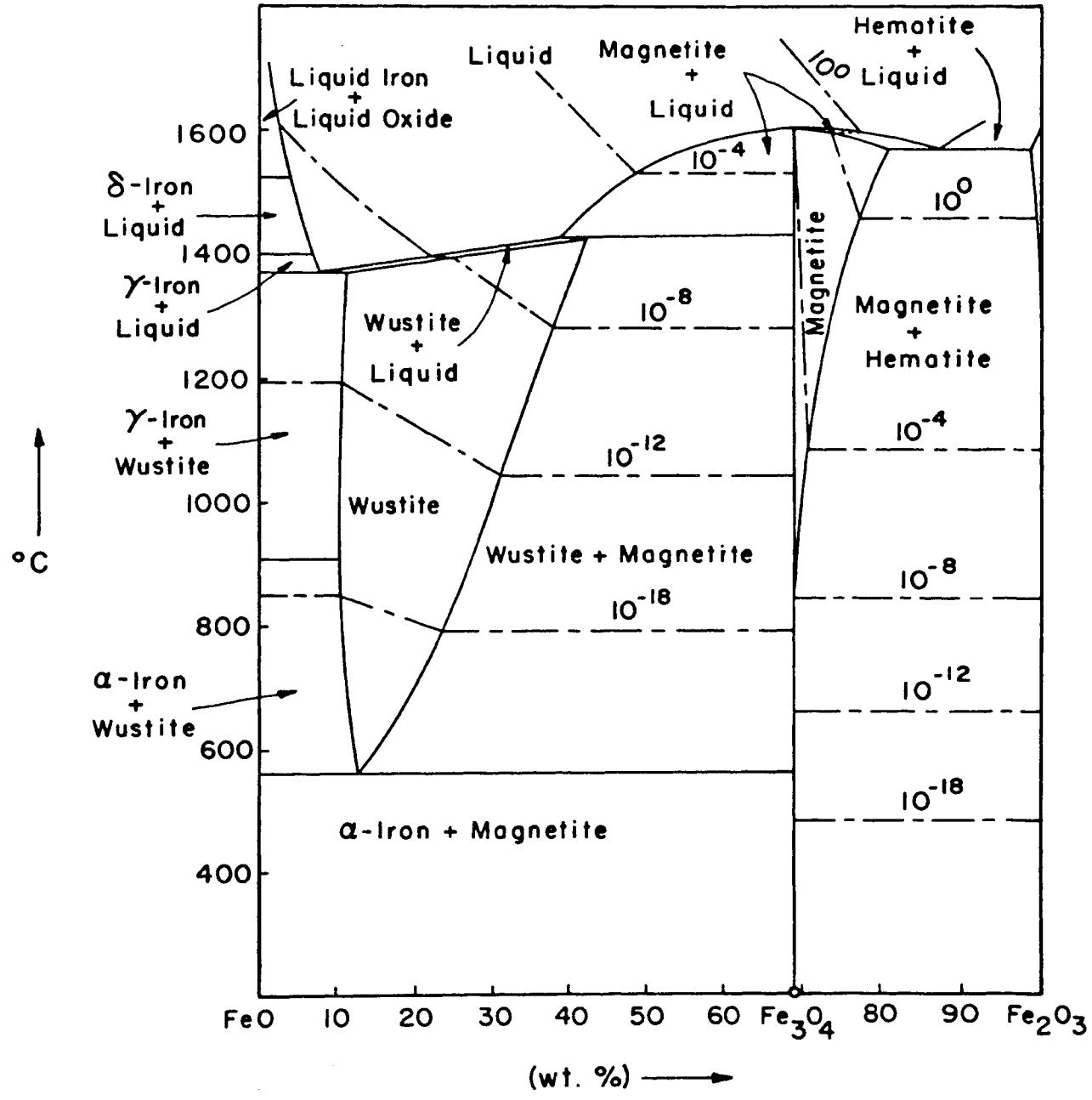

Figure 3. Phase Diagram for the FeO-Fe_2O_3 System. After Darken and Gurry[1,2], and Phillips and Muan[3].

(c) At the temperatures of interest to this investigation, the equilibrium oxygen pressures at the metallic iron + liquid oxide phase boundary are 5.0×10^{-10} and 2.86×10^{-9} atm. at 1450°C and 1550°C respectively[2].

(d) Magnetite of composition Fe_3O_4 melts at 1450°C at an oxygen pressure of 5.0×10^{-6} atm., and at 1550°C at an oxygen pressure of 4.0×10^{-4} atm.[2].

The activities of Fe, "FeO", Fe_2O_3, and Fe_3O_4 in liquid oxides have been calculated[1,2] by the usual Gibbs-Duhem integrations from the known oxygen activities, which can be defined as the square root of the equilibrium oxygen pressure of the gas phase.

The System $CaO-SiO_2$

A phase diagram of the $CaO-SiO_2$ system has been published by Muan and Osborn[4] based on the studies of a number of investigators, mainly Day, Shepherd and Wright[5], Rankin and Wright[6], and Greig[7]. The diagram is shown in Figure 4. The following comments are pertinent to our work: Two immiscible liquids coexist at high silica contents, there is virtually no solid solubility between the end members, several compounds have stable existence within the system, and several of them occur in different modifications. α-dicalcium silicate ($2CaO \cdot SiO_2$) and tricalcium silicate ($3CaO \cdot SiO_2$) have melting points well above the temperatures of this investigation, while rankinite ($3CaO \cdot 2SiO_2$) and

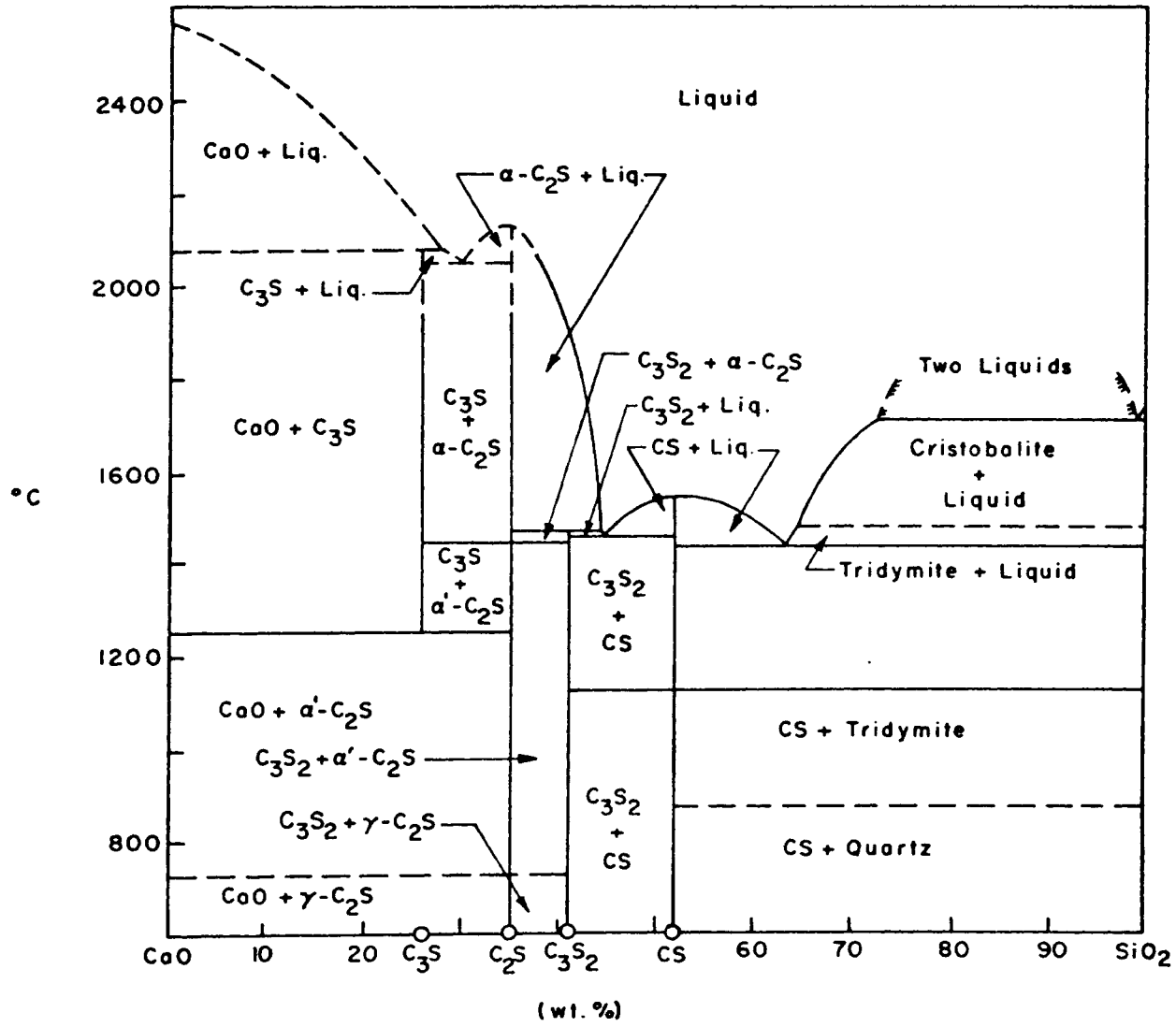

Figure 4. Phase Diagram for the System $CaO-SiO_2$, from Muan and Osborn[4].

Abbreviations: $C_3S = 3CaO \cdot SiO_2$, $C_2S = 2CaO \cdot SiO_2$, $C_3S_2 = 3CaO \cdot 2SiO_2$, $CS = CaO \cdot SiO_2$.

metacalcium silicate ($CaO \cdot SiO_2$) decompose and melt at 1464°C and 1544°C respectively.

The standard free energy of formation of dicalcium silicate, from CaO and SiO_2, has been compiled by Kelley[8] and Elliott, Gleiser, and Ramakrishna[9] from data in the literature[10,11,12]. Recent EMF cell measurements of Benz and Wagner[13] were in good agreement with those compilations. There are some uncertainties in the standard free energies of formation of tricalcium silicate as will be mentioned later in thermodynamic evaluations.

Activity-composition relations in $CaO-SiO_2$ melts have been determined by various investigators[14,15,16,17] at temperatures ranging from 1450°C to 1650°C. The comparison of reported activities showed considerable disagreement in the high-CaO region. Baird and Taylor[16] and Kay and Taylor[17] have measured the silica activities in the $CaO-SiO_2-Al_2O_3$ system at 1450°C and 1550°C. Monocalcium silicate-saturated slags of that system at 1450°C contained between two and ten percent alumina. However, the extrapolation of iso-silica activity curves to the $CaO-SiO_2$ join were assumed to represent the activity composition relations along the $CaO-SiO_2$ binary at that temperature. As will be shown later, the results of this investigation are in good agreement with those of Baird and Taylor and Kay and Taylor at both temperatures; their relations are reproduced in Figure 5.

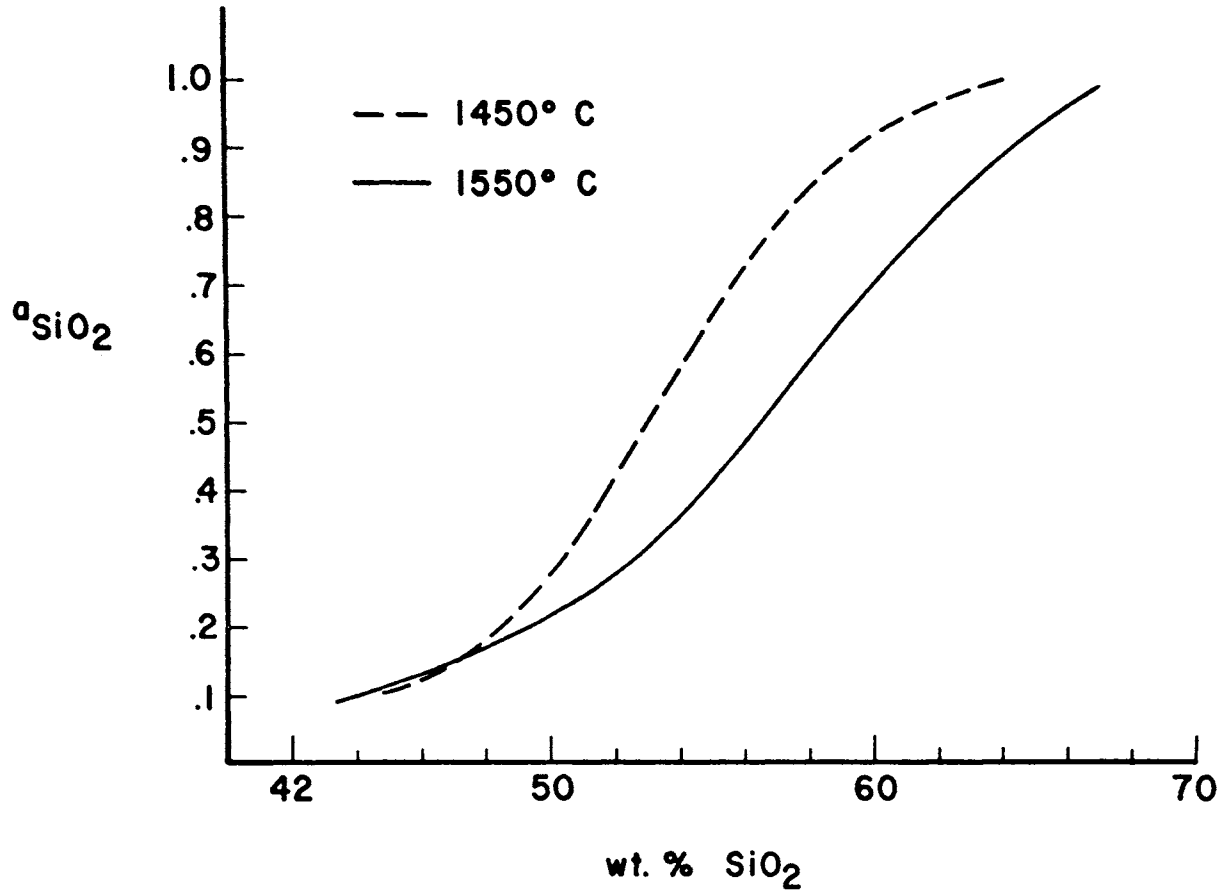

Figure 5. Silica Activities in the $CaO-SiO_2$ System at 1450°C and 1550°C. After Baird and Taylor[16], and Kay and Taylor[17].

The System $CaO-FeO-Fe_2O_3$

A large number of investigations on the CaO-iron oxide system have been reported in the literature. Phase relations in that system were studied at three levels of oxygen pressures. Phillips and Muan[18,19] have shown that the ternary system could satisfactorily be approximated to a $CaO-Fe_2O_3$ binary in air and at 1 atm. oxygen pressure. The diagram showing the phase relations in air is given in Figure 6. Some noteworthy features are: There is some solubility of CaO in iron oxide but almost none of Fe_2O_3 in CaO. Magnetite melts at 1596°C. Compounds $2CaO \cdot Fe_2O_3$, $CaO \cdot Fe_2O_3$, and $CaO \cdot 2Fe_2O_3$ are stable in the temperature ranges shown on the diagram. Phase relations at 1 atm. oxygen pressure are nearly the same as those in air; the low-CaO part of the diagram however, shows some decrease in liquidus temperatures and stability ranges of $CaO \cdot 2Fe_2O_3$ and magnetite.

Allen and Snow[20] and Tromel, Jager and Schurman[21] have studied the phase relations when the system is in contact with metallic iron. The resulting CaO-"FeO" diagram shows that there is appreciable solid solubility of CaO in "FeO" but a limited solubility of "FeO" in CaO. Hahn[22] has found that the solubility of wustite in lime and of lime in wustite, at a given temperature, depend critically on the oxygen pressure of the gas phase.

The composition of liquid slags of the $CaO-FeO-Fe_2O_3$ system were determined by Larson and Chipman[23] as a function of oxygen pressure of the gas phase at 1550°C. In a

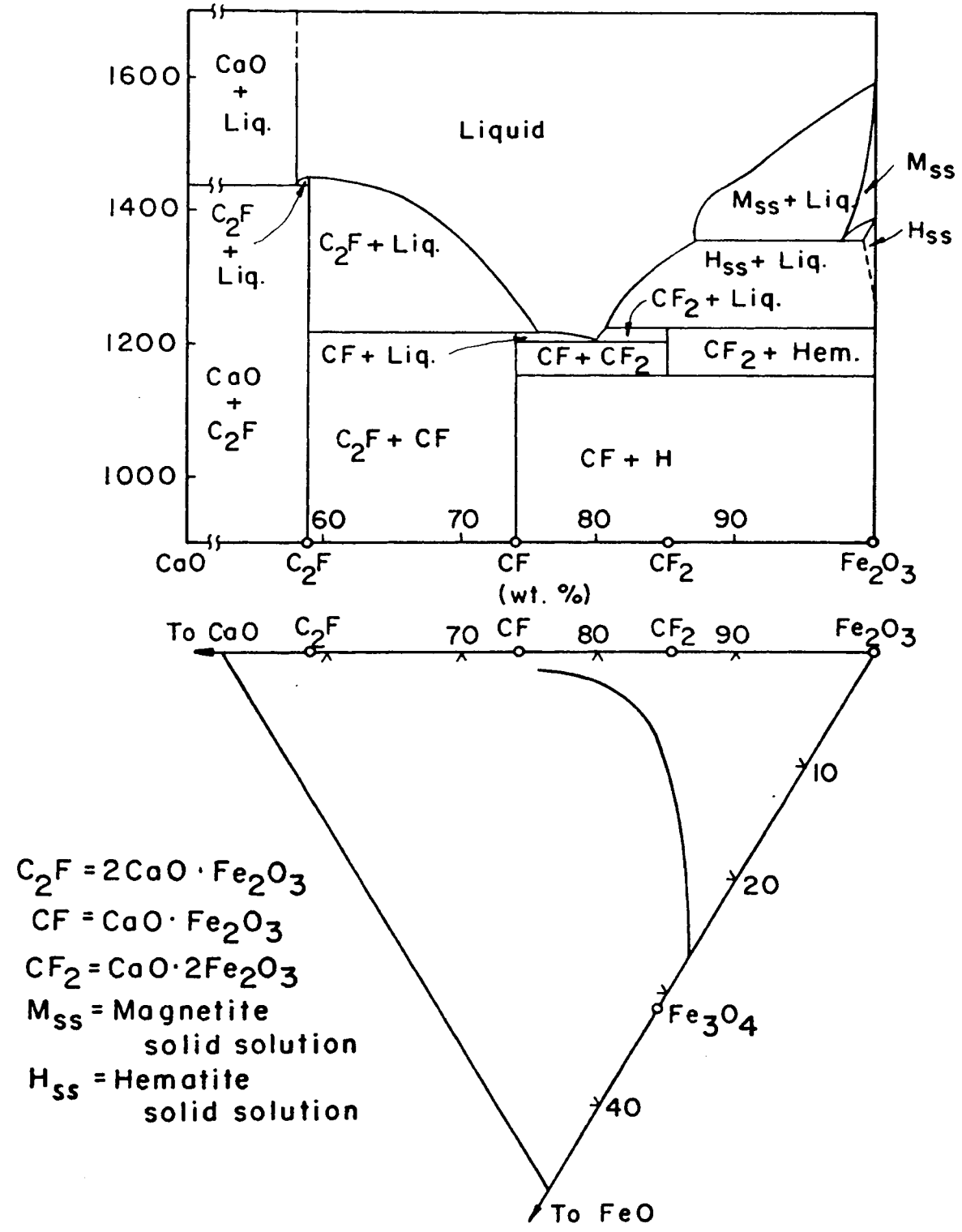

Figure 6. Phase Diagram for the System $CaO-Fe_2O_3$. Curve on Lower Figure Shows the Liquidus Compositions. After Phillips and Muan[18].

subsequent paper[24] they calculated the activities of "FeO", Fe_2O_3, and CaO. Turkdogan[25] has obtained much lower CaO activities using the same data[23]. Figures 7(a) and 7(b) show the activities of "FeO" and CaO as published by these investigators.

The System $FeO-Fe_2O_3-SiO_2$

The phase relations in the $FeO-Fe_2O_3-SiO_2$ system were extensively studied by Muan[26], who established the liquidus surface of the system throughout the entire composition triangle together with the oxygen pressures in equilibrium with several condensed phases.

Activity-composition relations have been determined by Schuhmann and Ensio[27] at 1350°C, and by Turkdogan[28], who combined the experimental data of White[29], and Turkdogan and Bills[30], at 1550°C. The diagram showing the relations at 1550°C is drawn in Figure 8(a). Figure 8(b) shows the same relations at 1450°C obtained by extrapolations between 1350°C and 1550°C diagrams.

The System $CaO-FeO-Fe_2O_3-SiO_2$

The experimental data on phase relations within the $CaO-FeO-Fe_2O_3-SiO_2$ system is not sufficiently complete to construct a tetrahedral model. Data was previously available at only two levels of oxygen pressures. The parent Ca-Fe-Si-O quaternary has been studied as a CaO-"FeO"-SiO_2 "ternary" in contact with metallic iron[20,31], and as a $CaO-Fe_2O_3-SiO_2$ "ternary" when the atmosphere was air[32,33].

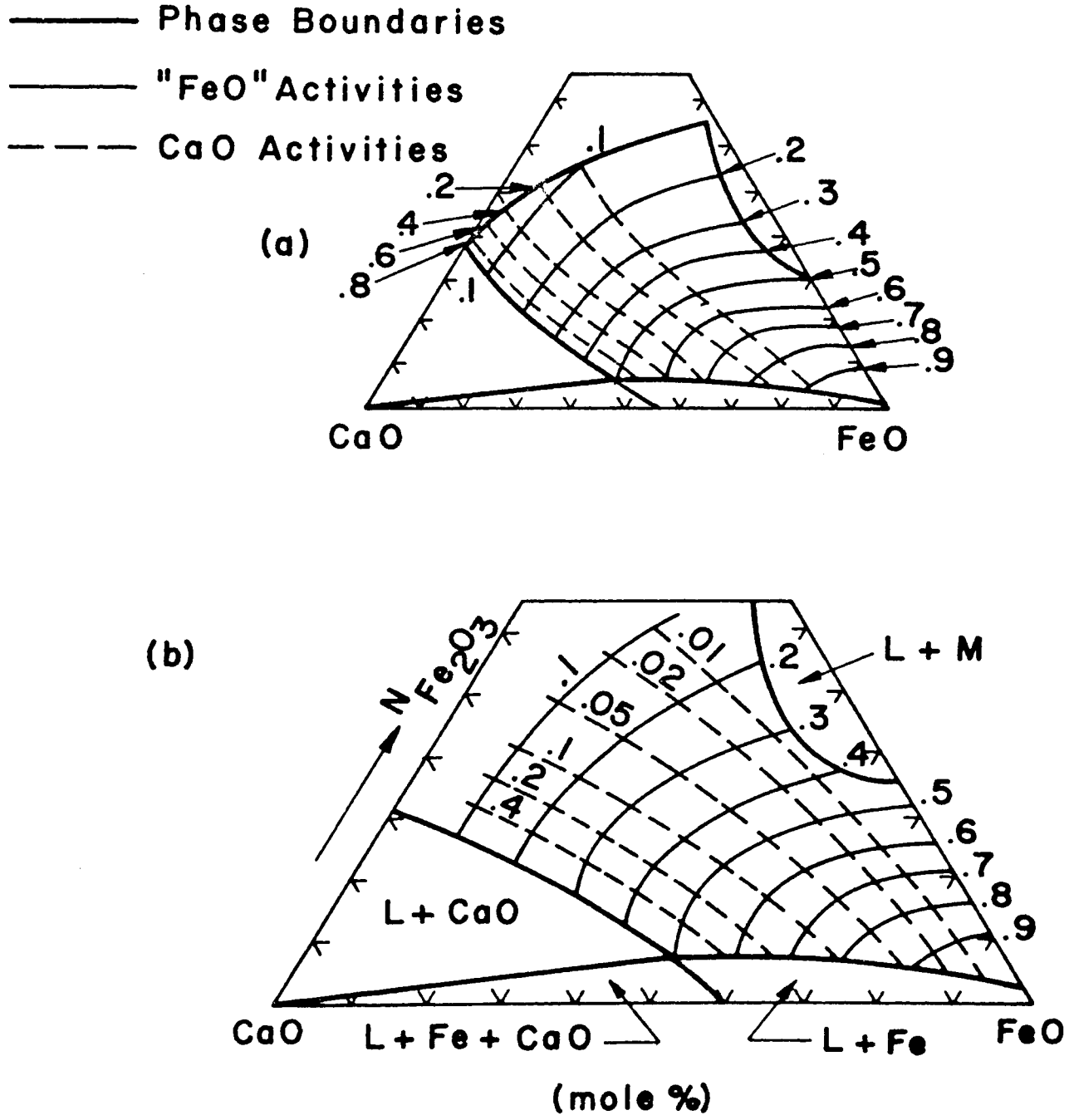

Figure 7. Activity-Composition Relations in the $CaO-FeO-Fe_2O_3$ System at 1550°C, after

(a) Larson and Chipman[24], and

(b) Turkdogan[25].

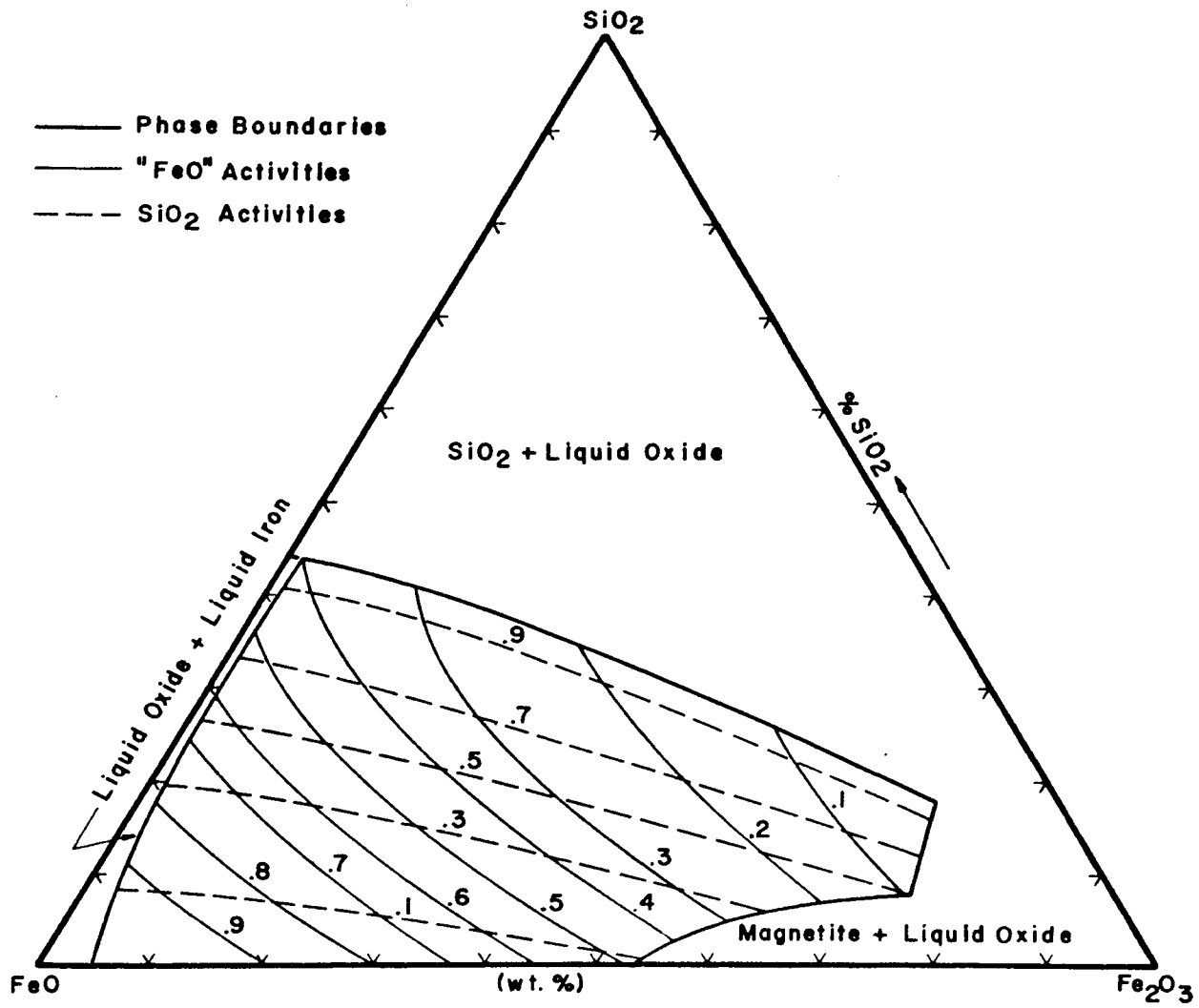

Figure 8a. Activities of FeO and SiO_2 in the Melts of the System $FeO-Fe_2O_3-SiO_2$ at 1550°C. After Turkdogan[28].

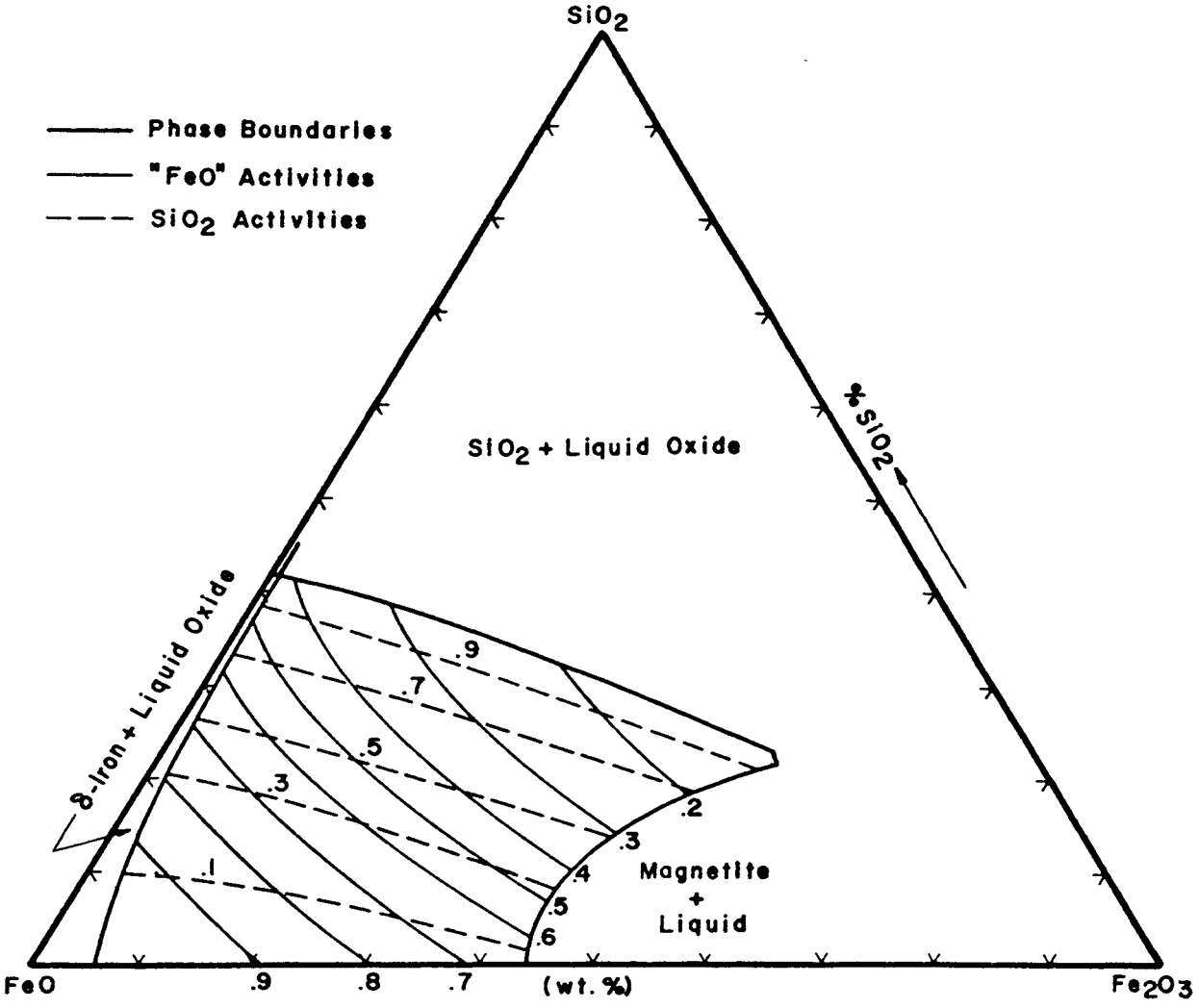

Figure 8b. Activities of FeO and SiO_2 in the Melts of the System $FeO-Fe_2O_3-SiO_2$ at 1450°C. From Extrapolations between Turkdogan[28] and Schuhmann and Ensio[27].

The isothermal sections of these systems at 1450°C and 1550°C are pertinent to this work, and they are drawn[34] in Figures 9 and 10.

Activities of "FeO" in slags of the system (CaO + MgO) - $FeO-SiO_2$ have been established by Fetters and Chipman[35] and later by Taylor and Chipman[36] by determining the effect of slag composition on the equilibrium oxygen content of the metal at 1600°C. Because of reactions taking place between the liquid phase and the MgO crucibles used to contain the melts, their slags had MgO contents ranging from less than one percent up to about twenty percent. The "FeO" activities were calculated by dividing the oxygen contents of the metal by 0.23 which is the oxygen content of the metal when it is in equilibrium with pure liquid "FeO". The relations are reproduced in Figure 11. Gorl, Oeters, and Scheel[37] have recently measured the oxygen content of the metal in equilibrium with slags saturated with dicalcium silicate, tricalcium silicate and lime in the CaO-"FeO"-SiO_2 system at 1600°C. Their values are in disagreement with those of Taylor and Chipman[36] above 10 wt% SiO_2.

The "FeO" activities in $CaO-FeO-Fe_2O_3-SiO_2$ melts at 1550°C were determined by Larson and Chipman[24] by gas equilibration measurements at three constant CaO/SiO_2 sections. No attempts were made to deliniate the phase boundaries. Because of difficulties involved in containing the melts in platinum crucibles at very low oxygen pressures,

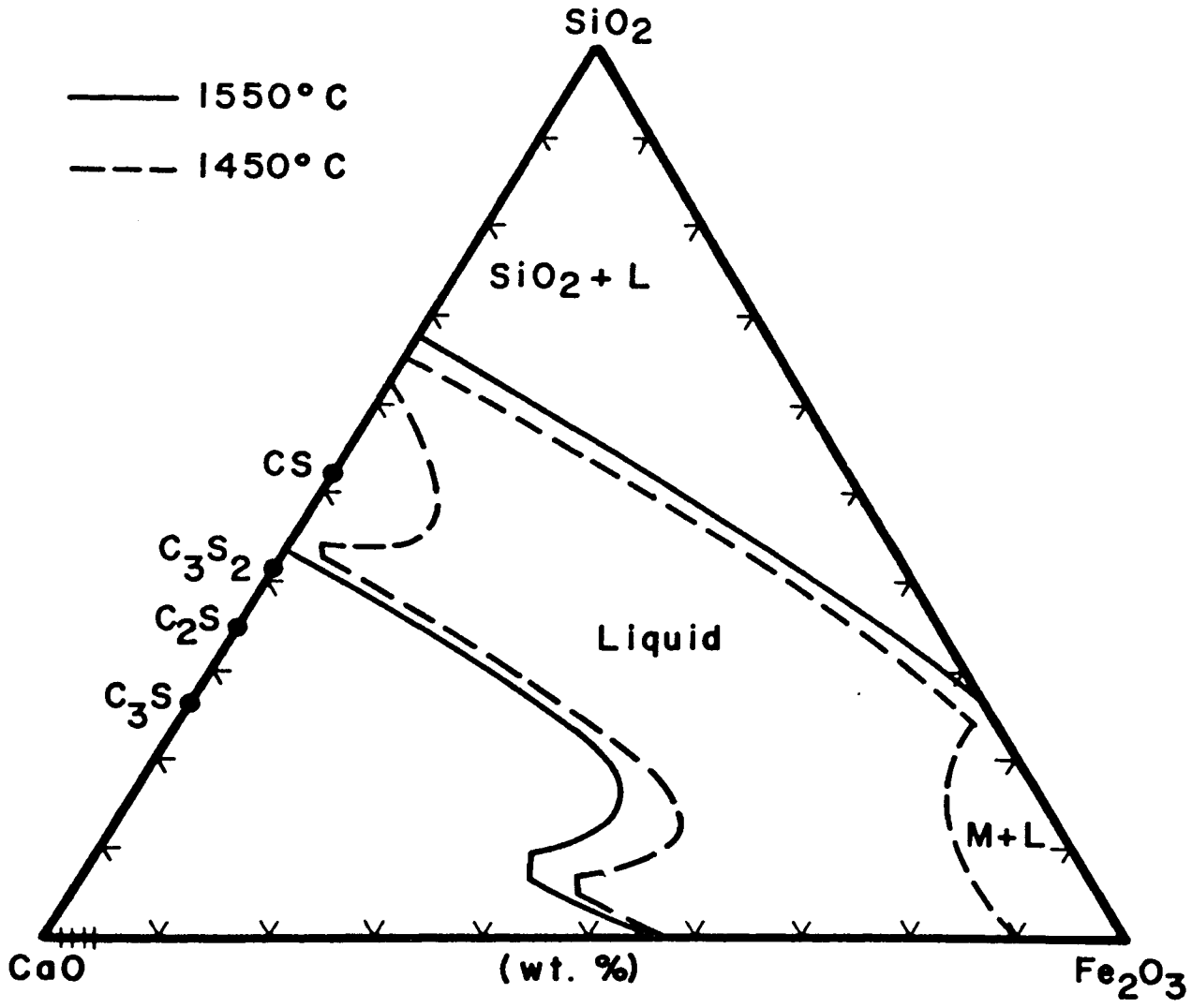

Figure 9. Isothermal Sections of the System $CaO-Fe_2O_3-SiO_2$ at 1450°C and 1550°C.

Abbreviations: CS = $CaO \cdot SiO_2$, C_3S_2 = $3CaO \cdot 2SiO_2$, C_2S = $2CaO \cdot SiO_2$, C_3S = $3CaO \cdot SiO_2$, M = Magnetite, L = Liquid.

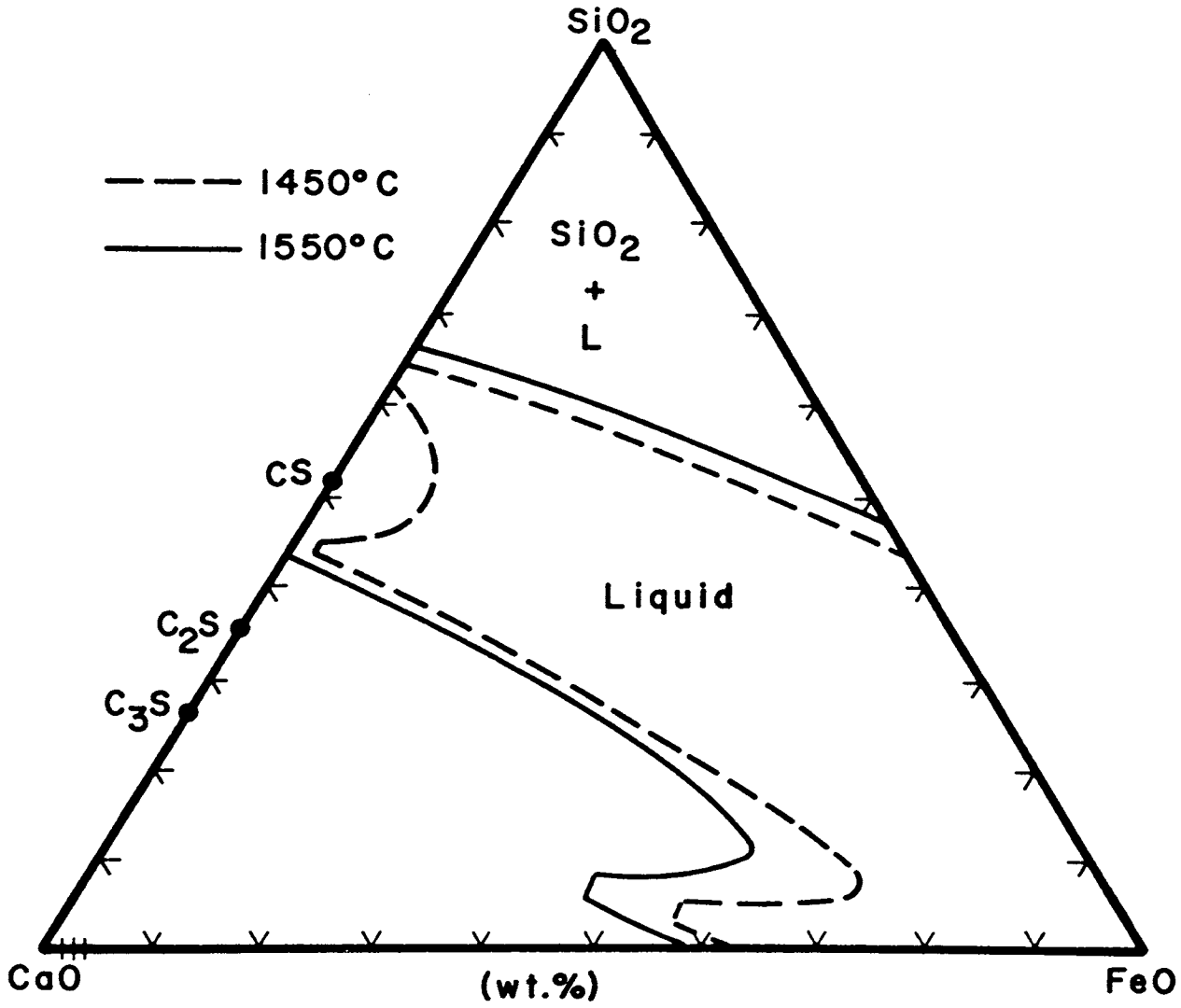

Figure 10. Isothermal Sections of the System $CaO-FeO-SiO_2$ at 1450°C and 1550°C.

Abbreviations: CS = $CaO \cdot SiO_2$, C_2S = $2CaO \cdot SiO_2$, C_3S = $3CaO \cdot SiO_2$.

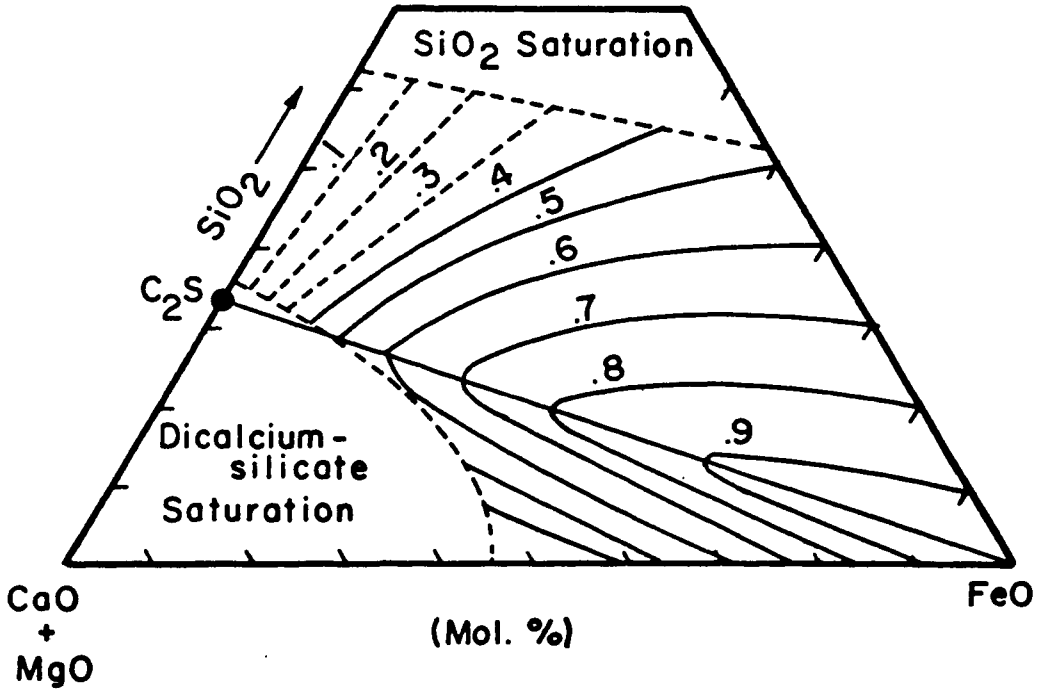

Figure 11. "FeO" Activities in the Melts of the System (CaO + MgO)-FeO-SiO_2 at 1600°C. After Taylor and Chipman[36].

they used the data of Fetters and Chipman[35] at 1600°C to obtain the composition and oxygen pressure of the slags in equilibrium with iron.

CHAPTER III

EXPERIMENTAL PROCEDURE

General Procedure

In order to determine the phase equilibria and activity-composition relations in the ternary and quaternary systems at 1450°C and 1550°C, mixtures of oxides and silicates of desired compositions were equilibrated with gas mixtures of known oxygen partial pressures. After equilibrium had been attained the samples were quenched to room temperature, removed from the crucibles and prepared for examination and analysis. Phase boundaries were determined by examining the quenched samples by microscopic and x-ray diffraction methods. The composition of all one phase and some two-phase samples was determined by chemical analysis.

Furnaces and Temperature Control

Two different furnaces were employed throughout this investigation. Most equilibration runs have been made in a silicon carbide resistance-type tube furnace capable of reaching temperatures up to about 1600°C. A vertical mullite tube, 36" long and 1½" I.D., served as the reaction chamber. A ground glass joint with a side arm for gas admission was sealed to the bottom of the tube, which was designed to permit quenching of the sample without disturbing the atmosphere in the furnace. The top of the tube was satisfactorily sealed by a thin refractory blanket placed between the top of the tube and the circular rim plate of the sample holder.

The temperature of this furnace was controlled by a Barber-Colman 472 Capacitrol controller with the aid of a Pt-Pt 13% Rh thermocouple, which regulated the temperature to within ±2°C.

Some equilibrium runs were carried out in a molybdenum-wound vertical tube furnace, in which the temperature was controlled to ±2°C by a commercial null-point regulator using a tungsten-rhenium thermocouple. A 3" hot zone in which the temperature was 4°C cooler 1½" from the hot spot was established in both furnace tubes.

Temperature Measurements

The actual sample temperature was measured at the beginning and just before the end of each run by a Pt-Pt 10% Rh thermocouple inserted next to the sample (see Figure 12). This thermocouple was frequently standardized against a reference thermocouple of the same composition calibrated by the National Bureau of Standards at 1450°C and 1550°C. Both thermocouples were also periodically calibrated against the melting points of silver (961°C), gold (1063°C), and palladium (1553°C). The temperatures measured and controlled as described above were estimated to be correct to ±5°C.

Atmosphere Control

The source of oxygen for the samples to be equilibrated at 1 atm. O_2 was tank oxygen of 99.95% min. purity. A cylinder of oxygen and nitrogen, premixed and analyzed by the

Matheson Company, was the source of gas of $Po_2 = 10^{-2.0}$ atm.* Air was mixed with prepurified grade Matheson nitrogen to obtain $Po_2 = 5.0x10^{-2}$. Oxygen pressures in the range of $Po_2 = 10^{-3}$ to about $Po_2 = 10^{-11}$ were obtained by either pure CO_2 or by mixtures of CO_2 and CO. Po_2 values could be calculated from tables of thermodynamic data on the free energy of formation of CO and CO_2[38].

The method of mixing CO and CO_2 in the exact desired proportions was similar to that used by Darken and Gurry[1], and later by Muan[26], except that CO_2 and CO were mixed after passing them individually through the calibrated flowmeter tubes of a Model 665 Matheson Gas Proportioner. Each flowmeter tube was periodically calibrated with a soap bubble column. This column consisted of a glass buret tube of known volume with a small reservoir of soap solution at the bottom, in series with the flowmeter. The rate at which a thin soap film passed up the column permitted a calculation of the flow rate of gas through the flowmeter tube. A series of mutually interchangeable flowmeter tubes of different flow ranges was at hand so that a wide range of mixing ratios could be obtained. Depending on the individual gases flowing through the tubes an accuracy of $10^{\pm 0.005}$ atm. was reproducible in mixing; for example, 80.2 vol. % CO + 19.8 vol.

---

*The symbol Po_2 will be used throughout this thesis to indicate the partial pressure of oxygen of the gas phase, expressed in atmospheres, in equilibrium with the condensed phase(s).

% CO_2 to get a $Po_2 = 10^{-9.300 \pm 0.005}$ at 1450°C, as estimated from errors in reading the millimetric scales of the flowmeters.

CO_2, supplied by Matheson Company, was of Coleman Instrument grade with a reported purity of 99.99% min. by volume. This gas was further purified by passing it over a copper gauze at 550°C. The purity of Matheson C.P. grade CO was in excess of 99.5% min. with 8 ppm. max. O_2, so this gas did not need any further purification. Several mixtures of CO_2 + CO, prepared and analyzed by Matheson Company, were also available.

Starting Materials

Table I summarizes the oxides prepared from Fisher Certified analytical grade reagents. The following compounds were prepared from CaO, Fe_2O_3, and SiO_2:

Calcium Ferrites: Ten gram samples of dicalcium ferrite ($2CaO \cdot Fe_2O_3$), monocalcium ferrite ($CaO \cdot Fe_2O_3$), and calcium diferrite ($CaO \cdot 2Fe_2O_3$) were synthesized by weighing proper amounts of CaO and Fe_2O_3, and grinding them together for at least 20 minutes in an agate mortar under reagent grade acetone to ensure complete mixing. The resulting powders were dried, remixed and pressed into 3/4" diameter, 3/8" long pellets and then were reacted in air for at least 24 hours at a temperature about 25°C below their respective solidus temperatures (as estimated from the phase diagram of Phillips and Muan[18]). These pellets were then ground to pass -200 mesh. The above steps of mixing, reacting, and

TABLE I

OXIDE	METHOD OF PREPARATION
SiO_2	Silica was prepared by dehydrating the precipitated silicic acid of 99.97% min. purity in a platinum dish at 1300°C for 24 hours. The product, tridymite, was then ground to -200 mesh.
CaO	Lime was obtained by thermal decomposition of pure $CaCO_3$ in a platinum dish at 1200°C for 24 hours in air. The product was cooled, immediately weighed and transferred to sealed teflon bottles.
Fe_2O_3	Hematite of 99.93% purity was dried at 700°C for 12 hours in an alumina crucible. The product was ground to -100 mesh.
Fe_3O_4	Magnetite of composition Fe_3O_4 was obtained by heating -100 mesh Fe_2O_3 at 1100°C for 24 hours under $Po_2 = 10^{-10}$ atm. in a platinum crucible. The crucible was slowly cooled to about 800°C without changing the CO/CO_2 ratio; further cooling was quickly made under a purified nitrogen atmosphere.
"FeO"	Wustite was obtained by heating -100 mesh Fe_2O_3 at 1100°C for 36 hours in a platinum crucible under $Po_2 = 10^{-12.5}$ atm. The product, averaging $Fe_{.945}O$, was cooled to room temperature as described for magnetite.

regrinding were repeated until the x-ray diffraction patterns and chemical analysis confirmed the complete formation of the particular compound in question.

Calcium Silicates: Ten gram samples of rankinite ($3CaO \cdot 2SiO_2$), dicalcium silicate ($2CaO \cdot SiO_2$), monocalcium silicate ($CaO \cdot SiO_2$), and tricalcium silicate ($3CaO \cdot SiO_2$) were synthesized by using the same procedure outlined for calcium ferrite compounds, except pellets were reacted at 1300°C.

Sample Equilibration

Samples, which weighed about 800 mg, were packed firmly into Pt crucibles made from platinum tubing of ½" O.D., 5 mil wall thickness. Four or five different samples were suspended in their crucibles with extremely thin platinum loops which were in turn placed on the hooks of the sample holder (see Figure 12). As soon as the samples were lowered into the hot zone of the furnace, the reaction tube was sealed and flushed with a rapid flow of gas. The gas flow was then reduced to about 150 cm^3/min, which was sufficient to minimize the effects of thermal diffusion[1].

The time required to reach equilibrium was determined by holding a high silica sample under a low oxygen pressure for different lengths of time. It was observed that at 1450°C the sample attained a uniform final composition after 20 hours. This same procedure indicated that 8 hours was necessary to reach equilibrium at 1550°C. Actual samples were equilibrated for 40 hours and 18 hours at 1450°C and

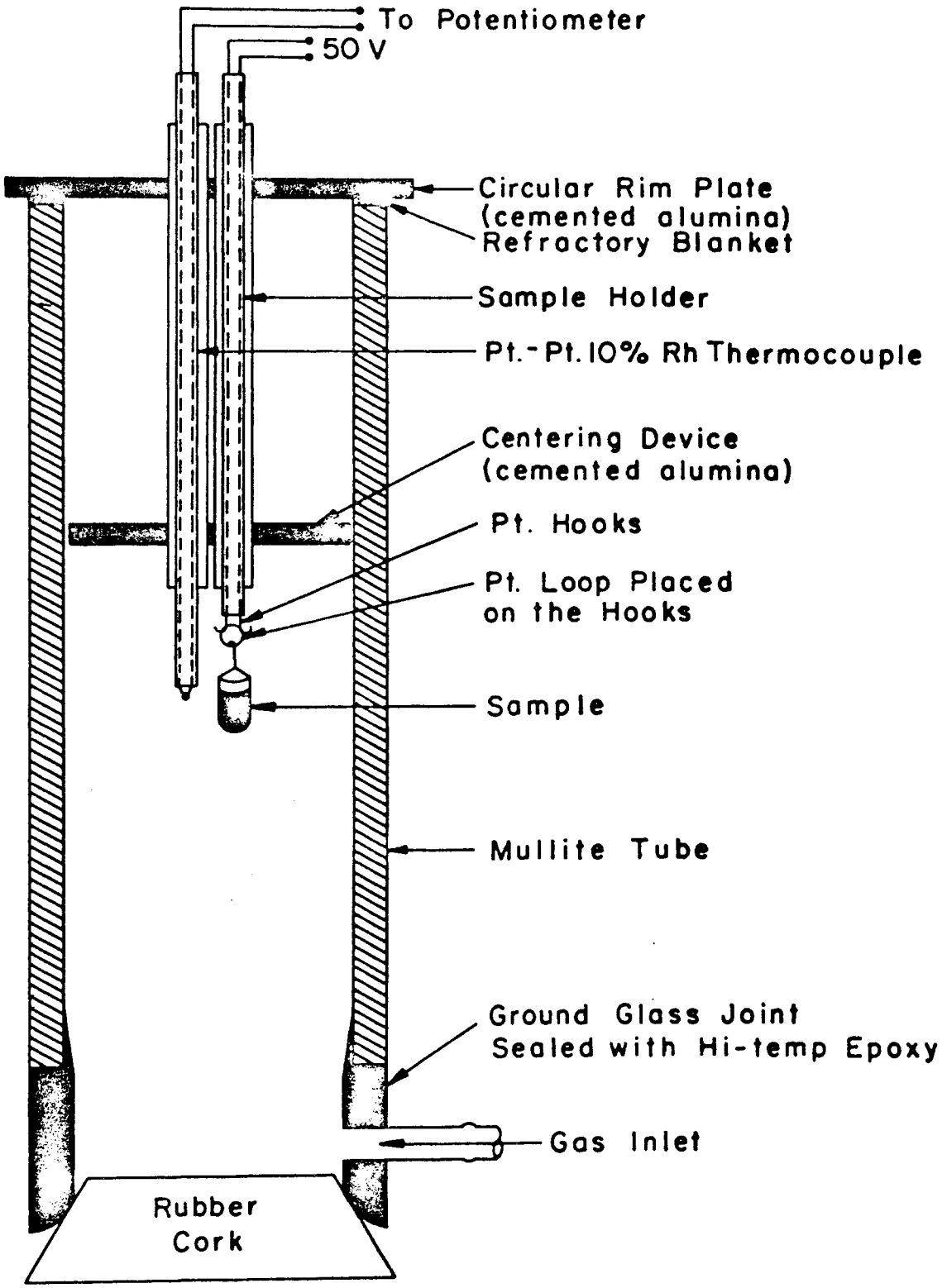

Figure 12. Part of the Apparatus Showing the Furnace Tube, Sample Holder, Thermocouple and the Sample Arrangement.

1550°C respectively. Samples with low silica contents reached equilibrium faster.

After equilibrium was attained, the crucibles were quenched to room temperature by applying about 50 volts across the platinum wires of the sample holder. The thin platinum loops vaporized and allowed the sample to drop into the quenching medium in less than a second. This technique provided a quench with no disturbance of the furnace atmosphere. For most of the samples the quenching medium was distilled water, except isopropyl alcohol was used for samples containing lime as a solid phase. Quenching into mercury was found to be unsatisfactory because of difficulties in completely separating the mercury from the sample. Comparisons of chemical analysis of several identical samples, quenched in mercury and water, showed that within the limits of analytical error, their final compositions were identical. Thus, it was concluded that under the conditions of this work, the water has no effect on the sample composition during quenching. This is probably because of such a small surface area and time of exposure.

The usefulness of platinum as a crucible material is limited by its tendency for alloying with iron from the melts containing iron oxides. Appreciable amounts of iron can be dissolved in platinum at oxygen pressures below 10^{-4} atm., according to the proposed reaction:

$$FeO \longrightarrow \underline{Fe}(Pt) + \tfrac{1}{2}O_2 \ .$$

Therefore for equilibration runs below $Po_2 = 10^{-3}$ atm. the

platinum crucibles used in this work were presaturated with iron by equilibrating them with lime-iron oxide mixtures having an iron activity nearly equal to that expected in the sample[39,40]. For slag compositions where no data were available, particularly for those containing silica, the crucibles were repeatedly equilibrated with the same mixture of slightly higher "FeO" content until the chemical analysis of total iron in the slag showed no loss to the crucible.

Chemical analyses performed on slags taken from top and bottom parts of various crucibles showed identical compositions, hence it was judged that the liquid slags were uniform and did not need any mechanical agitation.

Examination of Quenched Samples and Chemical Analyses

In order to identify any solid phases present for the estimation of phase boundaries, some of the quenched samples were removed from the crucibles and mounted in liquid epoxy resin which permeated the pores and cracks of the specimens before hardening and greatly facilitated polishing. The mounted specimens were polished with Linde "A" abrasive, suspended in alcohol instead of water when lime was expected as a solid phase. Phase determinations were made with a reflected light microscope in which the appearance of the solid phase was compared to the appearance of phases of known identity in previously prepared samples. Samples containing dicalcium silicate could easily be identified by transmitted light microscopy in which the sample was lightly ground, and immersed in refraction index liquid.

Chemical analyses were performed volumetrically to determine the composition of samples. The amounts of divalent iron, total iron, and CaO were established by dissolving about 200 mg -60 mesh sample in HCl for each analysis. After necessary treatments the resulting solutions were titrated by standard dichromate and permanganate methods[41]. The accuracy of analytical methods were checked against identical samples analysed by two commercial laboratories, and also comparing with the results of Darken and Gurry[2] on $FeO-Fe_2O_3$ mixtures. It was estimated that ferrous and ferric iron determinations were accurate to ±1%, while CaO analysis was accurate to ±0.5%. The details of analytical methods are described in Appendix I.

No attempts were made to determine quantitatively the relative amounts of liquid and solid phases present.

CHAPTER IV

EXPERIMENTAL RESULTS

The experimental results of this investigation are presented in two forms. Tables II through XI of Appendix II contain the chemical compositions of the samples after equilibration with various Po_2 at 1450°C and 1550°C. The phases present at the equilibration temperatures, as identified by the methods discussed earlier, are also listed. The Figures 13, 14, and 16-23 summarize the data given in these tables in the form of isothermal phase diagrams.

$CaO-FeO-Fe_2O_3$ SYSTEM

Presentation of Results

Figures 13 and 14 show the isothermal phase diagrams of that system at 1450°C and 1550°C respectively. Light solid curves are the boundary lines separating the single liquid phase* from the liquid + solid two-phase regions. Curved dash-dot lines passing through the open circles in the liquid field represent the constant Po_2 isobars. Straight line portions of the isobars, drawn through the black circles, correspond to liquid + solid phase areas. The magnetite + liquid phase boundary was determined by

---

*It is important to remember that a gas phase is always present in equilibrium with the condensed phase(s).

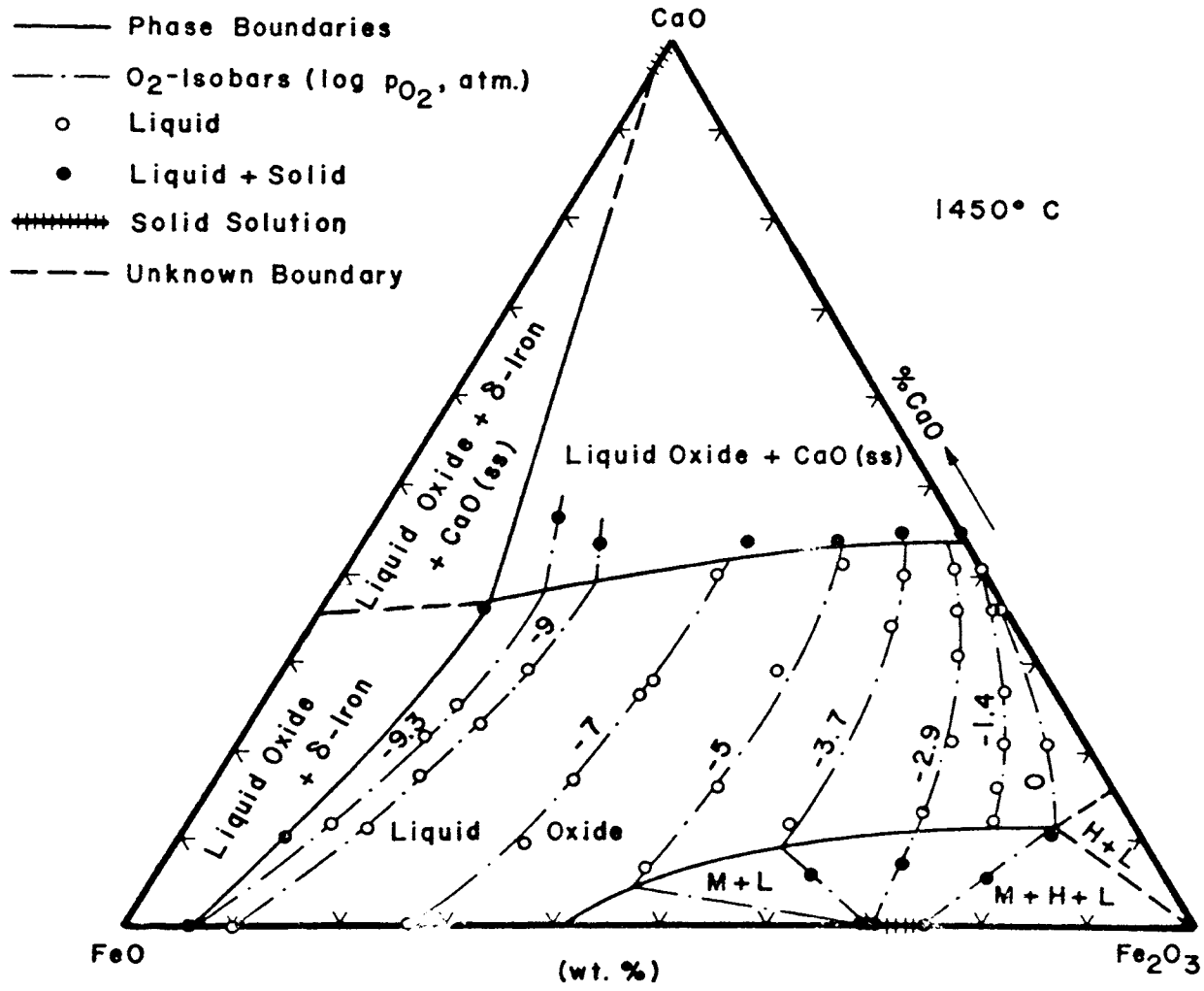

Figure 13. The Isothermal Phase Diagram for the CaO-FeO-Fe_2O_3 System.

Abbreviations: M = Magnetite, H = Hematite, L = Liquid Oxide

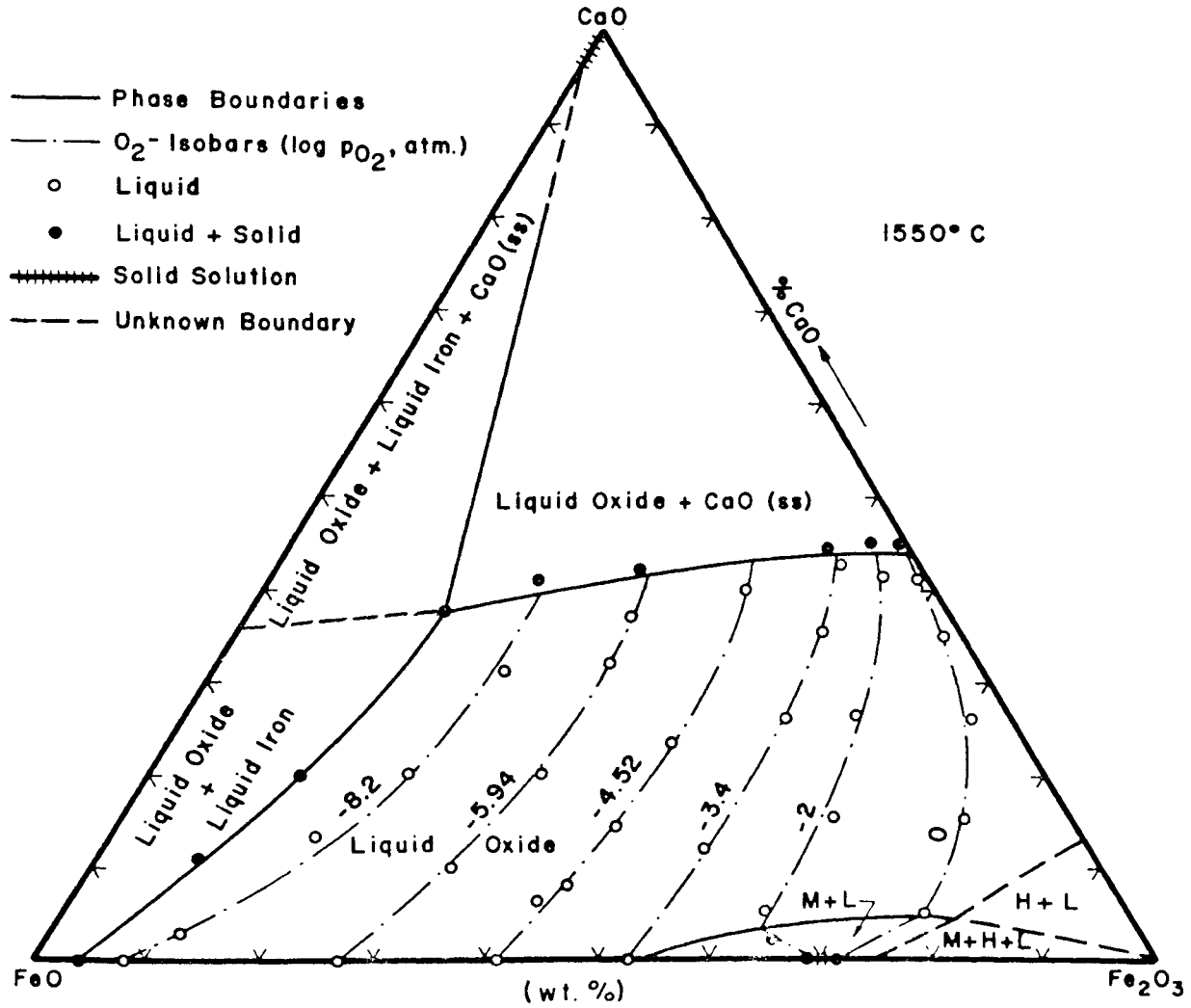

Figure 14. The Isothermal Phase Diagram for the CaO-FeO-Fe_2O_3 System.

Abbreviations: M = Magnetite, H = Hematite, L = Liquid.

connecting the points of intersection of iso-Po_2 curves with the respective iso-Po_2 lines. The extension of this boundary to FeO-Fe_2O_3 join was first estimated and then confirmed from the work of Darken and Gurry[2]. Open and black circles show the results of chemical analysis as expressed in terms of weight % CaO, FeO, and Fe_2O_3, in 100% liquid, and liquid + solid samples respectively.

The extent of nonstoichiometry in the magnetite phase is indicated by hashed marks along the FeO-Fe_2O_3 binary. Since no experiments were done above Po_2 = 1 atm. the dashed boundary line passing through the Fe_2O_3 corner was inferred from Phillips and Muan's work[3], neglecting the very small nonstoichiometry. Other dashed curves are the unknown boundaries.

At high lime contents the liquid phase was saturated with a series of CaO-"FeO" solid solutions. From the available phase diagrams[4] the amount of "FeO" in these solutions was estimated to increase approximately from zero to eight weight percent, at both temperatures, as Po_2 decreased from 10° to the Po_2 in equilibrium with iron. The CaO(ss) + liquid phase boundary was drawn by passing it through the average of the data points where the 100% liquid and the first trace of the solid phase was observed.

At 1450°C the composition and Po_2 of liquids along the liquid + metallic iron phase boundary were determined by equilibrating the samples in iron crucibles. The control of

$\frac{P_{CO_2}}{P_{CO}}$ was quite critical in these runs, for iron crucibles were severely oxidized when this ratio was slightly higher than that represented by the liquid + metallic iron boundary. Therefore, in this case, the samples were always equilibrated from the CaO-FeO side until there was no visible oxidation of the crucibles. Compositions and Po_2 of samples containing a very small amount of fine, dispersed metallic iron were assumed to represent this boundary.

A lack of suitable crucible materials did not permit any data to be obtained along the above boundary at 1550°C. Therefore points along the liquid oxide + liquid iron boundary were taken from Larson and Chipman[23] (see Table XII, Appendix II).

Discussion of Results

The results summarized in Figures 13 and 14 show, as expected, that the region of stability of magnetite is smaller at 1550°C than it is at 1450°C. For example, at Po_2 = 1 atm. at 1450°C liquid in equilibrium with solid magnetite contains 10.5% CaO, whereas at 1550°C it contains only 4.5% CaO. Hematite is completely unstable at both temperatures under all oxygen pressures of this work. The position of the phase boundary at lime saturation does not show any substantial change with temperature.

The dicalcium ferrite ($2CaO \cdot Fe_2O_3$) phase was reported to be stable both in air and at 1 atm. Po_2 up to 1449°C[18].

During the early stages of this work a few experiments were made in order to establish the stability region of this phase as a function of temperature and oxygen pressure. The dicalcium ferrite was found to melt at 1457°C at Po_2 = 1 atm., and at 1426°C when Po_2 was 10^{-1} atm. Since, within the limits of experimental error, the primary crystallization field of dicalcium ferrite is very small or non-existent it was not shown in the isothermal phase diagram of Figure 13.

To a first approximation, a liquid mixture of ferrous and ferric oxides can be considered to consist of ferrous and ferric ions distributed randomly among a matrix of oxygen ions. The shape of the oxygen isobars of Figures 13 and 14 suggests that Fe^{3+} ions become stabilized relative to Fe^{2+} ions with increasing additions of CaO to an otherwise pure iron oxide liquid.

The effect of temperature on Fe^{3+} stability can be illustrated by choosing a stability parameter, for example the ratio $\frac{n_{Fe_2O_3}}{n_{FeO}+n_{Fe_2O_3}}$ in liquid CaO-FeO-Fe_2O_3 oxides. The ratios calculated from Figures 13 and 14 are plotted against log Po_2 in Figure 15 for two levels of constant CaO contents. At all oxygen pressures this ratio is lower at 1550°C than at 1450°C, indicating favored Fe^{2+} stabilities at higher temperatures. Hence, in general it can be said that for a given CaO content and Po_2, the solubility of oxygen in CaO-FeO-Fe_2O_3 melts decreases with increasing temperatures.

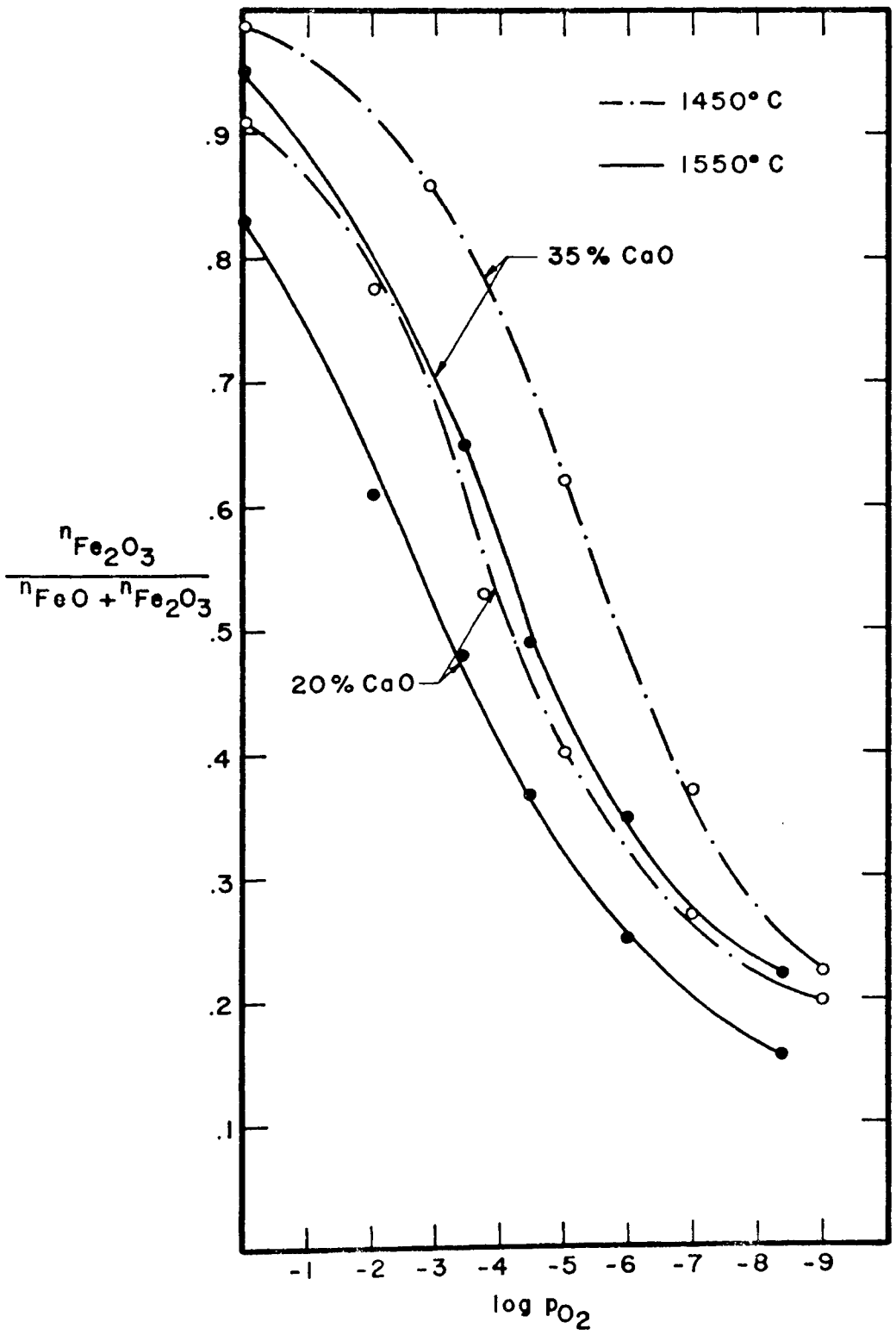

Figure 15. The Effect of Temperature on the Relative Fe^{3+} Stability of the Ternary $CaO-FeO-Fe_2O_3$ Melts at Two Levels of CaO.

$CaO-FeO-Fe_2O_3-SiO_2$ SYSTEM

Presentation of Results

Figures 16 to 19 and 20 to 23 show the isothermal phase diagrams of that system at 1450°C and 1550°C. The light lines are the phase boundaries, dash-dot lines are the constant Po_2 isobars, and the dashed lines are the inferred[26] or undetermined phase boundaries. Isobars and boundaries were drawn by methods described for the ternary system. Hashed marks indicate the existence of solid solutions, either determined experimentally or estimated from previous works[4,26]. Open and black circles are the results of chemical analyses as expressed in terms of weight % SiO_2, CaO, FeO, and Fe_2O_3 in 100% liquid, and in liquid + solid samples respectively. The limits of variation in the final intended silica contents were ±0.5% at 5 and 10% silica sections, and ±1.0% at 20 and 30% silica sections at both temperatures. At 1450°C the liquid + metallic iron phase boundaries for all constant silica sections were determined in iron crucibles as described for the ternary system. Since both iron and platinum crucibles were molten under extremely reducing oxygen potentials along these boundaries at 1550°C, no data could be obtained with the present technique. As will be described in the next chapter, extrapolations were made in the "ternary" CaO-"FeO"-SiO_2 system from data at 1450°C of this work and the 1600°C diagram of Taylor and Chipman[36] to obtain the composition and Po_2 of a few

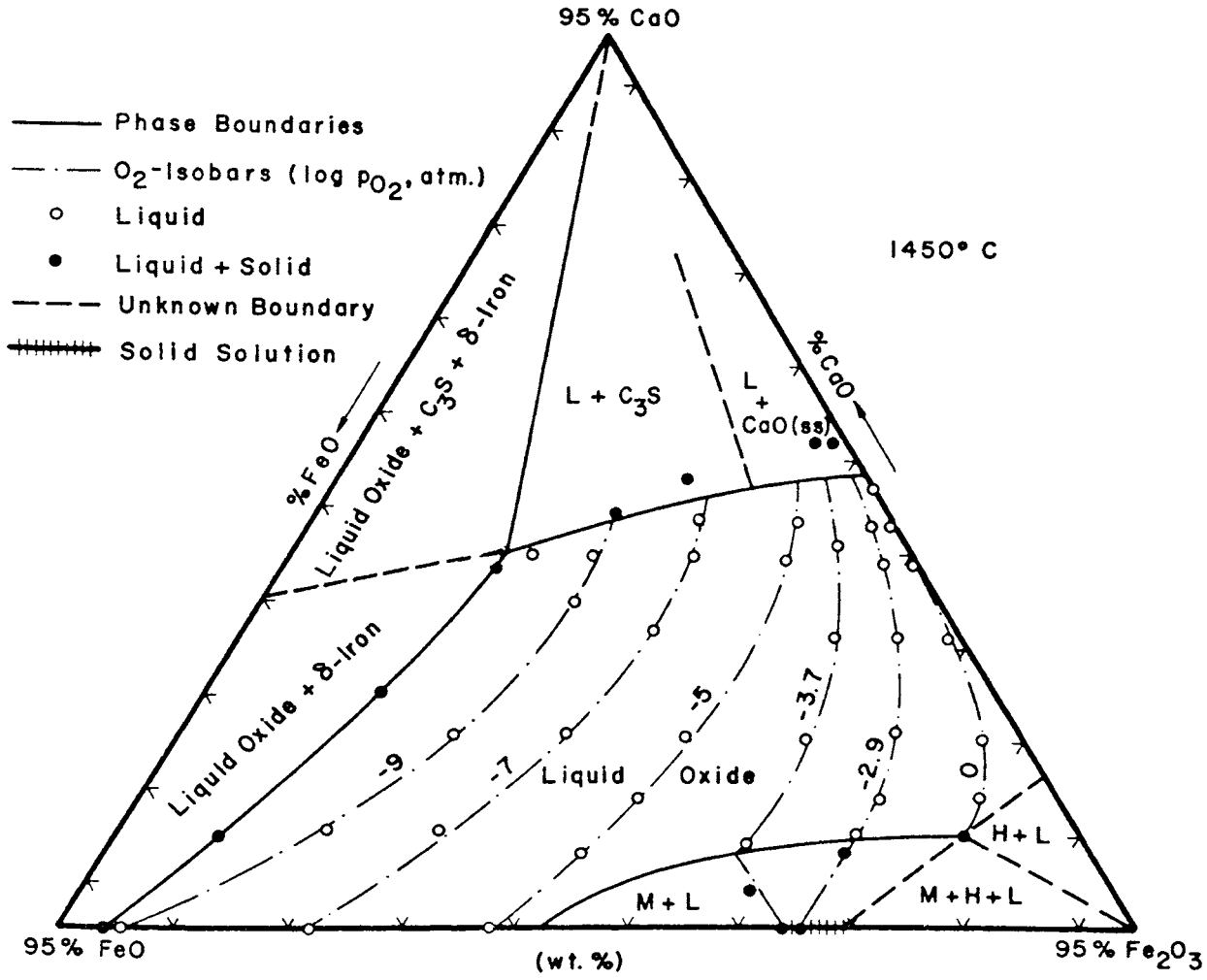

Figure 16. The 5% SiO_2-Isothermal Phase Diagram for the CaO-FeO-Fe_2O_3-SiO_2 System.

Abbreviations: M = Magnetite, H = Hematite, L = Liquid Oxide, C_3S = $3CaO \cdot SiO_2$.

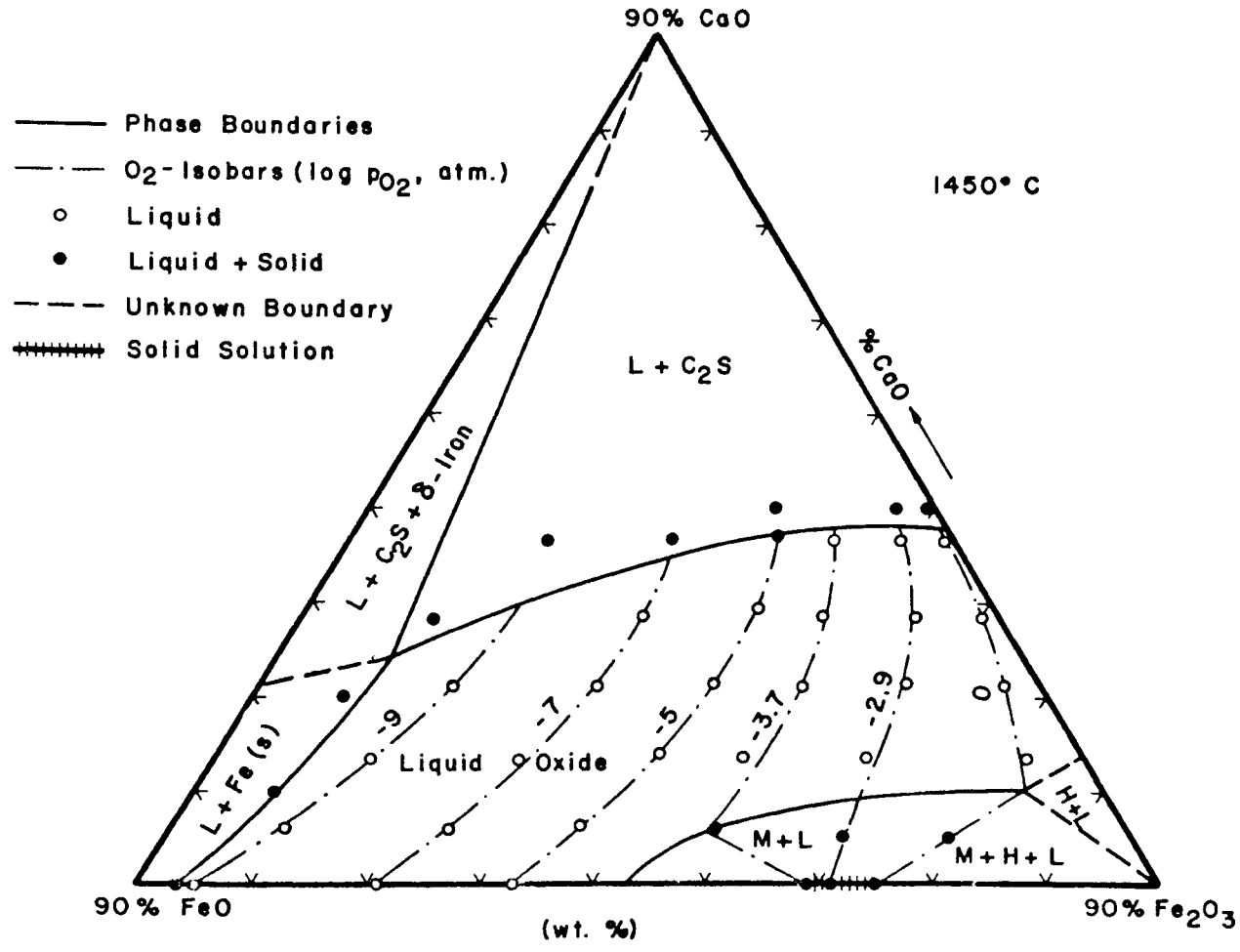

Figure 17. The 10% SiO_2-Isothermal Phase Diagram for the CaO-FeO-Fe_2O_3-SiO_2 System.

Abbreviations: M = Magnetite, H = Hematite, L = Liquid Oxide, C_2S = 2CaO·SiO .

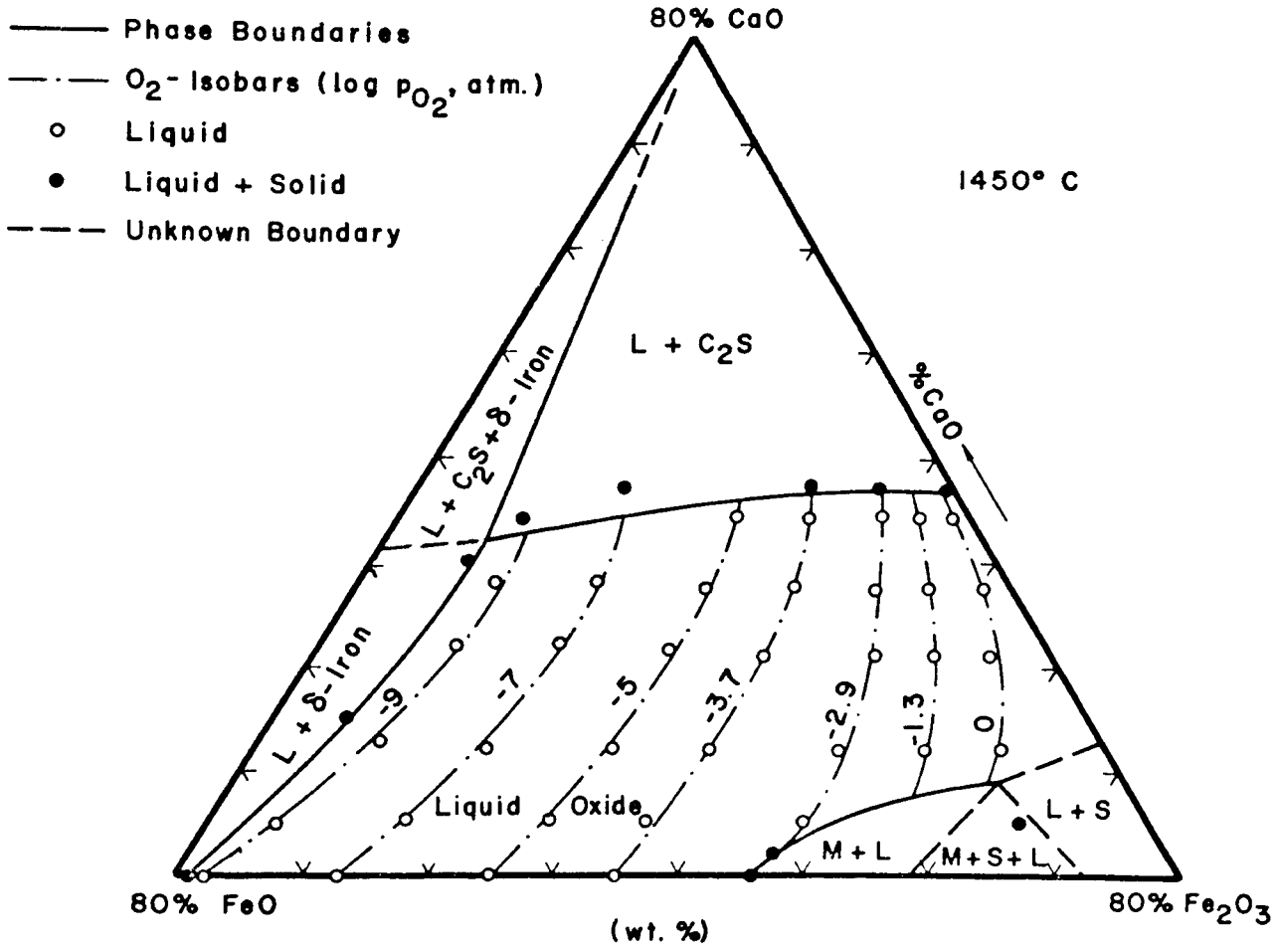

Figure 18. The 20% SiO_2-Isothermal Phase Diagram for the CaO-FeO-Fe_2O_3-SiO_2 System.

Abbreviations: M = Magnetite, S = Silica, L = Liquid Oxide, C_2S = $2CaO \cdot SiO_2$.

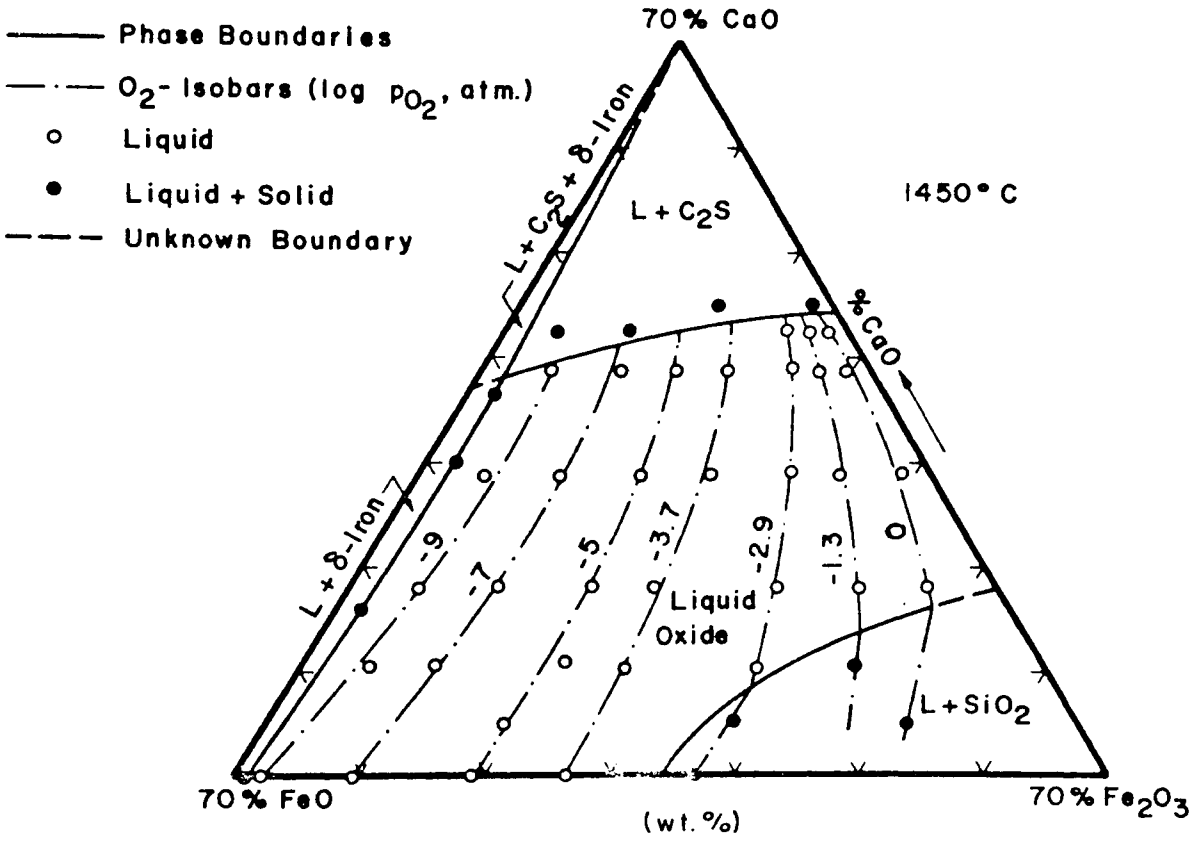

Figure 19. The 30% SiO_2-Isothermal Phase Diagram for the CaO-FeO-Fe_2O_3-SiO_2 System.

Abbreviations: L = Liquid Oxide, C_2S = $2CaO \cdot SiO_2$.

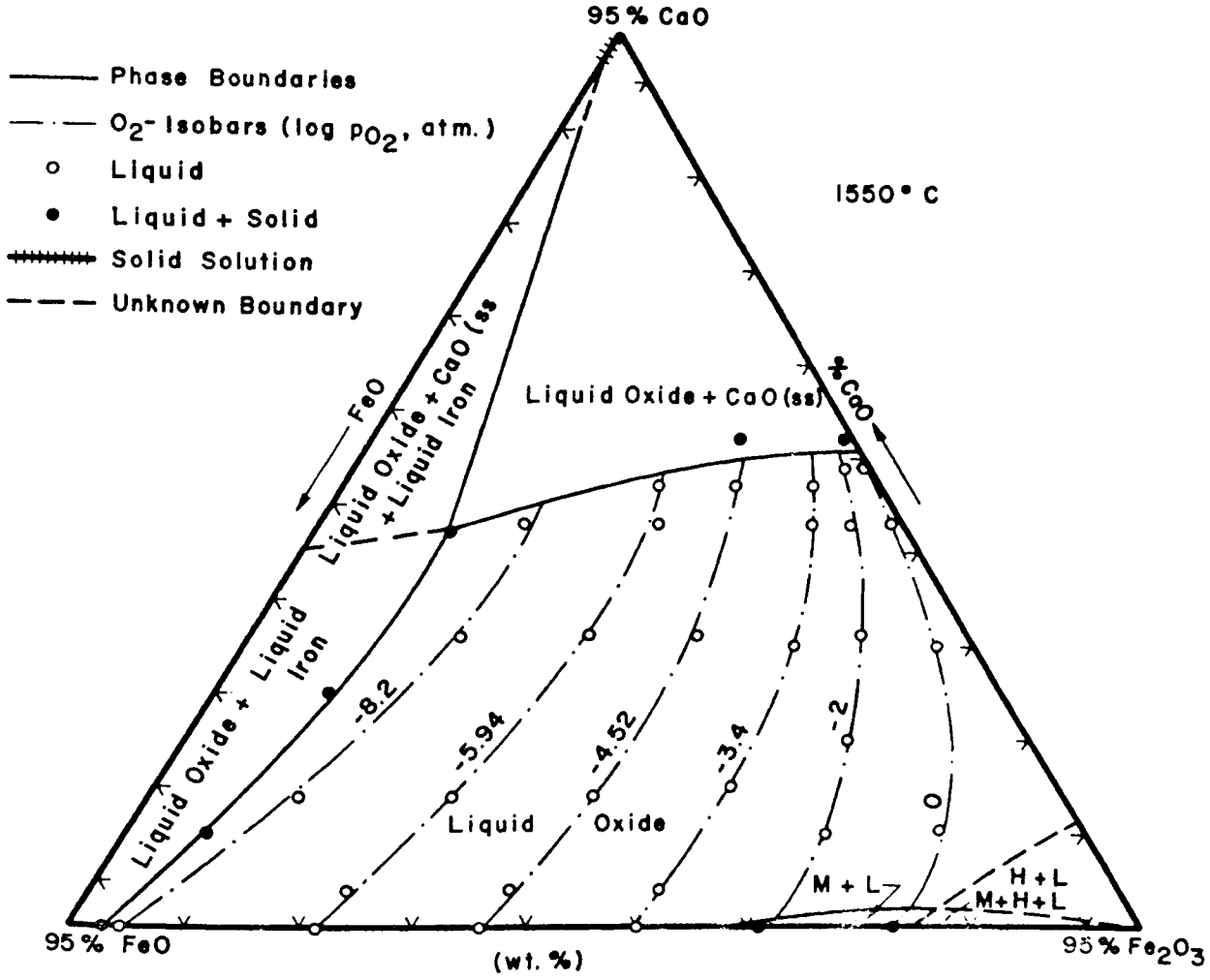

Figure 20. The 5% SiO_2-Isothermal Phase Diagram for the CaO-FeO-Fe_2O_3-SiO_2 System.

Abbreviations: M = Magnetite, H = Hematite, L = Liquid Oxide.

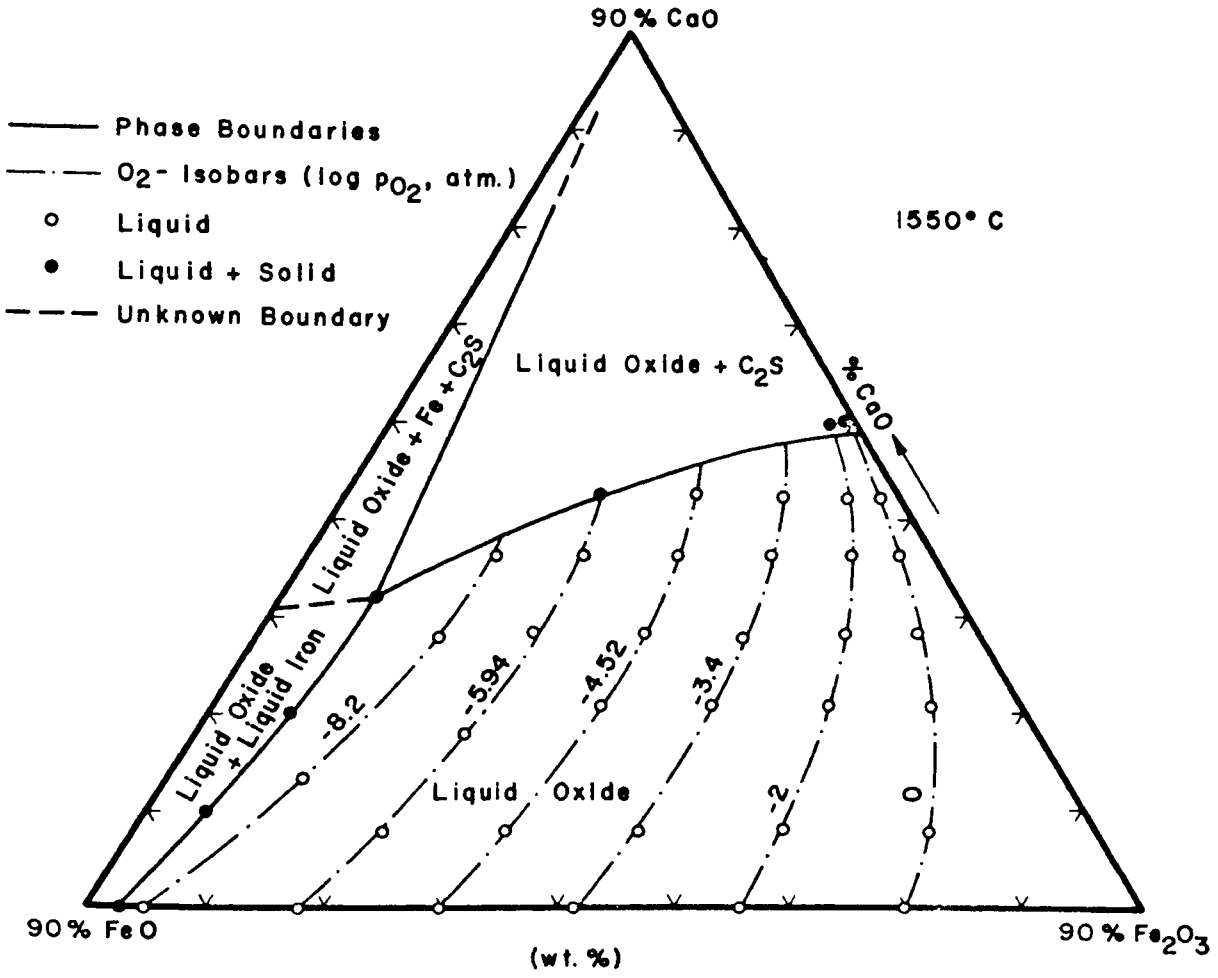

Figure 21. The 10% SiO_2-Isothermal Phase Diagram for the CaO-FeO-Fe_2O_3-SiO_2 System.

Abbreviations: C_2S = $2CaO \cdot SiO_2$.

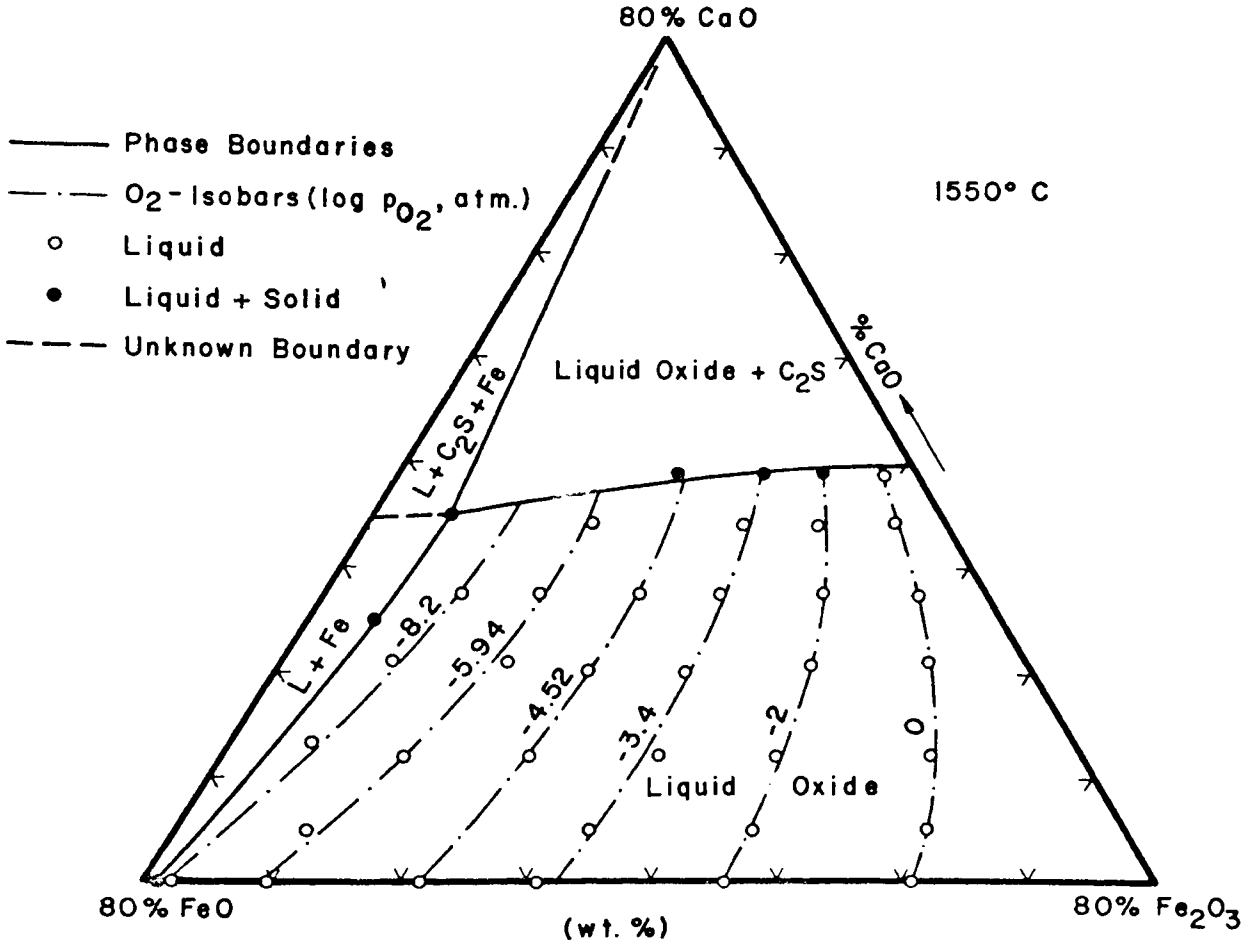

Figure 22. The 20% SiO_2-Isothermal Phase Diagram for the $CaO-FeO-Fe_2O_3-SiO_2$ System.

Abbreviations: L = Liquid Oxide,

$C_2S = 2CaO \cdot SiO_2$.

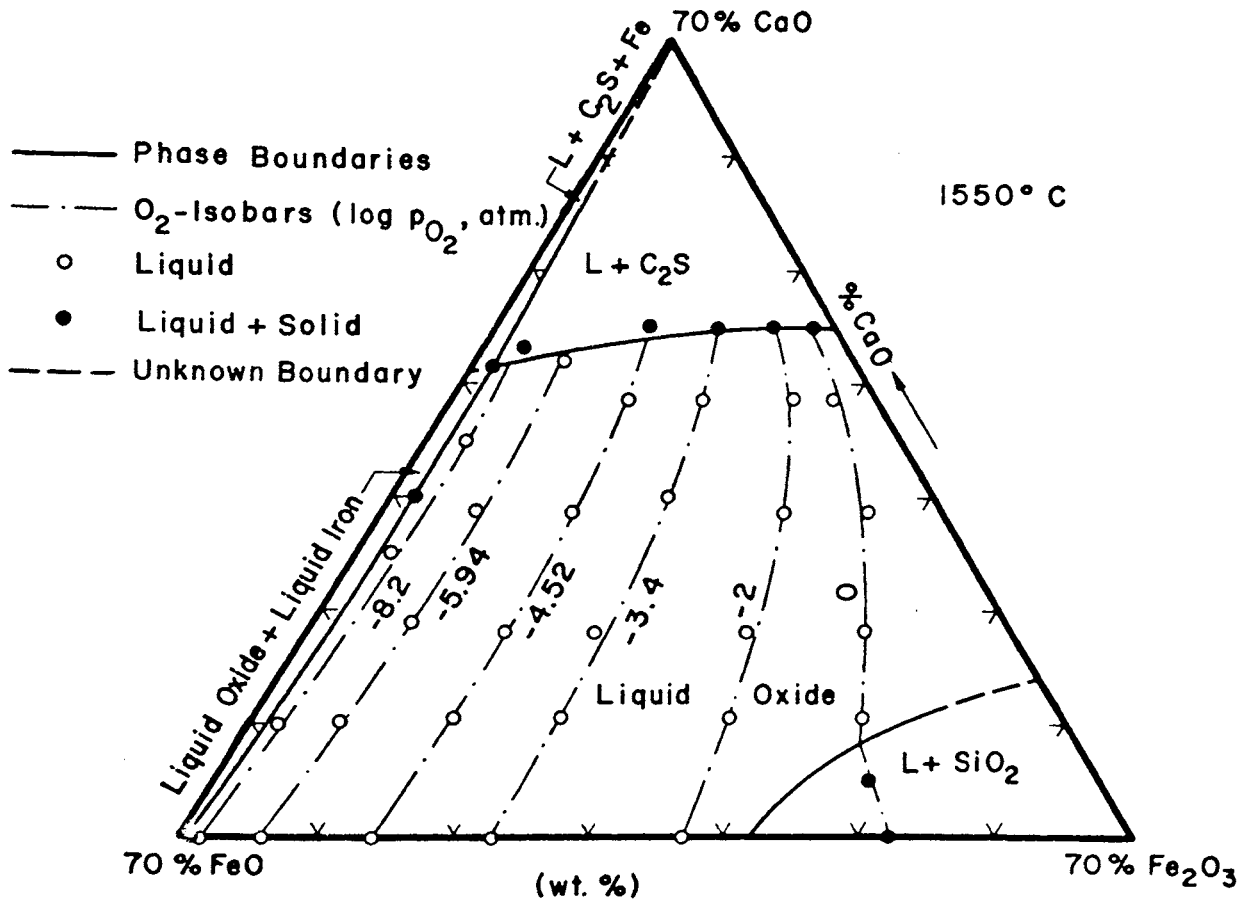

Figure 23. The 30% SiO_2-Isothermal Phase Diagram for the CaO-FeO-Fe_2O_3-SiO_2 System.

Abbreviations: L = Liquid Oxide,

C_2S = $2CaO \cdot SiO_2$.

points to draw the liquid oxide + liquid iron boundaries of Figures 20 through 23 (see Appendix II, Table XII).

Discussion of Results

Isothermal phase diagrams presented for constant silica sections are similar in appearance to the ternary diagrams; however, certain important differences are noted. At a constant temperature, the stability of magnetite decreases very rapidly with increasing silica additions. The detailed structural considerations, and critical evaluation of several existing models on constitution of solid and liquid oxide mixtures are beyond the scope of this thesis. However, it should be mentioned that the ionic theory of slags has contributed much to the understanding of slag constitution. Lumsden[42], using this theory, has qualitatively explained the effect of silica additions on solid or liquid iron oxide mixtures, and has shown that at a certain silica content the solution becomes highly unstable and silica separates in a solid or liquid form. Low-lime, high Po_2 regions of Figures 18 and 19 at 1450°C, and of Figure 23 at 1550°C probably correspond to this situation.

At 1450°C the stable solid phase at high lime contents in the 5% SiO_2 section (Figure 16) was observed to be essentially pure lime in the range of Po_2 = 1 atm. to 10^{-5} atm. At $Po_2 = 10^{-7}$ tricalcium silicate (C_3S) has appeared as the stable solid phase. The dashed boundary line separating CaO

(ss) and C_3S was drawn by assuming that these two phases had a stable coexistence with the liquid at $Po_2 = 10^{-6}$ atm. The composition of C_3S was projected to the 95% CaO corner of the diagram for ease of representation. When compared to the 1450°C ternary diagram, the 5% SiO_2 section shows an increased region of liquid oxide stability as evidenced by the movement of the CaO(ss) boundary toward the CaO corner. The 10% silica section of the quaternary system (Figure 17) shows a decreasing region of liquid oxide stability, with the high-lime stable phase being dicalcium silicate. Presumably C_2S and C_3S were in stable coexistence with the liquid somewhere between 5 to 10% SiO_2 at 1450°C. In this and similar Figures boundary lines passing through the C_2S point in the quaternary systems are projected to the top apex of each diagram. The 20% SiO_2 section (Figure 18) has the same features of the 10% SiO_2 section, except that the tridymite is in equilibrium with magnetite near the 80% Fe_2O_3 corner of the diagram. The magnetite-silica phase boundary was inferred from Muan[26]. The 30% silica section (Figure 19) shows an increased region of SiO_2 stability, no magnetite is present and the liquid oxide field has expanded compared to the 10 and 20% SiO_2 sections, indicating that C_2S stability is decreasing.

Figures 20 through 23, showing the isothermal phase diagrams at 1550°C, have essentially the same features as those described earlier at 1450°C, except that the liquid oxide has an increased region of stability with elevated temperature. Magnetite stability in the 5% SiO_2 section (Figure 20)

is much less than that at 1450 °C, and the high-lime stable solid phase is a series of CaO-"FeO" solid solutions. No magnetite is present in 10%, 20% and 30% SiO_2 sections. The cristobalite modification of silica is the low-lime high-Po_2 stable solid phase in 30% SiO_2 section. Tricalcium silicate (C_3S) was in stable coexistence with dicalcium silicate (C_2S) and liquid probably somewhere between 5 to 10% SiO_2. C_2S is the stable high-lime solid phase in all sections studied above 5% SiO_2.

Earlier studies[27,30] on $FeO-Fe_2O_3-SiO_2$ melts have proved that silica has the opposite effect of CaO on Fe^{3+} stability at a constant temperature and Po_2. Little, however, was quantitatively known[23] about the combined effects of CaO and SiO_2 on iron oxide melts. The data presented in Figures 16 through 23 can be used to construct various forms of two dimensional plots for comparison purposes. In Figure 24 the ratios $\frac{n_{Fe_2O_3}}{n_{FeO}+n_{Fe_2O_3}}$ of quaternary melts at 1450°C are plotted against log Po_2 for a constant CaO content of 20%. The graph clearly shows that while 5% SiO_2 addition results in slightly higher Fe^{3+} stability in the $Po_2 = 10^{-3}$ to 10^{-5} range, increased silica additions strongly reduce the stabilizing effect of CaO for Fe^{3+}. For example, a 20% silica addition to a $FeO-Fe_2O_3$-20% CaO melt at 1450°C is almost as effective in reducing Fe^{3+} stability as increasing the temperature of the ternary melt by 100°C. (Compare 20% SiO_2 curve of Figure 24 with 20% CaO

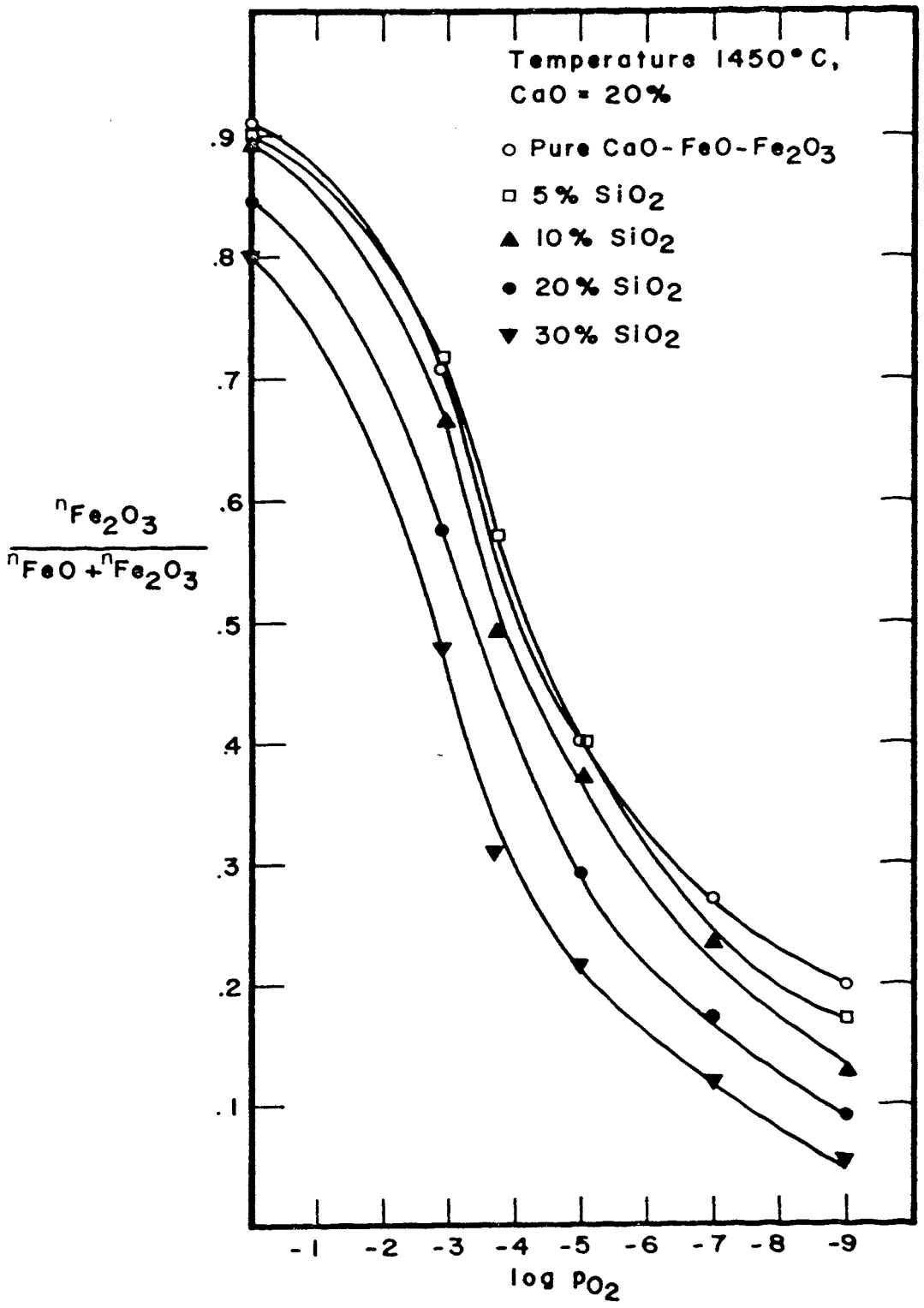

Figure 24. The Effect of Silica Additions on the Relative Fe^{3+} Stability of the $CaO-FeO-Fe_2O_3-SiO_2$ Melts Containing 20% CaO at 1450°C.

curve at 1550°C of Figure 15.) Obviously such diagrams can be prepared for any desirable CaO content at both temperatures.

Figure 25 shows the effect of temperature on Fe^{3+} stability in the 20% constant SiO_2 quaternary melts at two arbitrary levels of fixed CaO contents. Clearly, higher temperature reduces the stability of Fe^{3+}. The 5% CaO curve at 1450°C is coincident, within the limits of experimental error, with the 20% CaO curve at 1550°C. Hence, in going to higher operating temperatures increasing lime additions are necessary to preserve the low temperature oxygen solubility of quaternary $CaO-FeO-Fe_2O_3-SiO_2$ melts.

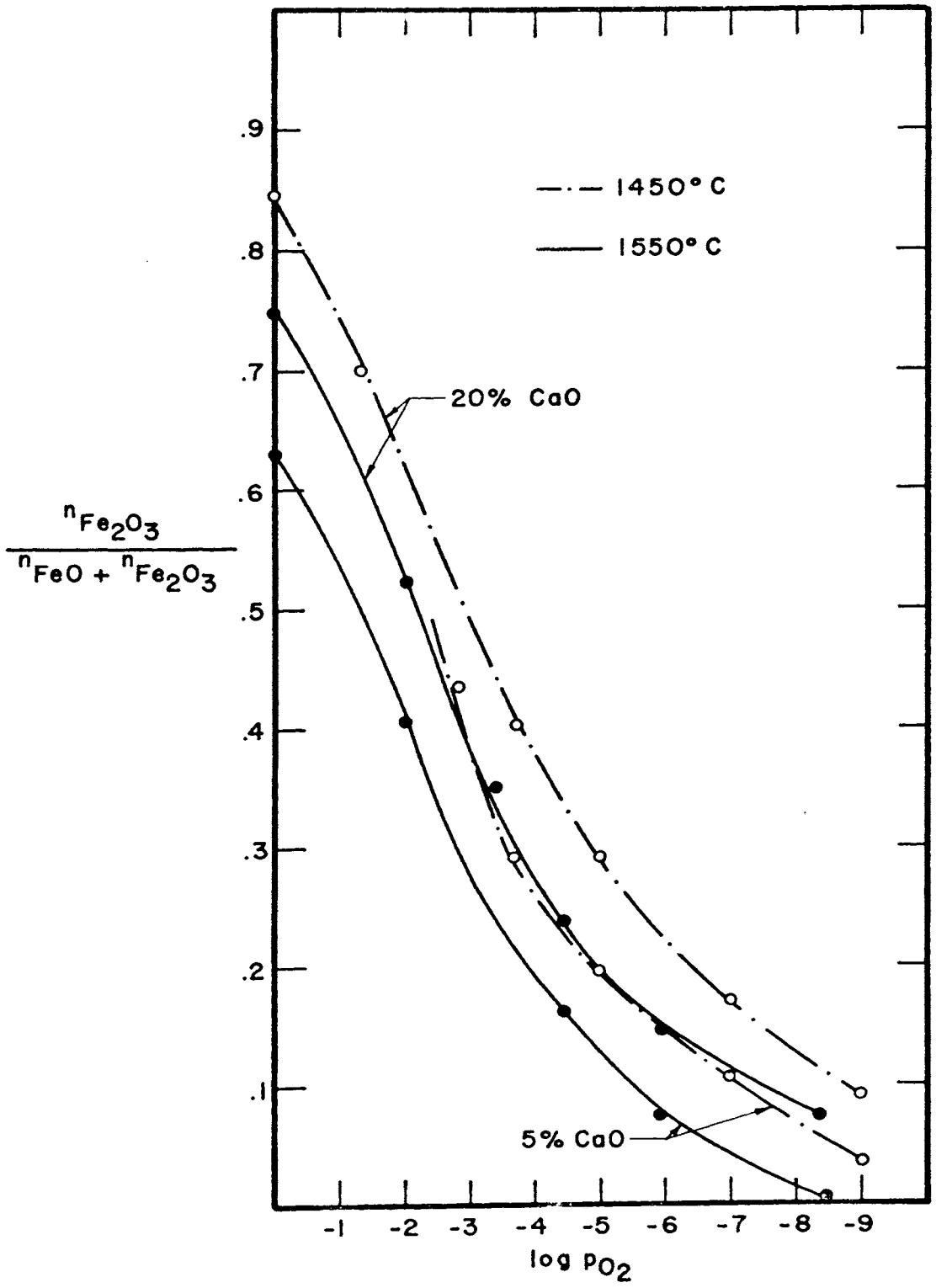

Figure 25. The Effect of Temperature on the Relative Fe^{3+} Stability of the $CaO-FeO-Fe_2O_3-SiO_2$ Melts Containing 20% SiO_2.

CHAPTER V

THERMODYNAMIC CONSIDERATIONS AND ACTIVITY CALCULATIONS

The Gibbs-Duhem equation has become an invaluable tool in calculating the activities of a multicomponent system from the experimentally determined activities of one of the components throughout the entire range of compositions of interest. In a recent paper dealing with slags and iron alloys Steinmetz and Thielmann[43] have summarized the Gibbs-Duhem methods developed for ternary systems since 1950. Although these methods were all[44,45,46,47,48] similar in principle, the one formulated by Schuhmann[47] was somewhat easier to apply to the experimental data of this investigation. A brief derivation of Schuhmann's method is given below.

At constant temperature and pressure the Gibbs-Duhem equation for a ternary system can be written as:

$$n_1 d\mu_1 + n_2 d\mu_2 + n_3 d\mu_3 = 0 \qquad (1)$$

where n_1, n_2, and n_3 are the moles and μ_1, μ_2, and μ_3 are the chemical potentials of components 1, 2, and 3 respectively. By definition,

$$\mu_1 = \left[\frac{\partial F}{\partial n_1}\right]_{n_2, n_3} \qquad (2a)$$

and

$$\mu_2 = \left[\frac{\partial F}{\partial n_2}\right]_{n_1,n_3} \tag{2b}$$

where F is the Gibbs Free Energy. Partial differentials of (2a) and (2b) are,

$$\left[\frac{\partial \mu_1}{\partial n_2}\right]_{n_1,n_3} = \left[\frac{\partial^2 F}{\partial n_2 \partial n_1}\right]_{n_3} \tag{3a}$$

and

$$\left[\frac{\partial \mu_2}{\partial n_1}\right]_{n_2,n_3} = \left[\frac{\partial^2 F}{\partial n_1, \partial n_2}\right]_{n_3} . \tag{3b}$$

Since the order of differentiation is immaterial, the right hand sides of (3a) and (3b) are the same, therefore

$$\left[\frac{\partial \mu_1}{\partial n_2}\right]_{n_1,n_3} = \left[\frac{\partial \mu_2}{\partial n_1}\right]_{n_2,n_3} . \tag{4}$$

Since μ_1 is a function of n_1, n_2, and n_3 only, at constant P and T, its total differential is

$$d\mu_1 = \left[\frac{\partial \mu_1}{\partial n_1}\right]_{n_2,n_3} dn_1 + \left[\frac{\partial \mu_1}{\partial n_2}\right]_{n_1,n_3} dn_2 + \left[\frac{\partial \mu_1}{\partial n_3}\right]_{n_1,n_2} dn_3 \tag{5}$$

Considering a path along which μ_1 and n_3 are constant, equation (5) reduces to

$$\left[\frac{\partial \mu_1}{\partial n_2}\right]_{n_1,n_3} = -\left[\frac{\partial \mu_1}{\partial n_1}\right]_{n_2,n_3}\left[\frac{\partial n_1}{\partial n_2}\right]_{\mu_1,n_3} \cdot \qquad (6)$$

Also from partial differentials

$$\left[\frac{\partial \mu_2}{\partial n_1}\right]_{n_2,n_3} = \left[\frac{\partial \mu_2}{\partial \mu_1}\right]_{n_2,n_3}\left[\frac{\partial \mu_1}{\partial n_1}\right]_{n_2,n_3}. \qquad (7)$$

Substituting right hand sides of (6) and (7) into (4) gives

$$\left[\frac{\partial \mu_2}{\partial \mu_1}\right]_{n_2,n_3}\left[\frac{\partial \mu_1}{\partial n_1}\right]_{n_2,n_3} = -\left[\frac{\partial \mu_1}{\partial n_1}\right]_{n_2,n_3}\left[\frac{\partial n_1}{\partial n_2}\right]_{\mu_1,n_3}$$

or, after simplifying

$$\left[\frac{\partial \mu_2}{\partial \mu_1}\right]_{n_2,n_3} = -\left[\frac{\partial n_1}{\partial n_2}\right]_{\mu_1,n_3} \cdot \qquad (8)$$

Equation (8) can conviently be expressed in terms of activities by substituting $d\mu_i = d\log_{10} a_i$, since $d\mu_i = RTd\ln a_i$ and the constant 2.303 RT cancels out of the equation. Hence,

$$\left[\frac{\partial \log a_2}{\partial \log a_1}\right]_{n_2,n_3} = -\left[\frac{\partial n_1}{\partial n_2}\right]_{a_1,n_3} \cdot \qquad (9)$$

Equation (9) can be integrated in a one phase field along a path of constant n_2 and n_3 , which means a compositional path of constant n_2/n_3 ratio, i.e., a straight line radiating from the corner corresponding to pure component 1. Upon integration of equation (9)

$$\log a^{II}_2 = \left\{ \log a^{I}_2 - \int_{\log a^{I}_1}^{\log a^{II}_1} \left[\frac{\partial n_1}{\partial n_2}\right]_{a_1, n_3} d\log a_1 \right\}_{n_2/n_3} . \qquad (10)$$

This integration can be performed along the path I-II of Figure 26 to evaluate $\log a^{II}_2$ when $\log a^{I}_2$ is known at the starting point and when experimental data on a_1 are sufficiently complete to permit the evaluation of the partial derivative $\left[\frac{\partial n_1}{\partial n_2}\right]_{a_1, n_3}$ as a function of $\log a_1$ along the entire path of integration.

The quantity $\left[\frac{\partial n_1}{\partial n_2}\right]_{a_1, n_3}$ appearing on the right hand side of equation (10) is the direction of the tangent to the iso-activity curve at a given point. It represents the composition of a binary mixture of 1 and 2, expressed as the ratio of moles of component 1 to moles of component 2, which can be added to the system without changing the activity of component 1. Figure 26(a) illustrates the graphical determination of $\left[\frac{\partial n_1}{\partial n_2}\right]_{a_1, n_3}$ for a given point P in the path I-II. The experimental data on a_1 are plotted on the composition triangle in the form of iso-activity curves along which a_1 is constant. Then, at P a tangent is drawn to the iso-activity curve and is extended to intersect the 1-2 side of the triangle. The point of intersection T, called the tangent-intercept, is $\left[\frac{\partial n_1}{\partial n_2}\right]_{a_1, n_3}$ for point P as read from composition scale along 1-2 and converted to a mole ratio

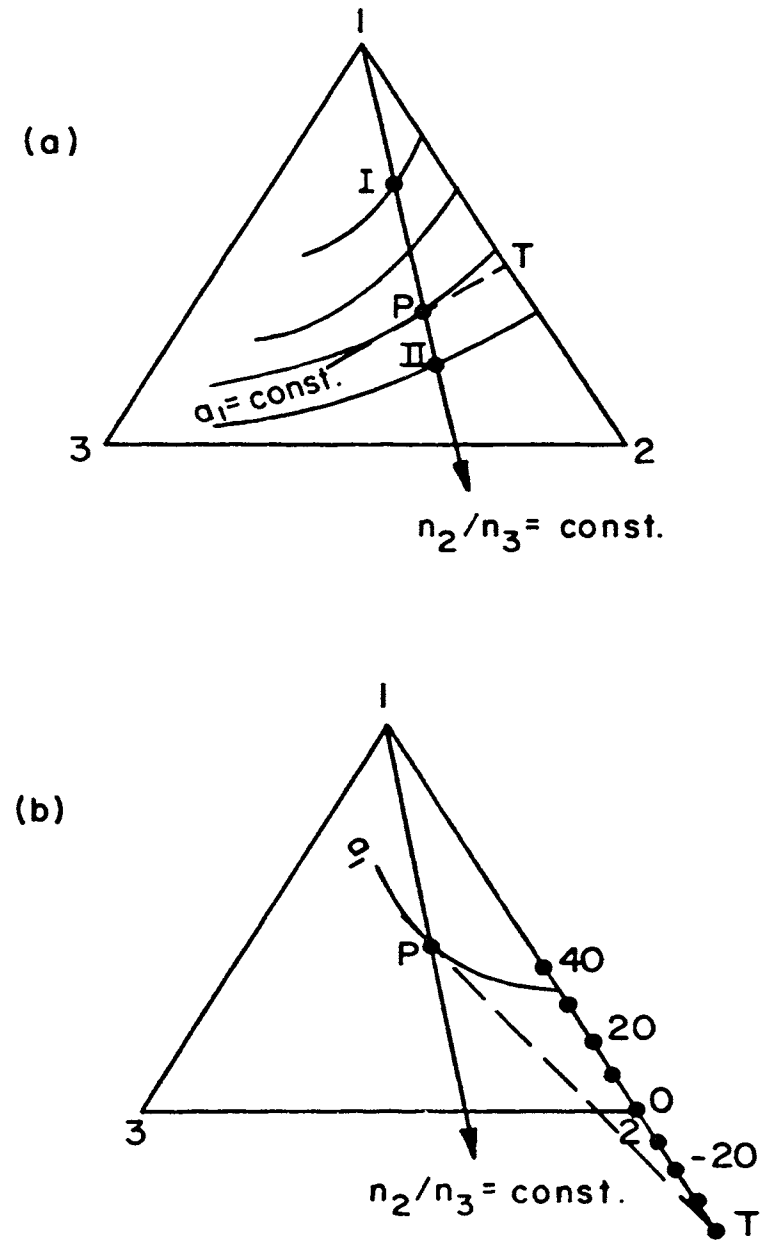

Figure 26. Idealized Composition Triangle Showing the Construction of (a) Positive Tangent-Intercepts, and (b) Negative Tangent-Intercepts (T).

of 1 to 2. In making a complete Gibbs-Duhem integration along a path such as I-II in Figure 26(a) the tangent-intercept procedure must be repeated at a sufficient number of points along I-II to establish the curve of $\left[\frac{\partial n_1}{\partial n_2}\right]_{a_1,n_3}$ against $\log a_1$. The integral in equation (10) is the area under this curve as $\log a_1$ varies from $\log a_1^{I}$ to $\log a_1^{II}$. For negative values of $\left[\frac{\partial n_1}{\partial n_2}\right]_{a_1,n_3}$ the intercept falls on an extension of the 1-2 side of the composition triangle as shown in Figure 26(b). Thus, the determination of negative tangent-intercepts requires the linear extension of the weight percent scales either in a positive direction above 100% or in a negative direction below 0%.

For the activities of the third component an equation of the same form as (10) can be derived simply by interchanging the relative roles of the three components in the derivation. Hence,

$$\log a_3^{II} = \left\{ \log a_3^{I} - \int_{\log a_1^{I}}^{\log a_1^{II}} \left[\frac{\partial n_1}{\partial n_3}\right]_{a_1,n_2} d\log a_1 \right\}_{n_2/n_3} . \qquad (11)$$

That is, the integration to determine $\log a_3^{II}$ is just the same as that to determine $\log a_2^{II}$ except that the tangent intercept T is measured on the 1-3 side of the triangle instead of on the 1-2 side. Equations (10) and (11) derived by Schuhmann's method are usually referred to as Gibbs-Schuhmann equations.

$CaO-FeO-Fe_2O_3$ SYSTEM

Equations (10) and (11) were applied to calculate the activities in that system at 1450°C and 1550°C. The results are presented in Tables XIII and XIV of Appendix III, together with the measured tangent intercepts.

Application of Gibbs-Schuhmann Equations

In order to apply equations (10) and (11) to the $CaO-FeO-Fe_2O_3$ system the activity of one of these components must be known. However, the only activity which is known from the experimental data is the activity or the partial pressure of oxygen of the gas phase in equilibrium with the melt. The activity of oxygen in the melt can be defined as the square root of Po_2. In order to use oxygen as one component the composition of the melts should be converted to the CaO, Fe, and O basis. Oxygen exclusive of that contained in CaO becomes component 1 in equations (10) and (11). The standard state for oxygen was chosen as 1 atm. For iron activities equation (10) reads:

$$\log a_{Fe}^{II} = \left\{ \log a_{Fe}^{I} - \int_{\log a_O^I}^{\log a_O^{II}} \left[\frac{\partial n_O}{\partial n_{Fe}} \right]_{a_O, n_{CaO}} d\log a_O \right\}_{n_{Fe}/n_{CaO}} \quad . \quad (12)$$

Experimental data given in terms of weight percent CaO, FeO, and Fe_2O_3 in Tables II and III of Appendix II were

recalculated to represent compositions in the CaO-Fe-O composition triangle. The iso-oxygen activities were then drawn as shown schematically in Figure 27. For several constant Fe/CaO ratios, values of $\left[\frac{\partial n_O}{\partial n_{Fe}}\right]_{a_O, n_{CaO}}$ were evaluated by measuring the tangent-intercepts along the Fe-O side of the diagram. The standard state for iron was chosen by making the activity of iron equal to unity along the metallic iron + liquid oxide phase boundary at the oxygen activity a_O^I in equilibrium with the melt. Therefore $\log a_{Fe}^I = 0$. Hence, the integration in equation (12) could be performed within the composition range OAB of Figure 27 where the sections along constant Fe/CaO ratios terminate at the metallic iron saturation boundary. The activities of "FeO" could then be calculated from the iron and oxygen activities by using the relationship

$$a_{"FeO"} = K \cdot (a_{Fe}) \cdot (a_O) \quad . \tag{13}$$

The standard state for "FeO" was chosen as pure liquid iron oxide in equilibrium with the metallic iron at both temperatures. For this standard state the oxygen activity is 2.23×10^{-5} at 1450°C and 5.35×10^{-5} at 1550°C[2]. After these values were introduced into equation (13) the proportionality constant K was calculated to be 4.50×10^4 at 1450°C and 1.87×10^4 at 1550°C. By using equation (13) with

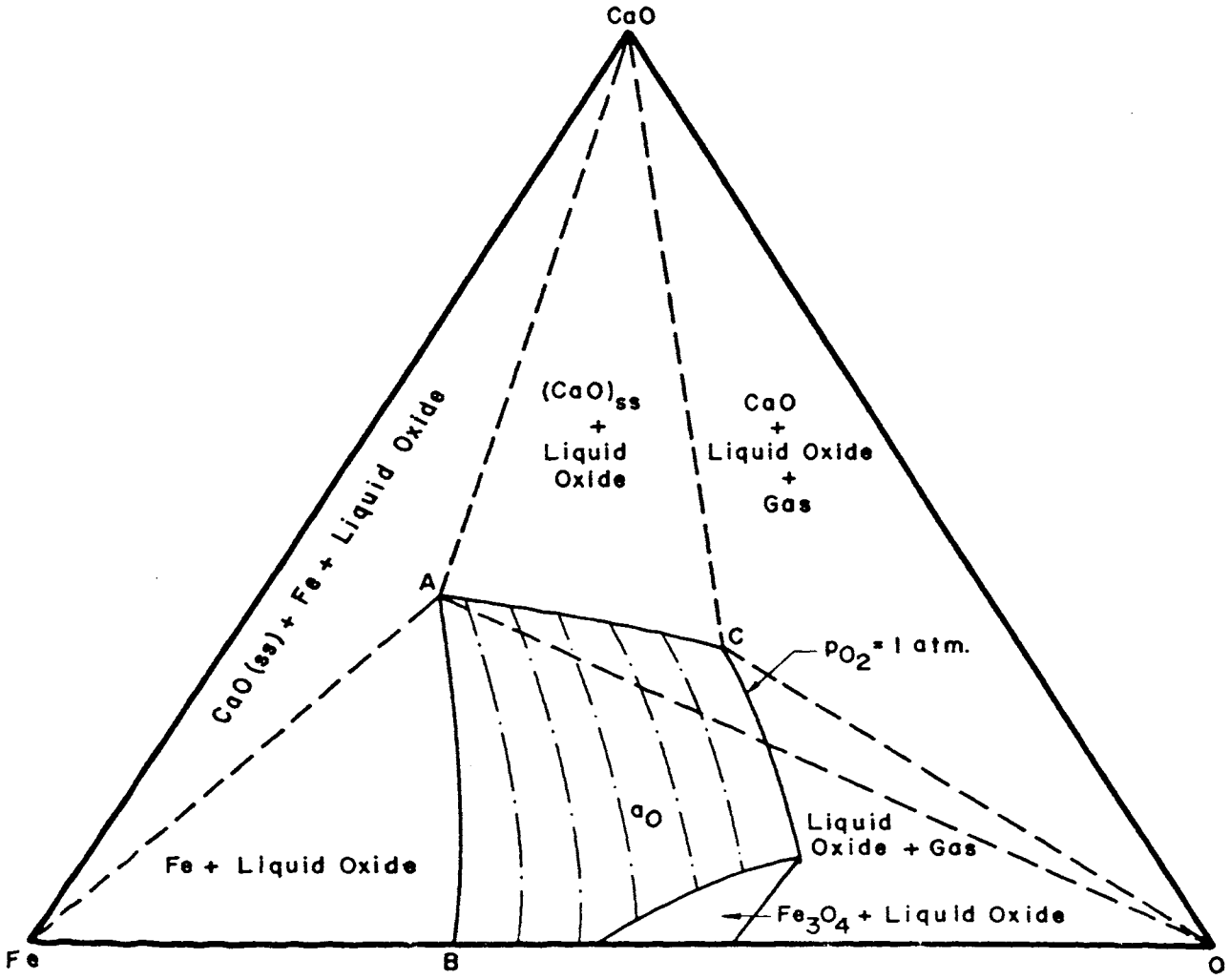

Figure 27. Schematic CaO-Fe-O Composition Triangle Showing the Iso-Oxygen Activity Curves.

appropriate K values "FeO" activities were calculated in the OAB field at both temperatures.

Equation (11) for CaO activities can be written as:

$$\log a_{CaO}^{II} = \left\{ \log a_{CaO}^{I} - \int_{\log a_O^I}^{\log a_O^{II}} \left[\frac{\partial n_O}{\partial n_{CaO}} \right]_{a_O, n_{Fe}} d\log a_O \right\}_{n_{Fe}/n_{CaO}} \quad . \quad (14)$$

The standard state for lime was chosen as pure solid CaO neglecting the small "FeO" solubility. Hence, $\log a_{CaO}^{I} = 0$, at the CaO(ss) saturation boundary. Equation (14) was used only once to determine the $\log a_{CaO}^{II}$ values along the line OA. Since $d\log a_O = 0$ along an iso-oxygen activity curve, the rest of the CaO activities could be calculated from a relatively simple binary Gibbs-Duhem integration (see equation 1) of the form:

$$\log a_{CaO} = \left\{ \log a_{CaO}^{*} - \int_{\log a_{Fe}^{*}}^{\log a_{Fe}} \left(\frac{n_{Fe}}{n_{CaO}} \right) d\log a_{Fe} \right\}_{a_O} \quad (15)$$

where $\log a_{CaO}^{*}$ and a_{Fe}^{*} values were equivalent to $\log a_{CaO}^{II}$ and a_{Fe}^{II} values obtained by integrations of equations (12) and (14) along OA.

Results of Activity Calculations

The results given in Tables XIII and XIV of Appendix III are summarized in the form of activity-composition diagrams as shown in Figures 28 and 29, at 1450°C and 1550°C respectively. Heavy lines outline the region of stability of the 100% liquid field from Po_2 = 1 atm. to the metallic iron + liquid oxide phase boundary. Light solid lines are the "FeO" activities, dashed lines represent the CaO activities. Fe_2O_3 activities were not calculated. Iso-activity curves were constructed by re-expressing the CaO-Fe-O compositions in terms of weight % CaO, FeO, Fe_2O_3 and transforming the "FeO" and CaO activities into that system.

Discussion of Activity-Composition Diagrams

Figures 28 and 29 show that at both temperatures CaO activities decrease rapidly with decreasing CaO content, following an approximately parallel course to the CaO(ss) boundary. The "FeO" activities, on the other hand, present a complex nature. In both diagrams an apparent symmetry is observed with respect to an imaginary line joining the point A and the dicalcium ferrite composition. In dealing with ionic nature of metallurgical slags, Chipman and Chang[49] have postulated the existence of Ca^{++} and $Fe_2O_5^{4-}$ ions in melts of the systems formed by calcium and iron oxides. They have tried to explain the shape of "FeO" activity curves by assuming that the local arrangements of the above

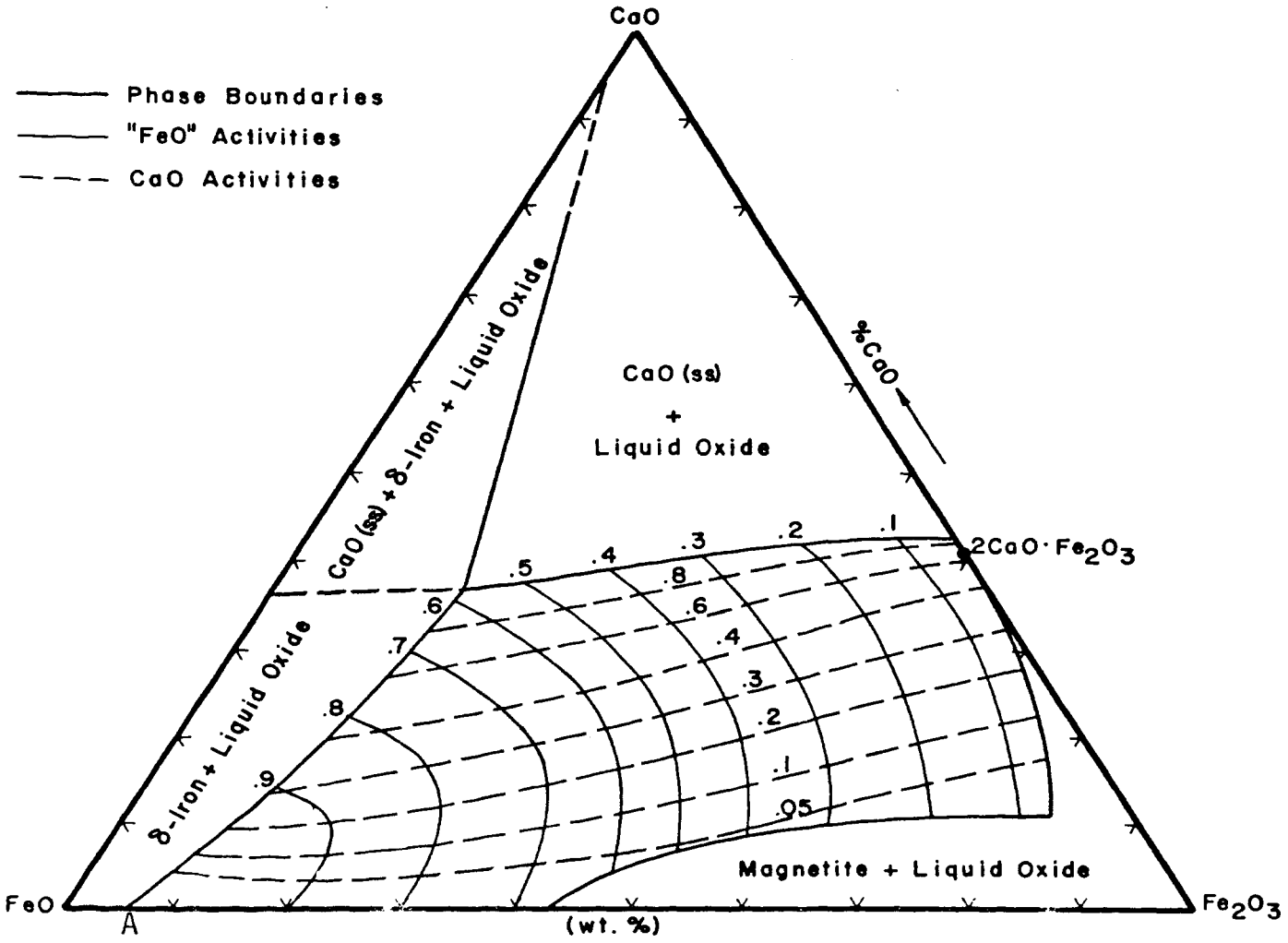

Figure 28. Activities of "FeO" and CaO in Melts of the System $CaO-FeO-Fe_2O_3$ at 1450°C.

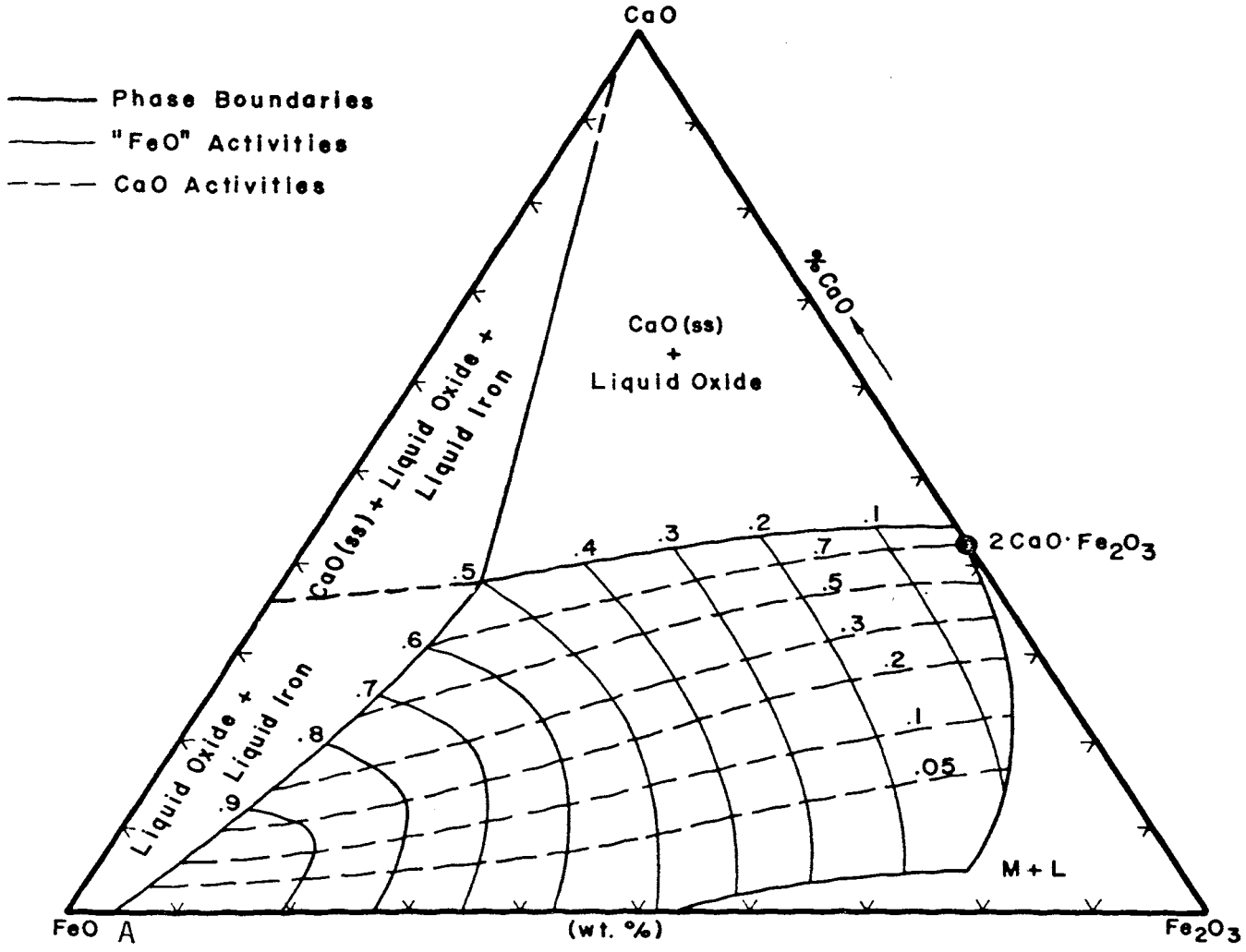

Figure 29. Activities of "FeO" and CaO in Melts of the System $CaO-FeO-Fe_2O_3$ at 1550°C.

ions approaching the gross $2CaO \cdot Fe_2O_3$ composition was energetically favored in preference to a completely statistical distribution. The existence of such ions, however, is not yet experimentally verified.

The effect of temperature on "FeO" activities is shown in Figure 30 at two arbitrary levels of lime contents. "FeO" activities are lower at 1550°C than at 1450°C. Similar diagrams constructed for CaO activities have shown that the CaO activities are also lower at 1550°C. These observations indicate that in addition to simple Ca^{2+} - $Fe_2O_5^{4-}$ groupings some complex interactions among the Fe^{2+}, $O^{=}$, Ca^{2+}, and Fe^{3+} ions may be taking place. Since a complete $CaO-FeO-Fe_2O_3$ phase diagram is unavailable at the present, no estimations can be made about the nature and the strength of such complex interactions.

The accuracy of activity calculations are affected by a number of factors, which can be classified as follows:

1.) Errors introduced during the determination of tangent intercepts.

2.) Errors in the subsequent Gibbs-Duhem graphical integrations.

3.) Cumulative experimental errors in the control of Po_2, and chemical analyses.

The first source of error was predominant in the composition field AOC of Figure 27. Erratic CaO activities would result from faulty measurements in that small field due to the inevitable uncertainties involved in drawing tangents to

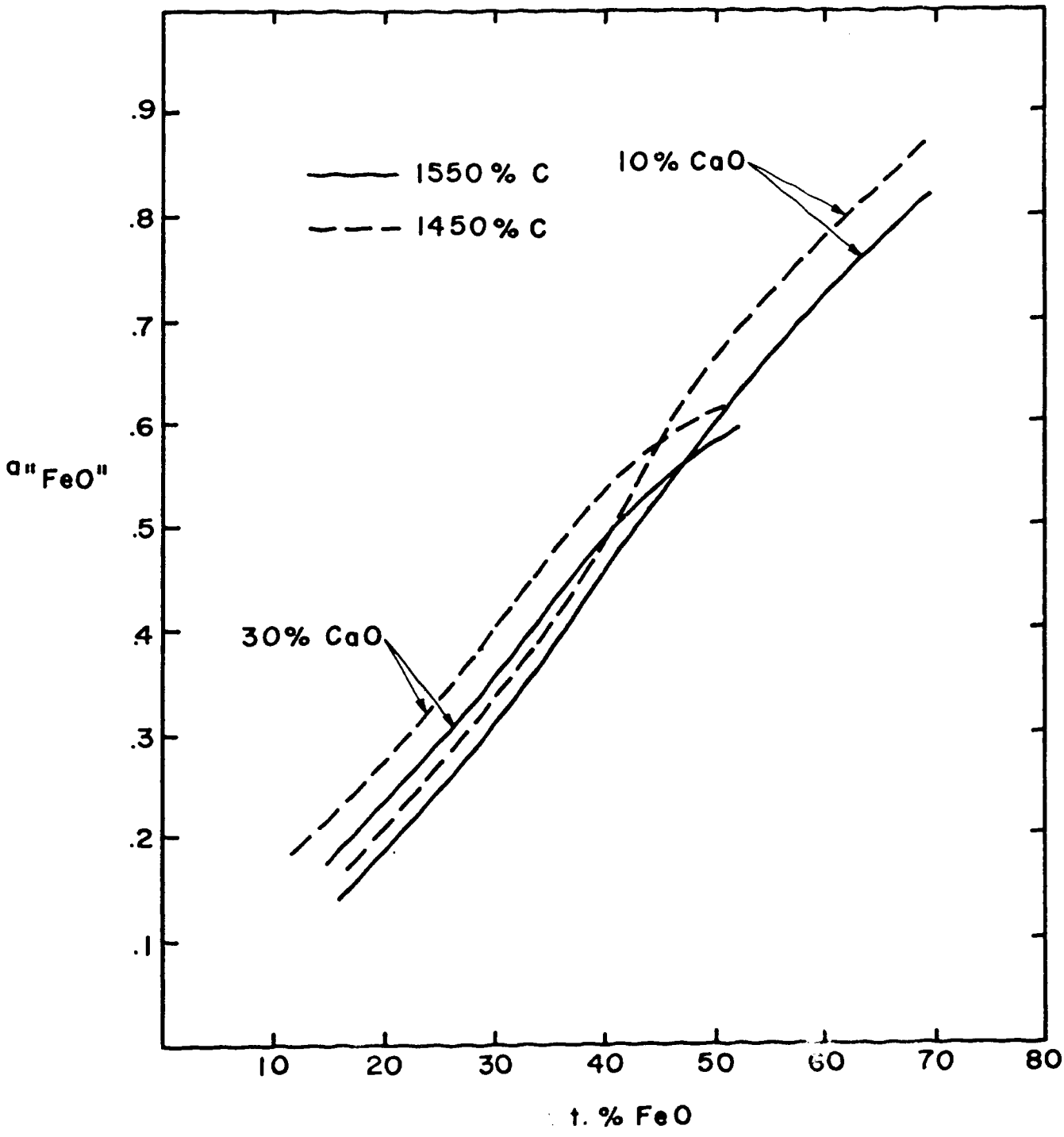

Figure 30. Effect of Temperature on "FeO" Activities of $CaO-FeO-Fe_2O_3$ Melts at Two Levels of CaO.

very small portions of iso-oxygen activity curves. Therefore, no measurements were made in that area above the line OA, at either temperature. The second source of error could be minimized by carefully counting the squares under Gibbs-Duhem curves; this source was estimated to contribute least to the error since in most cases smooth curves have resulted, both for CaO and Fe, which could be integrated quite accurately.

For the third source of error the accuracy of calculated iron activities, hence those of "FeO", could be checked along the magnetite saturation boundary. The standard free energy change of the following reaction was obtained from thermodynamic tables[50], at 1450°C:

$$3Fe(s) + 2O_2(g) \rightarrow Fe_3O_4(s) \qquad (16)$$
$$\Delta F^\circ = -138.2\ (\pm 1.2)\ \text{kcal/mole}$$

for which $\log K_{16} = \log a_{Fe_3O_4} - 3\log a_{Fe} - 2\log Po_2 = 17.52$.

Assuming that $a_{Fe_3O_4} = 1$ at the magnetite + liquid oxide boundary, iron activities could be calculated from $\log K_{16}$ with the known Po_2 values used at 1450°C of this work. Table XV summarizes the iron activities obtained by Gibbs-Schuhmann's method, and those by using equation (16). In the last row the ΔF° values calculated from integrated Fe activities are given.

TABLE XV

COMPARISON OF IRON ACTIVITIES

Po_2	10°	$10^{-2.9}$	$10^{-3.7}$	$10^{-5.0}$
$\log a_{Fe}$ (from (16))	-5.803	-3.870	-3.340	-2.470
$\log a_{Fe}$ (integration)	-5.750	-3.843	-3.322	-2.437
ΔF° kcal/mole	-135.8	-136.4	-136.8	-136.2

The differences between the tabulated value -138.2 kcal/mole and the calculated values at $Po_2 = 10^{\circ}$ and $10^{-2.9}$ may be explained by the excess oxygen dissolved in magnetite under these conditions. For the two lower Po_2 the differences of 0.2 and 0.8 kcal/mole from the lower limit are probably due to cumulative errors involving the control of Po_2, chemical analyses, and the location of magnetite boundary. Other data for Fe_3O_4[9] gives -137.4±2.0 kcal/mole for ΔF° of reaction (16).

In the high-lime region another check could be made by considering the following reaction:

$$2CaO(s) + Fe_2O_3(s) = 2CaO \cdot Fe_2O_3(s) \qquad (17)$$

for which $\log K_{17} = -2\log a_{CaO} - \log a_{Fe_2O_3}$

by assuming that the activity of dicalcium ferrite is unity at the $2CaO \cdot Fe_2O_3$ point. Considering also,

$$2FeO(l) + \tfrac{1}{2}O_2(g) = Fe_2O_3(s) \qquad (18)$$

$$\log K_{18} = \log a_{Fe_2O_3} - 2\log a''_{FeO}{}'' - \tfrac{1}{2}\log Po_2 \ .$$

$\log K_{18}$ was obtained from thermodynamic tables of Coughlin[50] as 2.32±.1 at 1450°C. At the dicalcium ferrite point $Po_2 = 1$, and $a_{FeO} = 0.012$, hence $\log a_{Fe_2O_3} = -1.64$ assuming that the standard state of Fe_2O_3 is pure solid hematite. At the same point the CaO activity at 1450°C was read as 0.65 from the activity diagram. Substituting these values back into $\log K_{17}$ gave:

$$\log K_{17} = 2.014 \ .$$

Using this value the standard free energy of formation of dicalcium ferrite from the oxides was calculated to be:

$$\Delta F^\circ = -4.575\ T\ \log K_{17} = -15.9 \text{ kcal/mole} \ .$$

Koehler, Barany, and Kelley[51] have measured the standard free energy of formation of this compound from its oxides and a value of -16.7±1.0 kcal/mole could be obtained from their data at 1450°C. The calculated $\Delta F^\circ = -15.9$ kcal/mole is in good agreement with the lower limit of their values.

The "FeO" activity-composition relations obtained at 1550°C are in good agreement with the "FeO" activities of both Larson and Chipman[24] and Turkdogan[25]. The CaO

activities at high-lime contents are in better agreement with those of Turkdogan; their shapes, however, resemble Chipman's curves. At low-lime contents, the CaO activities of Turkdogan are considerably higher than in the present work and that of Chipman. Both the magnetite and CaO(ss) boundaries are very similar to those of Turkdogan.

Method of Calculating Activities in a Quaternary System

Calculating the activities in a system of four or more components has been described in detail by Gokcen[48]. In addition to providing a new method, he has shown that the extensions of known ternary methods permit calculations in multi-component systems. Again, the method of Schuhmann, as modified for quaternary systems, was found to fit best to the experimental data. A short description of the derivations is given below; it will be assumed that the activities of component 1 are known, and those of 2, 3, and 4 will be calculated.

Component 2

The principal form of Gibbs-Duhem equation for a system of four components is:

$$n_1 d\mu_1 + n_2 d\mu_2 + n_3 d\mu_3 + n_4 d\mu_4 = 0 \qquad (19)$$

where n_1, n_2, n_3, and n_4 are the moles, and μ_1, μ_2, μ_3, and μ_4 are the corresponding chemical potentials of components 1, 2, 3, and 4 respectively. By definition,

$$\mu_1 = \left[\frac{\partial F}{\partial n_1}\right]_{n_2,n_3,n_4} \text{ and } \mu_2 = \left[\frac{\partial F}{\partial n_2}\right]_{n_1,n_3,n_4} . \qquad (20)$$

After differentiating equation (20),

$$\left[\frac{\partial \mu_2}{\partial n_1}\right]_{n_2,n_3,n_4} = \left[\frac{\partial^2 F}{\partial n_1 \partial n_2}\right]_{n_3,n_4}$$

and

$$\left[\frac{\partial \mu_1}{\partial n_2}\right]_{n_1,n_3,n_4} = \left[\frac{\partial^2 F}{\partial n_2 \partial n_1}\right]_{n_3,n_4} .$$

Since the order of differentiation is immaterial, the left hand sides of the above equations are the same; hence,

$$\left[\frac{\partial \mu_2}{\partial n_1}\right]_{n_2,n_3,n_4} = \left[\frac{\partial \mu_1}{\partial n_2}\right]_{n_1,n_3,n_4} . \qquad (21)$$

From the theory of partial differentials:

$$\left[\frac{\partial \mu_1}{\partial n_2}\right]_{n_1,n_3,n_4} = -\left[\frac{\partial \mu_1}{\partial n_1}\right]_{n_2,n_3,n_4}\left[\frac{\partial n_1}{\partial n_2}\right]_{\mu_1,n_3,n_4}$$

and

$$\left[\frac{\partial \mu_2}{\partial n_1}\right]_{n_2,n_3,n_4} = \left[\frac{\partial \mu_2}{\partial \mu_1}\right]_{n_2,n_3,n_4}\left[\frac{\partial \mu_1}{\partial n_1}\right]_{n_2,n_3,n_4}$$

Therefore,

$$\left[\frac{\partial \mu_2}{\partial \mu_1}\right]_{n_2/n_4, n_3/n_4} = -\left[\frac{\partial n_1}{\partial n_2}\right]_{\mu_1, n_3/n_4} . \qquad (22)$$

This equation is similar in form to that of equation (8) for ternary systems. Substituting $d\mu_i = RTd\log a_i$, we obtain, upon integration of (22),

$$\log a^{II}_2 = \left\{\log a^{I}_2 - \int_{\log a^{I}_1}^{\log a^{II}_1} \left[\frac{\partial n_1}{\partial n_2}\right]_{a_1, n_3/n_4} d\log a_1\right\}_{n_2/n_4, n_3/n_4} . \qquad (23)$$

The tetrahedron in Figure 31(a), represents the quaternary system in which the compositions are expressed in terms of weight %. The evaluation of tangent-intercepts $(\partial n_1/\partial n_2)\ a_1, n_3/n_4$ calls for construction of a_1 curves in a plane of constant n_3/n_4. In the tetrahedron the constant n_3/n_4 is the 1-2-W plane, since n_3/n_4 is constant along the lines 1-W and 2-W of triangles 1-3-4, and 2-3-4. Along any line 1-V, $(n_3+n_4)/n_2$ hence n_2/n_4 is constant. In a quaternary system, constant a_1 is represented by an appropriate surface in the tetrahedron; the intersections of 1-2-W with the constant a_1-surfaces are represented by the constant a_1-curves. As shown in Figure 31(b) the intercept of the tangent P -A with the edge 1-2 yields $(\partial n_1/\partial n_2)$ values. The

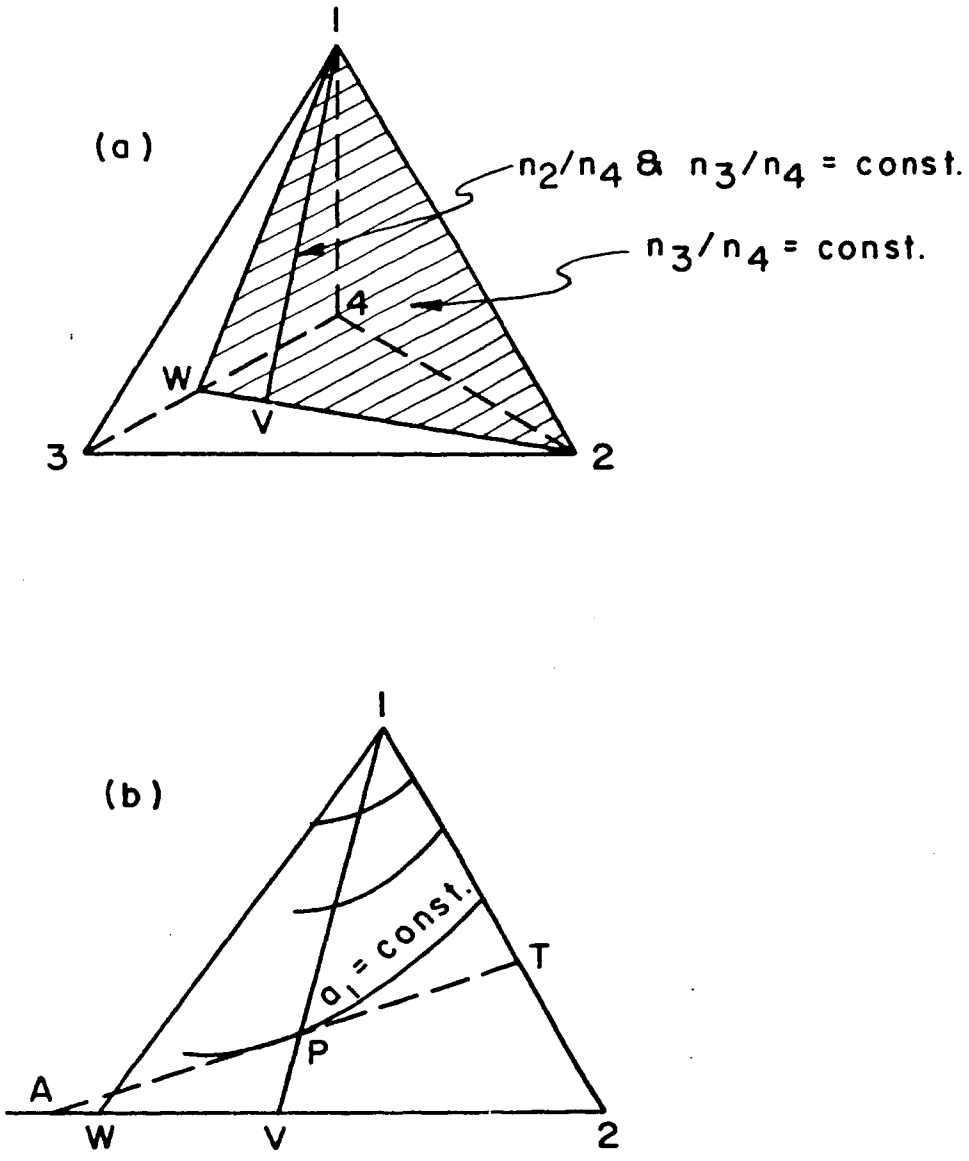

Figure 31. Idealized Composition Tetrahedron (a) Showing the Plane of Operation for Equation (23), and (b) the Construction of Tangent-Intercepts in that Plane.

right hand side integral of equation (23) may thus be evaluated, graphically, from a plot of these values against $\log a_1$.

Component 3

For the activities of component 3 equation (23) assumes the form,

$$\log a^{II}_3 = \left\{ \log a^{I}_3 - \int_{\log a^{I}_1}^{\log a^{II}_1} \left[\frac{\partial n_1}{\partial n_3}\right]_{a_1, n_3/n_4} d\log a_1 \right\}_{n_3/n_4, n_1/n_4} \quad . \quad (24)$$

Hence the evaluation of $(\partial n_1/\partial n_3)a_1, n_3/n_4$ must be made in a plane containing the edge 1-3 and intersecting 2-4.

Component 4

Once the activities of components 2 and 3 are determined as described above, those of the fourth component can be calculated from equation (19). Considering a path along which, say, a_3 is constant equation (19), in terms of activities, reduces to:

$$n_1 \, d\log a_1 + n_2 \, d\log a_2 + n_4 \, d\log a_4 = 0 \qquad (25)$$

or

$$d\log a_4 = -n_1/n_4 \, d\log a_1 - n_2/n_4 \, d\log a_2 \, .$$

Upon integrating this equation

$$\log a^{II}_4 = \left[\log a^{I}_4 - \int_{\log a^{I}_1}^{\log a^{II}_1} \frac{n_1}{n_4} d\log a_1 - \int_{\log a^{I}_2}^{\log a^{II}_2} \frac{n_2}{n_4} d\log a_2 \right]_{a_3} . \quad (26)$$

Obviously, for the evaluations of activities of component 2, 3, and 4, the terms $\log a^{I}_2$, $\log a^{I}_3$, and $\log a^{I}_4$ must be known at the starting points of integrations corresponding to the lower limit indicated by $\log a^{I}_1$.

$CaO-FeO-Fe_2O_3-SiO_2$ SYSTEM

Equations (23), (24) and (26) were applied to calculate the activities in that system at 1450°C and 1550°C. The results are presented in Tables XVI and XVII of Appendix IV.

Application of Gibbs-Schuhmann Equations

For reasons explained in the ternary activity calculations the compositions of $CaO-FeO-Fe_2O_3-SiO_2$ melts had to be recalculated to the $CaO-SiO_2$-Fe-O basis, whereby oxygen exclusive of that contained in CaO and SiO_2 became one component whose activities were experimentally determined in constant silica sections.

In order to calculate the iron activities equation (23) was written as:

$$\log a_{Fe}^{II} = \left\{ \log a_{Fe}^{I} - \int_{\log a_O^I}^{\log a_O^{II}} \left[\frac{\partial n_O}{\partial n_{Fe}}\right]_{a_O, \frac{n_{CaO}}{n_{SiO_2}}} d\log a_O \right\}_{\frac{n_{CaO}}{n_{SiO_2}}, \frac{n_{Fe}}{n_{CaO}}} \quad (27)$$

The iso-oxygen activity curves in several constant $\frac{n_{CaO}}{n_{SiO_2}}$ planes were constructed from the iso-Po_2 curves of constant silica sections. Figure 32(a) schematically shows one such plane where the tangent intercepts, $\left[\frac{\partial n_O}{\partial n_{Fe}}\right]_{a_O}$, were measured along the Fe-O side of the composition triangle Fe-O-(CaO+ SiO_2). These tangent-intercepts were evaluated in the field OAC of Figure 32(a) for several constant Fe/CaO paths originating from the O apex and terminating at the metallic iron saturation boundary AC. The standard states of iron and oxygen were defined the same way as described in the ternary system, thus along the line AC $\log a_{Fe}^{I} = 0$. Therefore, the integration on the right hand side of equation (27) could be performed in the area AOC to calculate the $\log a_{Fe}^{II}$ values.

The "FeO" activities were calculated from the above determined iron activities by using equation (13). The standard state of "FeO" was still chosen as pure liquid iron oxide in equilibrium with metallic iron at both temperatures. Hence, values of K from equation (13) remained the same as those calculated in the ternary system.

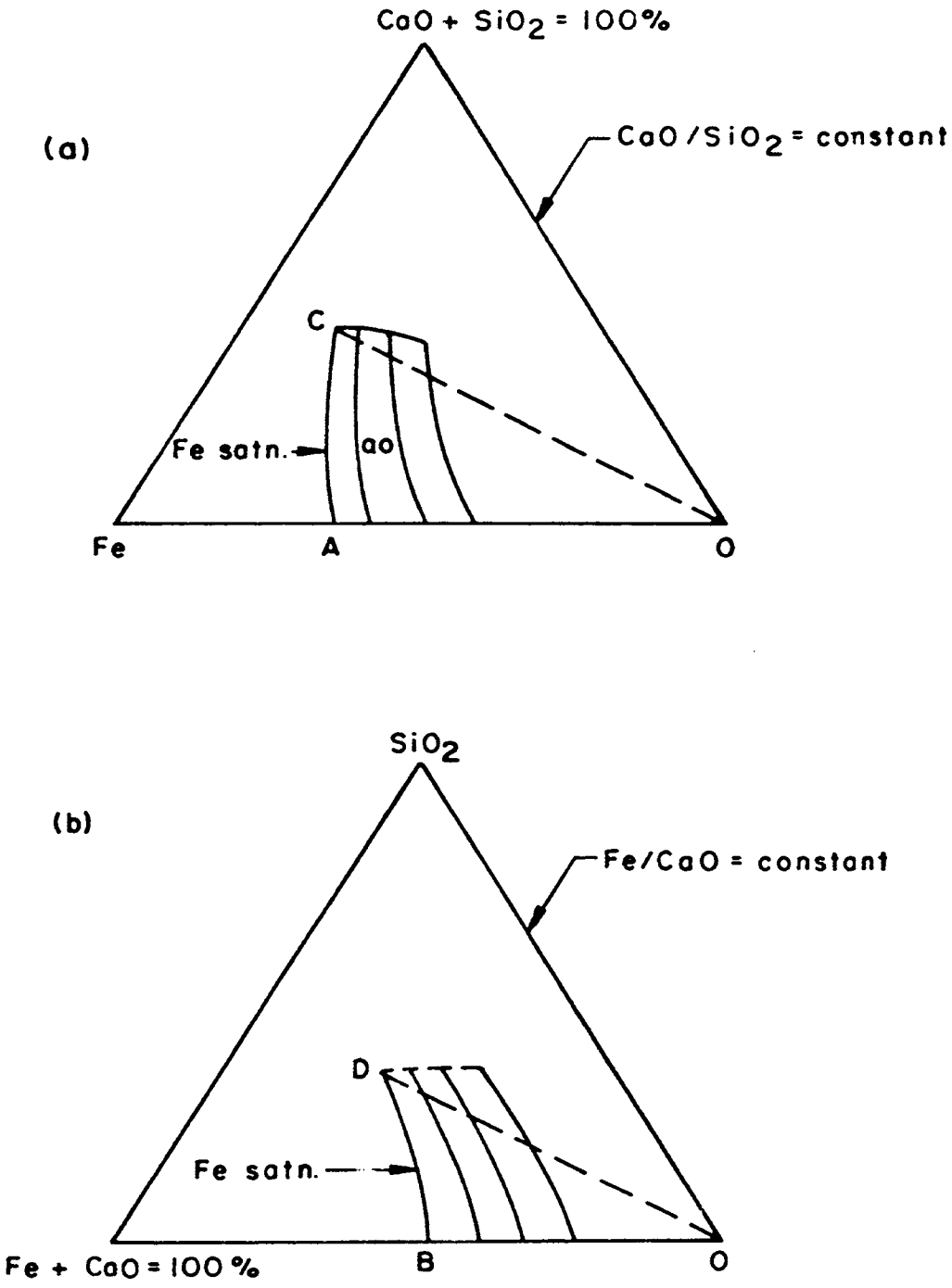

Figure 32. Schematic Diagrams Showing the Iso-Oxygen Activity Curves in (a) Constant $^{n}CaO/^{n}SiO_2$ Planes, and (b) Constant $^{n}Fe/^{n}CaO$ Planes.

For the silica activities equation (24) was rearranged as:

$$\log a^{II}_{SiO_2} = \left\{ \log a^{I}_{SiO_2} - \int_{\log a^{I}_{O}}^{\log a^{II}_{O}} \left[\frac{\partial n_O}{\partial n_{SiO_2}}\right] a_O, \frac{n_{Fe}}{n_{CaO}} \, d\log a_O \right\} \frac{n_{Fe}}{n_{SiO_2}}, \frac{n_{Fe}}{n_{CaO}} \quad (28)$$

The calculation of $\log a^{II}_{SiO_2}$ values were quite similar to that of iron activities, except the iso-oxygen activity curves were constructed in several constant $\frac{n_{Fe}}{n_{CaO}}$ planes, and the tangent-intercepts were measured along the SiO_2-O side of the SiO_2-O-(Fe+CaO) plane which is shown schematically in Figure 32(b). The complete evaluation of $\log a^{II}_{SiO_2}$ depends on a knowledge of $\log a^{I}_{O}$, and $\log a^{I}_{SiO_2}$ values corresponding to the lower limit of integration. Since the integration was carried out along constant Fe/SiO_2 compositional paths terminating at the iron-saturation boundary, the lower limit values were obtained by activity calculations involving the CaO-"FeO"-SiO_2 system in contact with metallic iron, as will be explained later.

The CaO activities were calculated by writing the equation (26) as:

$$\log a^{II}_{CaO} = \left[\log a^{I}_{CaO} - \int_{\log a^{I}_{Fe}}^{\log a^{II}_{Fe}} \frac{n_{Fe}}{n_{CaO}} \, d\log a_{Fe} \right.$$

$$- \int_{\log a_O^I}^{\log a_O^{II}} \frac{n_O}{n_{CaO}} \, d\log a_O \Big]_{a_{SiO_2}} \quad . \qquad (29)$$

In a constant silica section where the compositions were expressed in terms of weight percent CaO, SiO_2, Fe, and O, the lime activities could be calculated along several iso-SiO_2 activity curves by performing the two binary Gibbs-Duhem integrations which appear in the right hand side of equation (29). The standard state of CaO was chosen as pure solid lime. The lower limits of the integrals of (29), and the $\log a_{CaO}^I$ values corresponding to them were evaluated from calculations in the CaO-"FeO"-SiO_2 system in contact with iron, since these limits correspond to the CaO activities at the iron-saturation boundary.

Activities in the CaO-"FeO"-SiO_2 System in Contact with Iron

Complete evaluation of $\log a_i^{II}$ values of equations (27), (28), and (29) depends on an exact knowledge of the starting activities, $\log a_i^I$. The quaternary CaO-SiO_2-Fe-O system could be approximated to the ternary CaO-$\overset{"}{Fe}\overset{"}{O}$-$SiO_2$ system in contact with metallic iron in so far as the $\log a_i^I$ values represented the situation when the activities had to be known along the iron-saturation boundary. For this purpose, in order to plot the compositions in the CaO-$\overset{"}{Fe}\overset{"}{O}$-$SiO_2$ triangle, FeO and Fe_2O_3 were calculated as total FeO, assuming Fe_2O_3

to be equivalent to 2FeO, leaving the total further deficient by the amount of excess oxygen in the ferric oxide. The components CaO, FeO, and SiO_2 were then recalculated to total 100%.

After converting the compositions to mole fractions the "FeO" activities at 1450°C were plotted as shown in Figure 33. The same diagram at 1550°C, shown in Figure 34, could be drawn by extrapolations between the 1450°C "FeO" activities and those of Taylor and Chipman[36] given in Figure 11. The compositions and Po_2 of the points representing the liquid iron + liquid oxide phase boundary tabulated in Table XII of Appendix II were obtained by working back from equation (13) with the extrapolated "FeO" activities and the procedure outlined for the conversion of compositions.

In order to calculate the silica activities two different methods had to be applied. In the composition field X-Y-FeO_t of Figures 33 and 34 the Gibbs-Schuhmann equation (10) was written as:

$$\log a^{I}_{SiO_2} = \left\{ \log a^{*}_{SiO_2} - \int_{a^{*}_{"FeO"}}^{a^{I}_{"FeO"}} \left[\frac{\partial n_{FeO}}{\partial n_{SiO_2}} \right] d\log a_{"FeO"} \right\}_{n_{CaO}/n_{SiO_2}} \quad . \quad (30)$$

Choosing the standard state of silica as pure solid SiO_2, $\log a^{*}_{SiO_2} = 0$ at the silica saturation boundary. Hence $\log a^{I}_{SiO_2}$ values were calculated by graphical integration of (30) from the known "FeO" activities and the tangent-

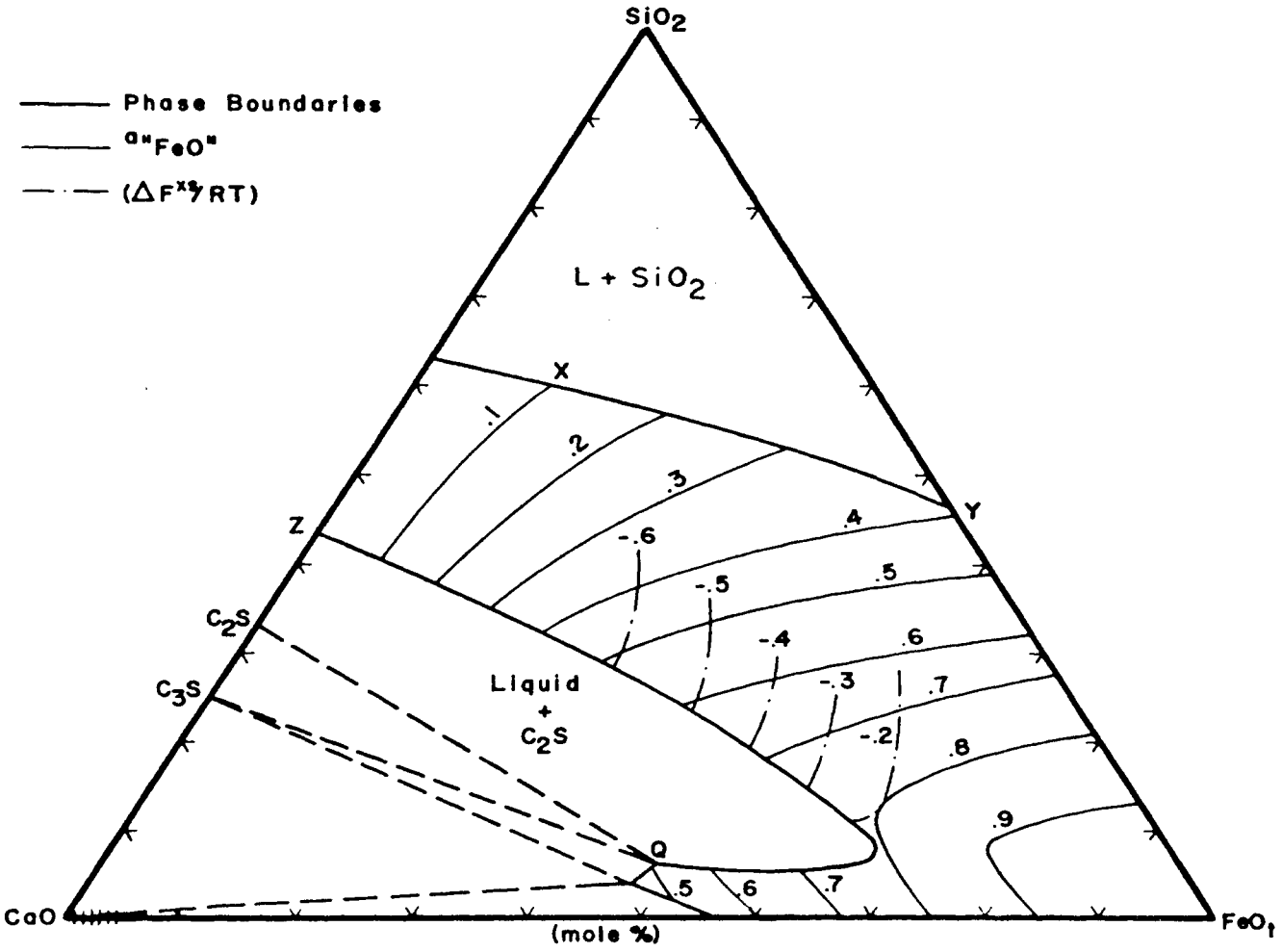

Figure 33. "FeO" Activities and the Excess Molar Free Energies of Mixing in Melts of the System CaO-"FeO"-SiO_2 at 1450°C.

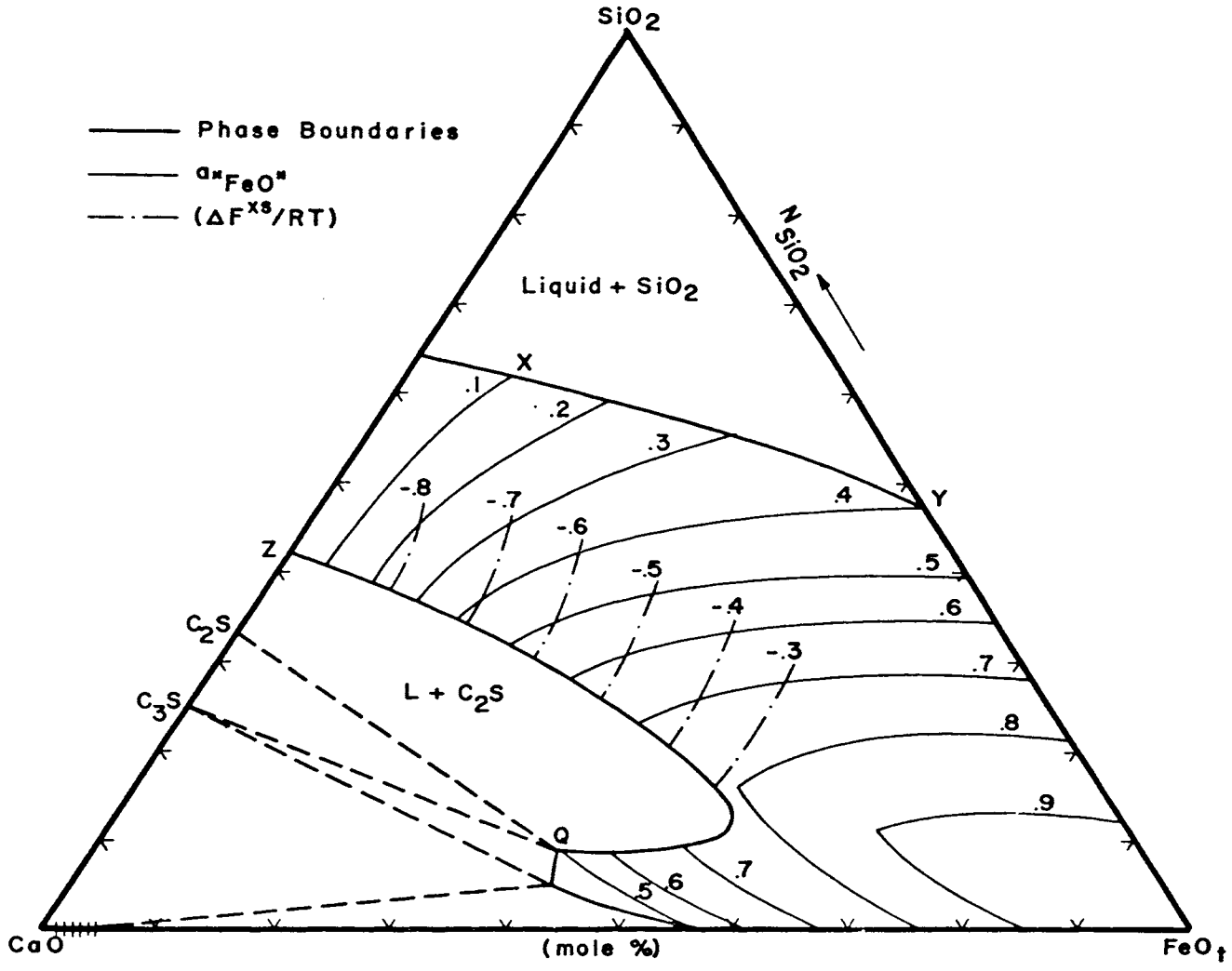

Figure 34. "FeO" Activities and the Excess Molar Free Energies of Mixing in Melts of the System CaO-"FeO"-SiO_2 at 1550°C.

intercepts measured along the FeO_t-SiO_2 side of the diagrams at several constant CaO/SiO_2 paths. For reasons obvious from Figures 33 and 34 Schuhmann's method could not be used below the line X-FeO_t. However, the extension of the iso-silica activities in the range $a_{SiO_2} = 1.0$ to $a_{SiO_2} = .4$ resulted in silica activities which were in good agreement with those of Taylor and his coworkers[16,17] along the CaO-SiO_2 join. Therefore, the relations reproduced in Figure 5 were assumed to be correct at both temperatures, and silica activity curves in the range $a_{SiO_2} = .1$ to $a_{SiO_2} = .4$ were drawn by joining the calculated points with those at the CaO-SiO_2 binary, as shown in Figures 35 and 36.

For calculating the silica activities lower than $a_{SiO_2} = .1$, Darken's method was used. Darken[44] has derived an equation to determine the ternary excess free energies in a molten system, which for the present case could be written as:

$$\Delta F^{xs}_t = RT(1-N_{FeO})\left[\Delta F^{xs}_b - \int_0^{N_{FeO}} \frac{\ln\gamma FeO}{(1-N_{FeO})^2} dN_{FeO}\right]_{N_{CaO}/N_{SiO_2}} \quad (31)$$

where ΔF^{xs}_t = ternary excess free energies,

ΔF^{xs}_b = excess free energies along the CaO-SiO_2 binary,

N_{FeO} = mole fraction of "FeO",

γ_{FeO} = activity coefficient of "FeO".

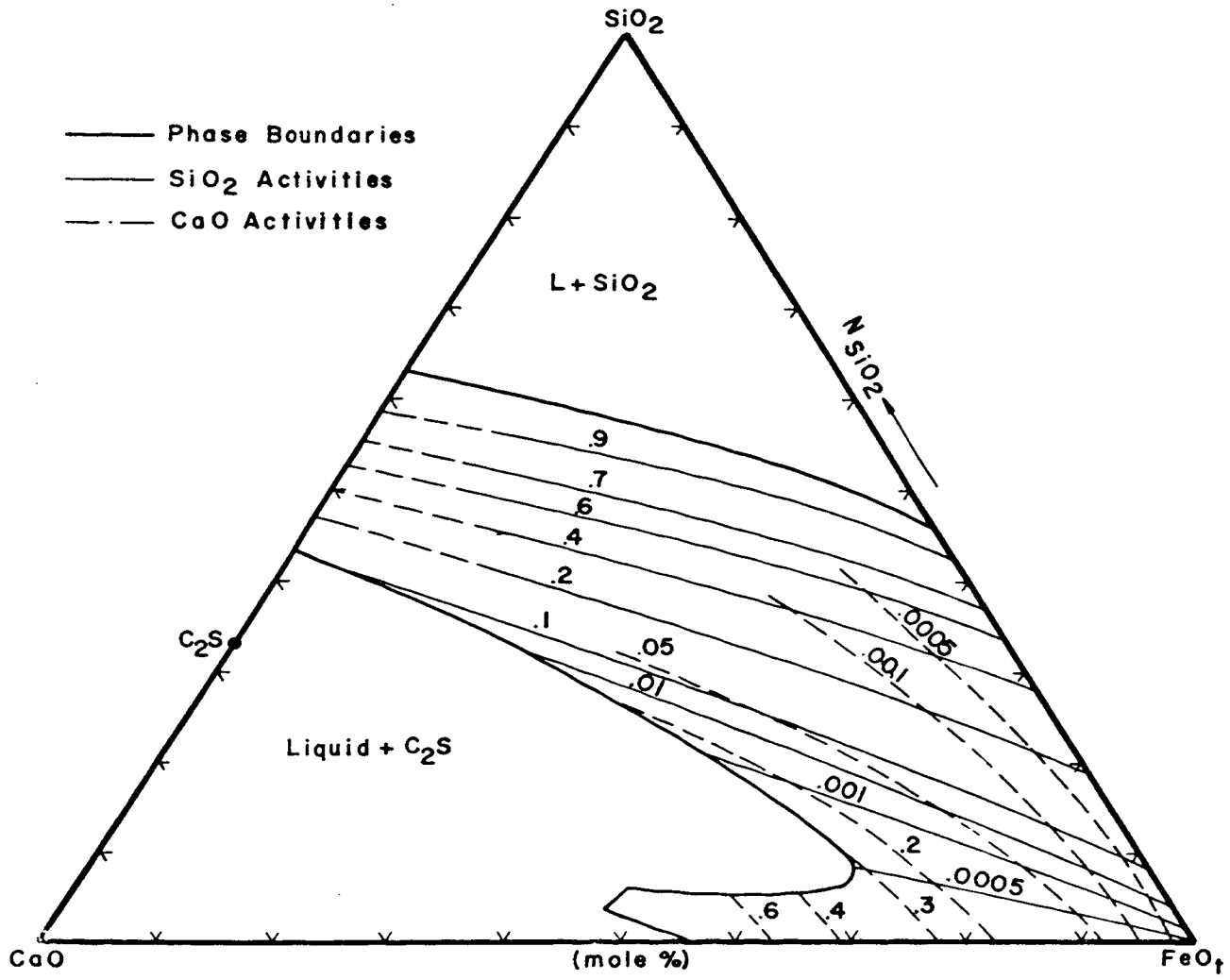

Figure 35. CaO and SiO_2 Activities in Melts of the System CaO-"FeO"-SiO_2 at 1450°C.

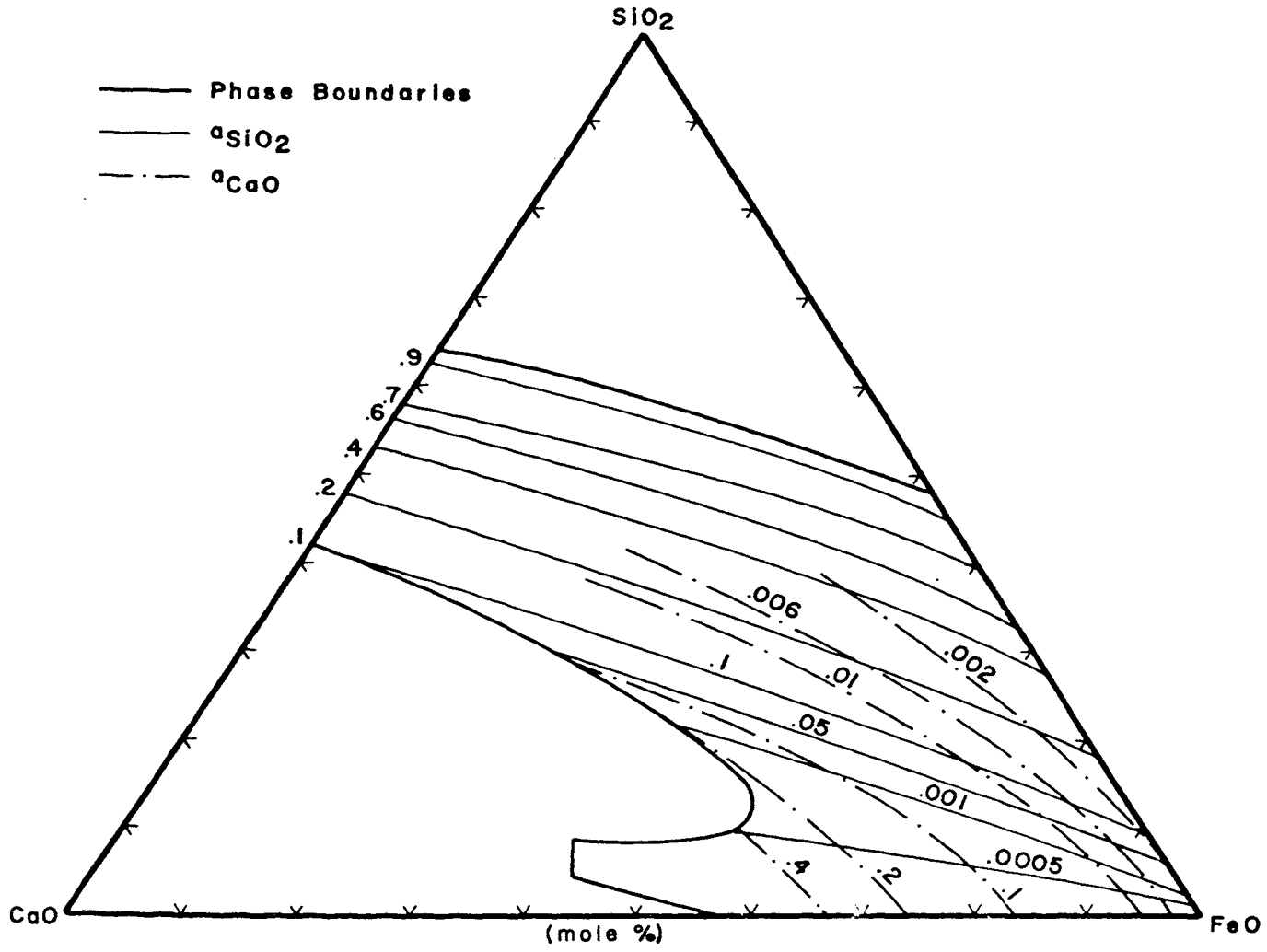

Figure 36. CaO and SiO_2 Activities in Melts of the System CaO-"FeO"-SiO_2 at 1550°C.

The stability field of solid monocalcium silicate at 1450°C was neglected and the liquids were assumed to be saturated with dicalcium silicate at point Z at both temperatures. Thus, considering the following reaction,

$$2CaO(s) + SiO_2(s) = 2CaO \cdot SiO_2 \qquad (32)$$

at point Z $$\log K_{32} = -2\log a_{CaO} - \log a_{SiO_2} \qquad (33)$$

$\log K_{32}$ values were obtained from literature[9] as 4.08 and 4.25 at 1550°C and 1450°C respectively. Therefore it was possible to solve for the $\log a_{CaO}$ values at point Z from the knowledge of silica activities[16,17], and calculate the rest of the lime activities from a binary Gibbs-Duhem integration along the $CaO-SiO_2$ binary. The excess free energies ΔF^{xs}_b were then evaluated by using the equation:

$$\Delta F^{xs}_b = RT(N_{CaO} \cdot \log\gamma_{CaO} + N_{SiO_2} \cdot \log\gamma_{SiO_2}). \qquad (34)$$

The ternary excess free energies could thus be calculated from the knowledge of binary excess free energies ΔF^{xs}_b, and the integration of the right hand side part of equation (31) along a number of CaO/SiO_2 paths near the dicalcium silicate saturation boundary. The iso-excess free energies obtained with the aid of equation (31) are drawn with dash-dot lines in Figures 33 and 34, and they are extended to the

dicalcium silicate saturation boundary. The silica and lime activities along this boundary could be calculated by simultaneous solution of equation (33) with

$$\Delta F^{xs}_{t} = RT(N_{CaO}\cdot\log\gamma_{CaO} + N_{SiO_2}\cdot\log\gamma_{SiO_2} + N_{FeO}\cdot\log\gamma_{FeO}). \quad (35)$$

The low silica activities shown in Figures 35 and 36 were drawn by joining the calculated silica activities along the C_2S saturation with those inferred from Figures 8(a) and 8 (b) along the FeO_t-SiO_2 binary.

The calcium oxide activities in the composition range of interest to this investigation were calculated with the help of a binary Gibbs-Duhem equation of the form

$$\log a^{I}_{CaO} = \left[\log a^{*}_{CaO} - \int_{a^{*}_{SiO_2}}^{a^{I}_{SiO_2}} \frac{n_{SiO_2}}{n_{CaO}} d\log a_{SiO_2}\right]_{a_{"FeO"}} \quad (36)$$

The $\log a^{*}_{CaO}$ and $a^{*}_{SiO_2}$ values were calculated at the C_2S saturation, and the integration was performed along several constant iso-"FeO" activity curves. The lime activities along the CaO-FeO_t join were taken from the relations given in Figures 28 and 29.

Results of Activity Calculations

The results given in Tables XVI and XVII of Appendix IV are summarized in the form of activity-composition diagrams

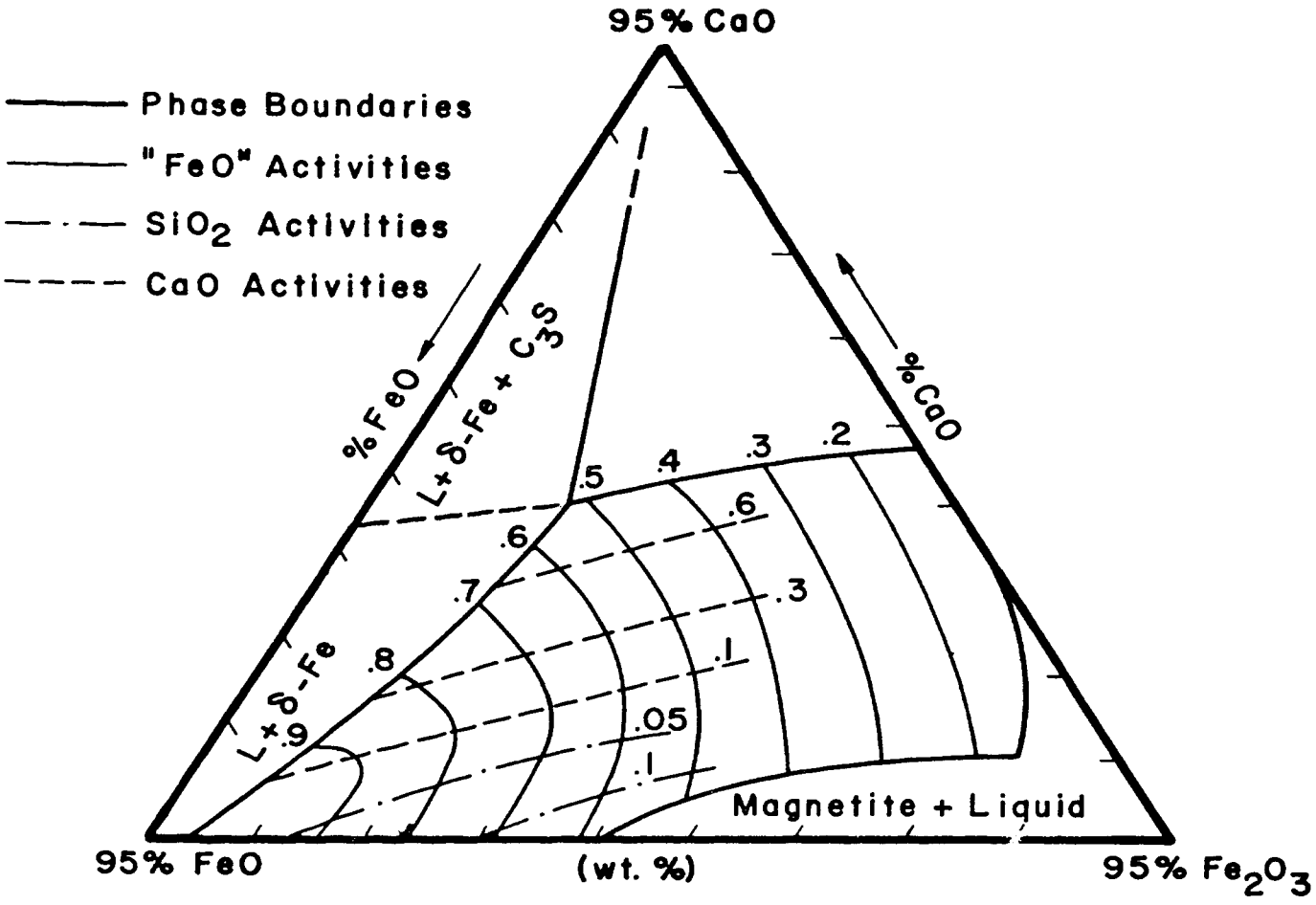

Figure 37. Activities of "FeO", CaO, and SiO_2 in Melts of the System $CaO-FeO-Fe_2O_3-SiO_2$ in the 5% SiO_2 Section at 1450°C.

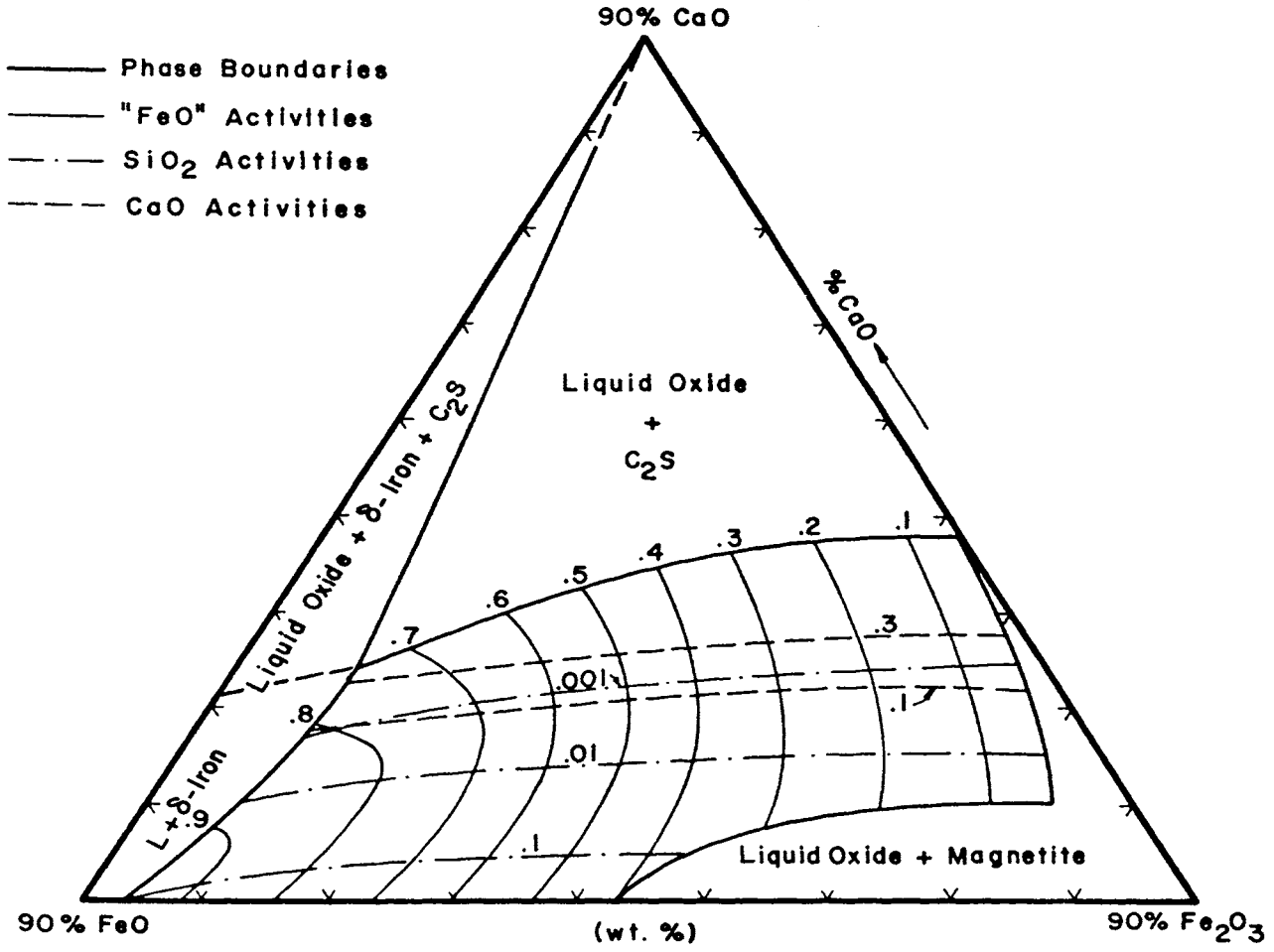

Figure 38. Activities of "FeO", CaO, and SiO_2 in Melts of the System CaO-FeO-Fe_2O_3-SiO_2 in the 10% SiO_2 Section at 1450°C.

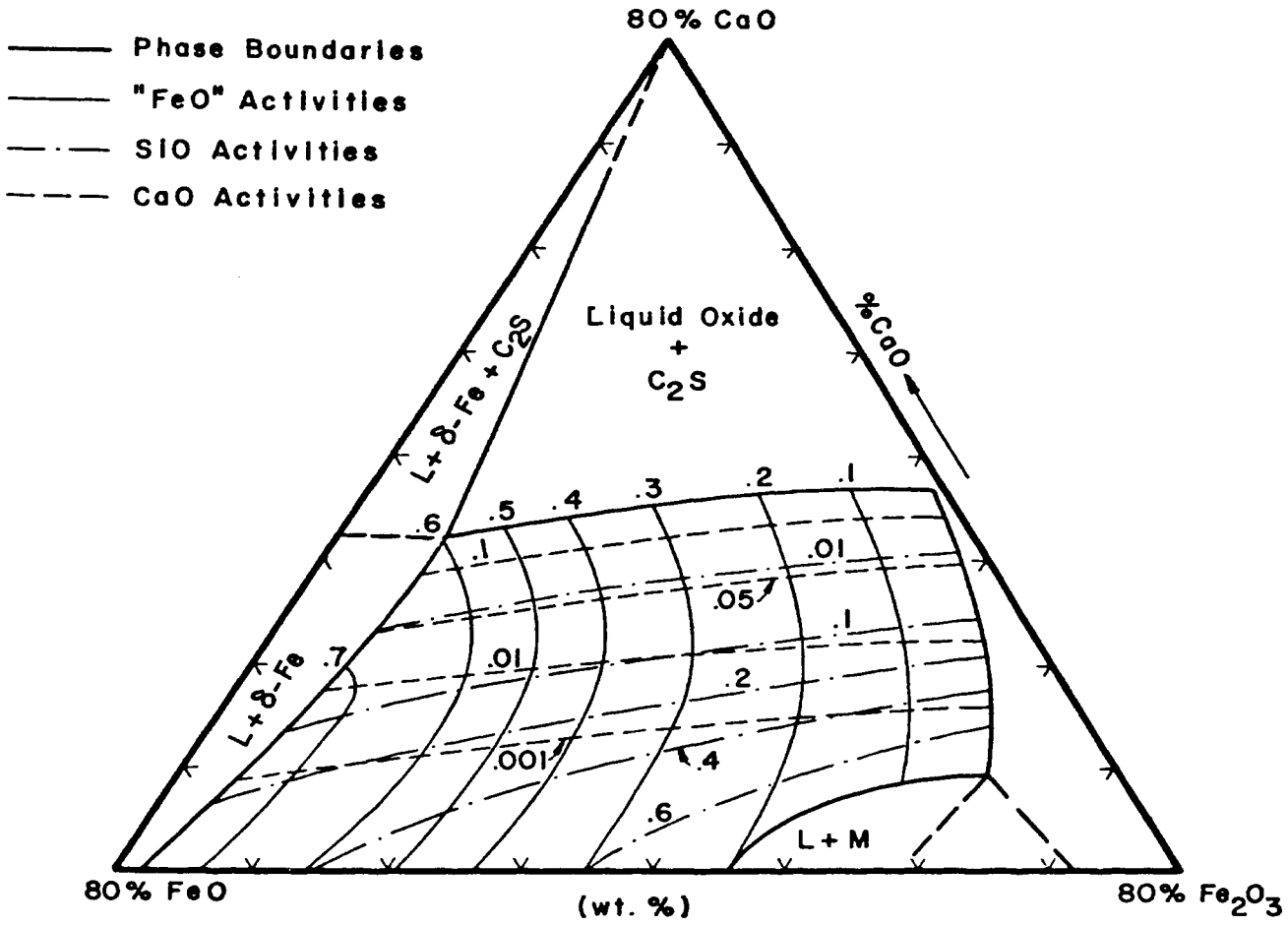

Figure 39. Activities of "FeO", CaO, and SiO_2 in Melts of the System CaO-FeO-Fe_2O_3-SiO_2 in the 20% SiO_2 Section at 1450°C.

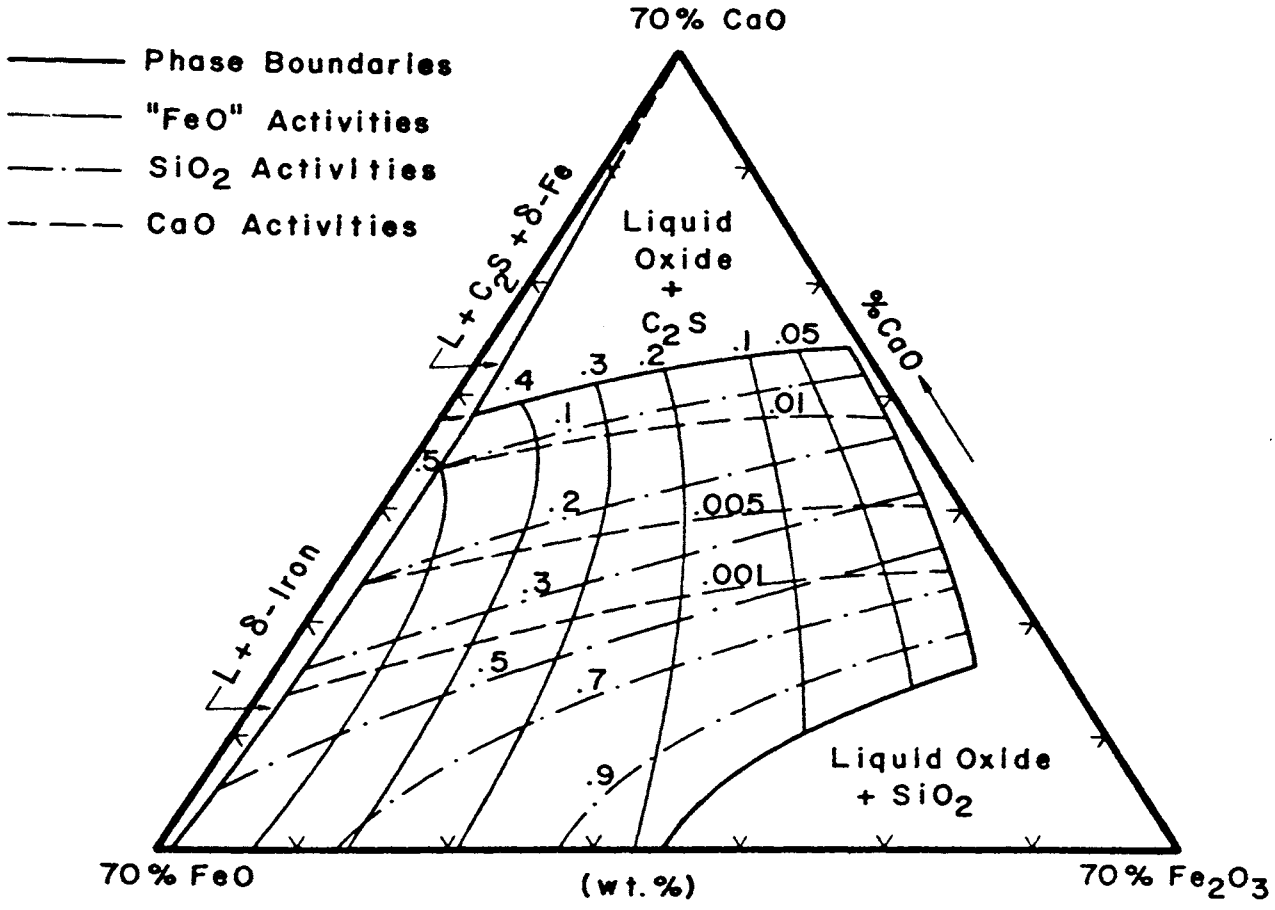

Figure 40. Activities of "FeO", CaO, and SiO_2 in Melts of the System CaO-FeO-Fe_2O_3-SiO_2 in the 30% SiO_2 Section at 1450°C.

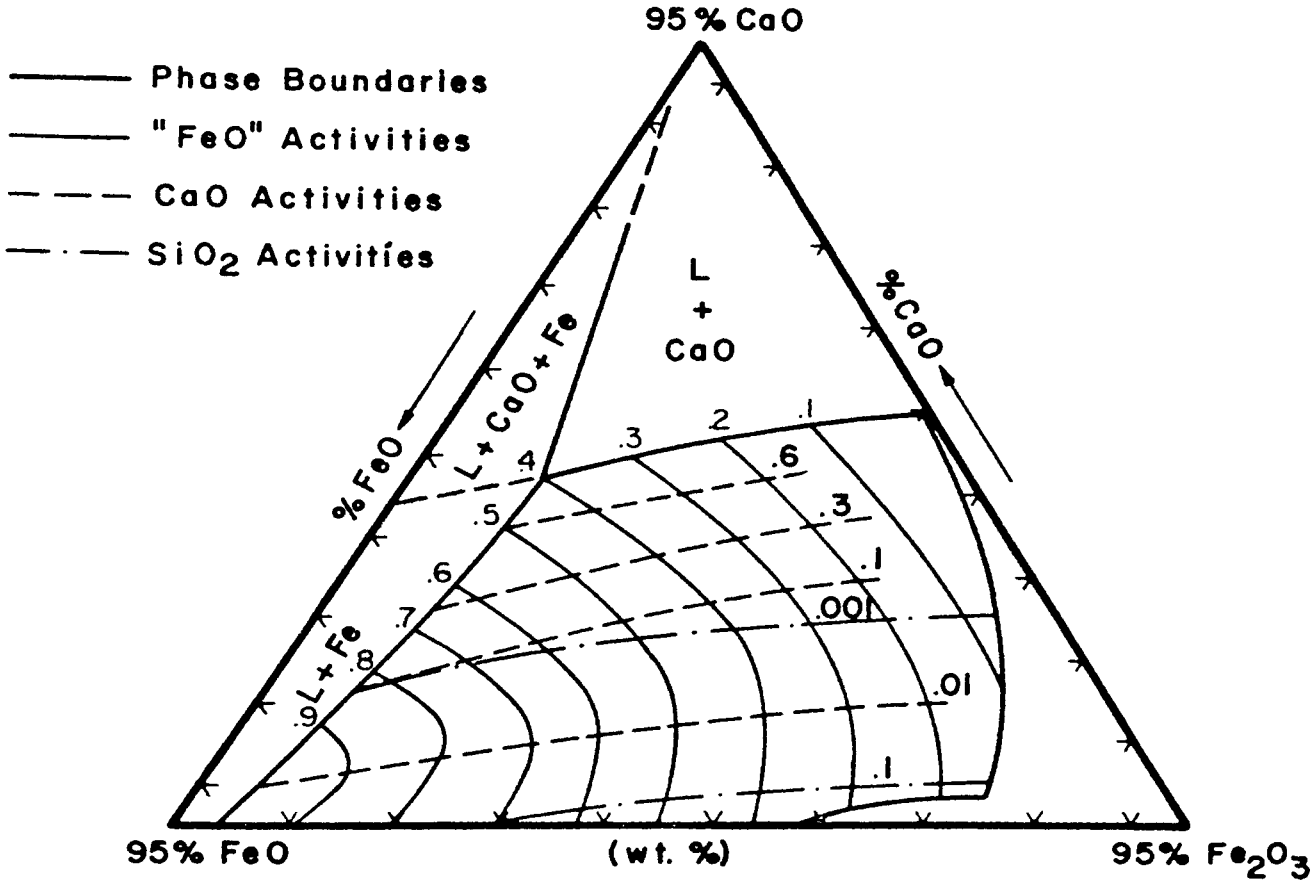

Figure 41. Activities of "FeO", CaO, and SiO_2 in Melts of the System CaO-FeO-Fe_2O_3-SiO_2 in the 5% SiO_2 Section at 1550°C.

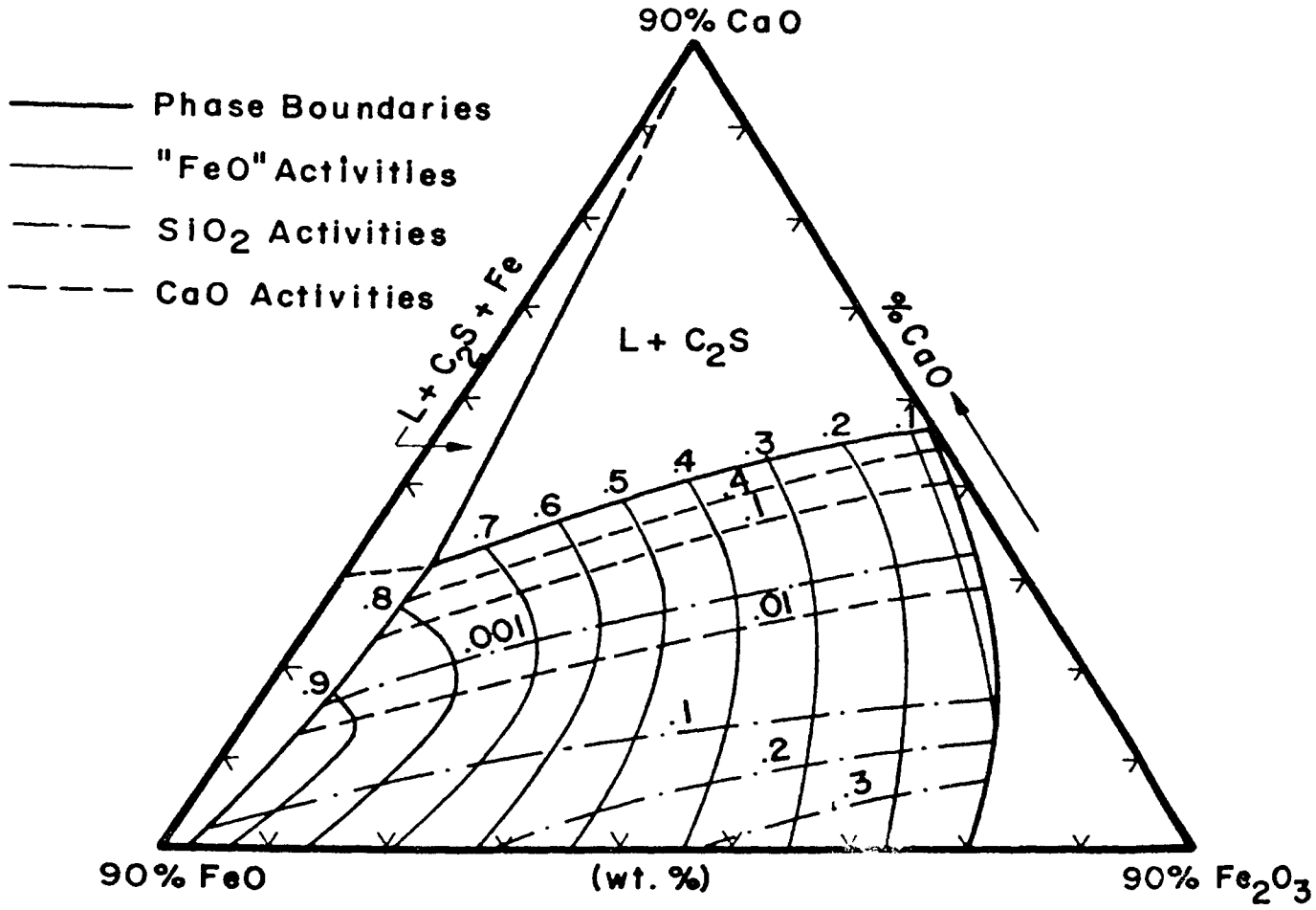

Figure 42. Activities of "FeO", CaO, and SiO_2 in Melts of the System CaO-FeO-Fe_2O_3-SiO_2 in the 10% SiO_2 Section at 1550°C.

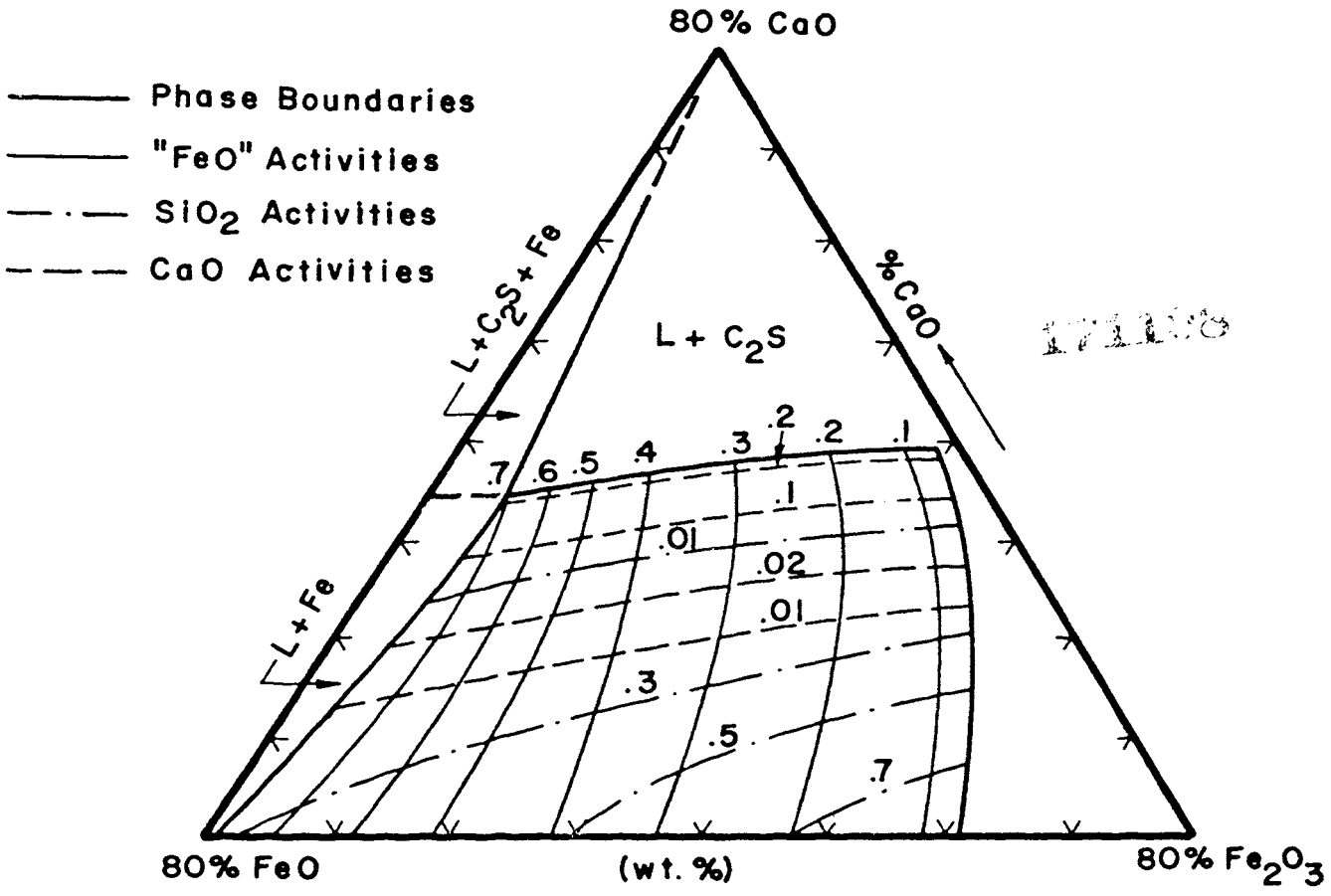

Figure 43. Activities of "FeO", CaO, and SiO_2 in Melts of the System $CaO-FeO-Fe_2O_3-SiO_2$ in the 20% SiO_2 Section at 1550°C.

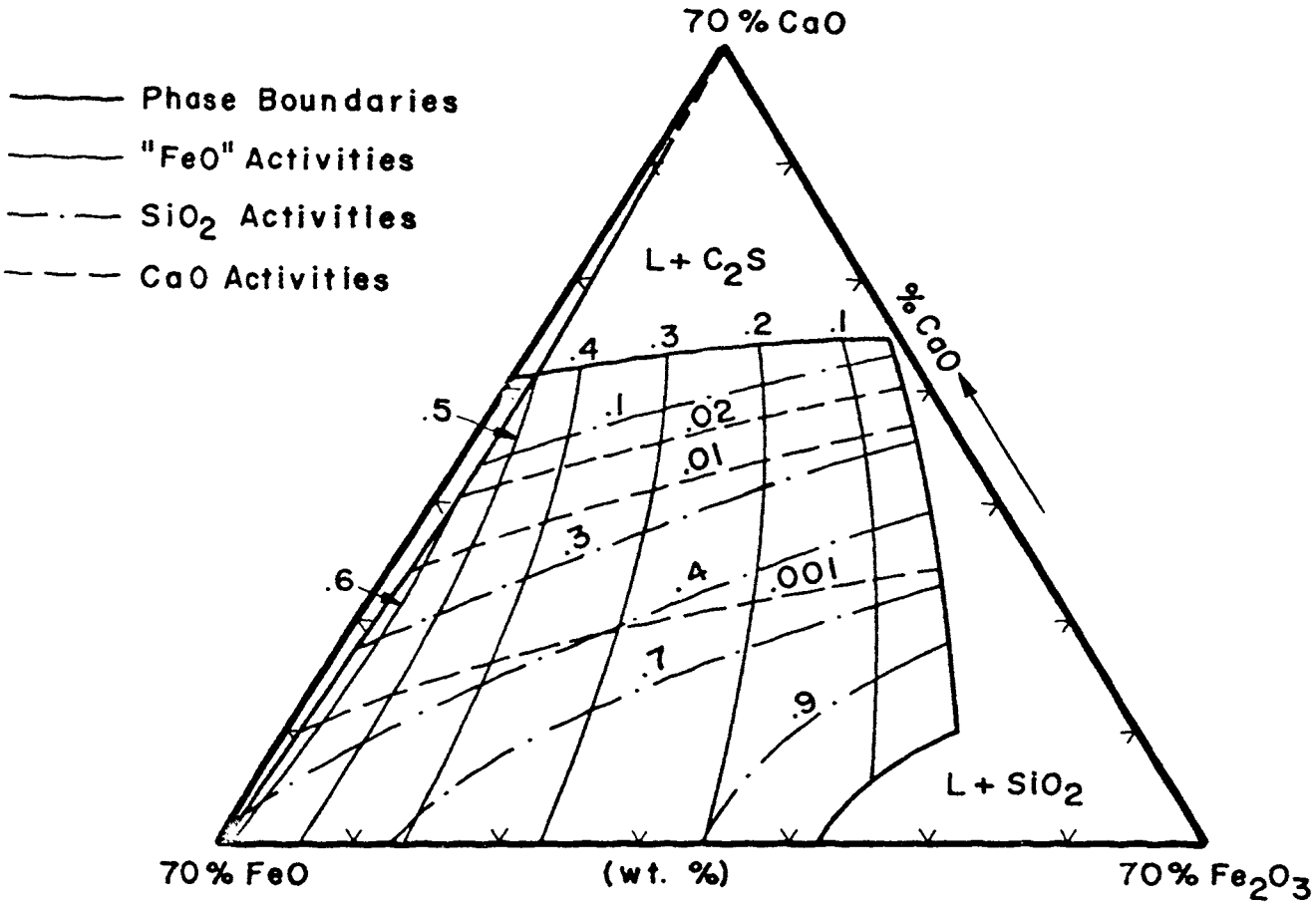

Figure 44. Activities of "FeO", CaO, and SiO_2 in Melts of the System CaO-FeO-Fe_2O_3-SiO_2 in the 30% SiO_2 Section at 1550°C.

as shown in Figures 37 to 40, and 41 to 44, at 1450°C and 1550°C respectively. Line symbols are the same as those used in the ternary activity graphs. Fe_2O_3 activities were not calculated.

Discussion of Activity-Composition Diagrams

Figures 37 through 40, and 41 through 44 show that the lime activities increase rapidly with increasing CaO content. Similarly the silica activities increase with increased SiO_2 additions, particularly at low lime contents. The "FeO" activities again show a complex nature; however, the symmetry noted in Figures 28 and 29 gradually diminishes as more silica is introduced into the system, so that at the 30% silica section no symmetry can be claimed.

Chipman and Chang[49] have assumed that the CaO-FeO-Fe_2O_3-SiO_2 melts are ionic and consist of species like Ca^{++}, Fe^{++}, Fe^{+}, $O^{=}$, $SiO_4^{=}$, and $Fe_2O_5^{4-}$. The mutual interactions between these species determine the shape of the iso-activity curves. Increased SiO_2 additions energetically favor the association of Ca^{++} and Fe^{++} ions with $SiO_4^{=}$ ions in preference with other groupings. Hence, the approach to the gross Ca_2SiO_4 composition would probably account for the very low lime and silica activities in the high-lime parts, of the 20% and 30% silica sections.

Figure 45 shows the effect of increased SiO_2 additions on "FeO" activities in a quaternary melt containing, for example, 15% CaO at 1450°C. The "FeO" activities are lower

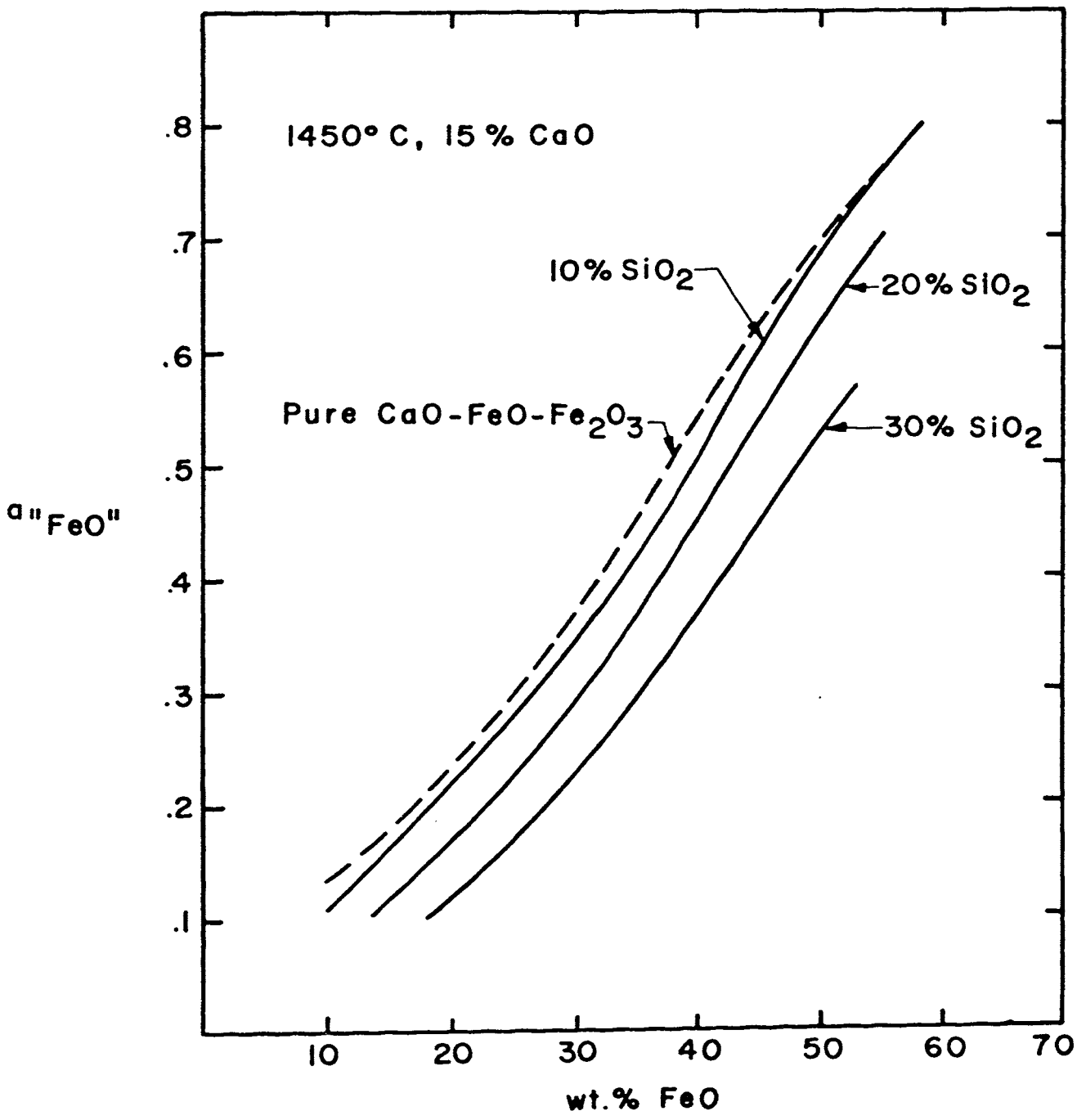

Figure 45. Effect of Increasing SiO_2 Addition on "FeO" Activities of $CaO-FeO-Fe_2O_3-SiO_2$ Melts Containing 15% CaO at 1450°C.

at higher SiO_2 contents probably because of the stronger interaction between divalent iron cations and silicate anion complexes.

The effect of temperature on "FeO" activities is shown in Figure 46 for two levels of SiO_2 contents at 15% CaO. Within the limits of errors involved in experiments and calculations temperature does not have a pronounced effect on the "FeO" activities. Diagrams similar to Figures 45 and 46 drawn for various CaO contents showed the same characteristics at both temperatures.

In addition to the factors discussed in the ternary activity calculations the accuracies of the quaternary activities are affected by the extrapolations and assumptions involved in the ternary CaO-"FeO"-SiO_2 system which was used to determine the reference activities in equations (27), (28), and (29). At 1450°C no data were obtained at silica contents higher than 30%. The high-SiO_2 "FeO" activities shown in Figure 35 were drawn on the basis of approximations between the low-SiO_2 "FeO" activities of this work at 1450°C, and those of Figure 11 at 1600°C. Consequently the silica, and therefore the lime, activities obtained by Schuhmann's and Darken's methods may not be absolutely correct. The results of these calculations were therefore omitted from the tables. Similarly, it is difficult to estimate the accuracy of reference CaO and SiO_2 activities at 1550°C since they were calculated from the extrapolated "FeO" iso-activity curves.

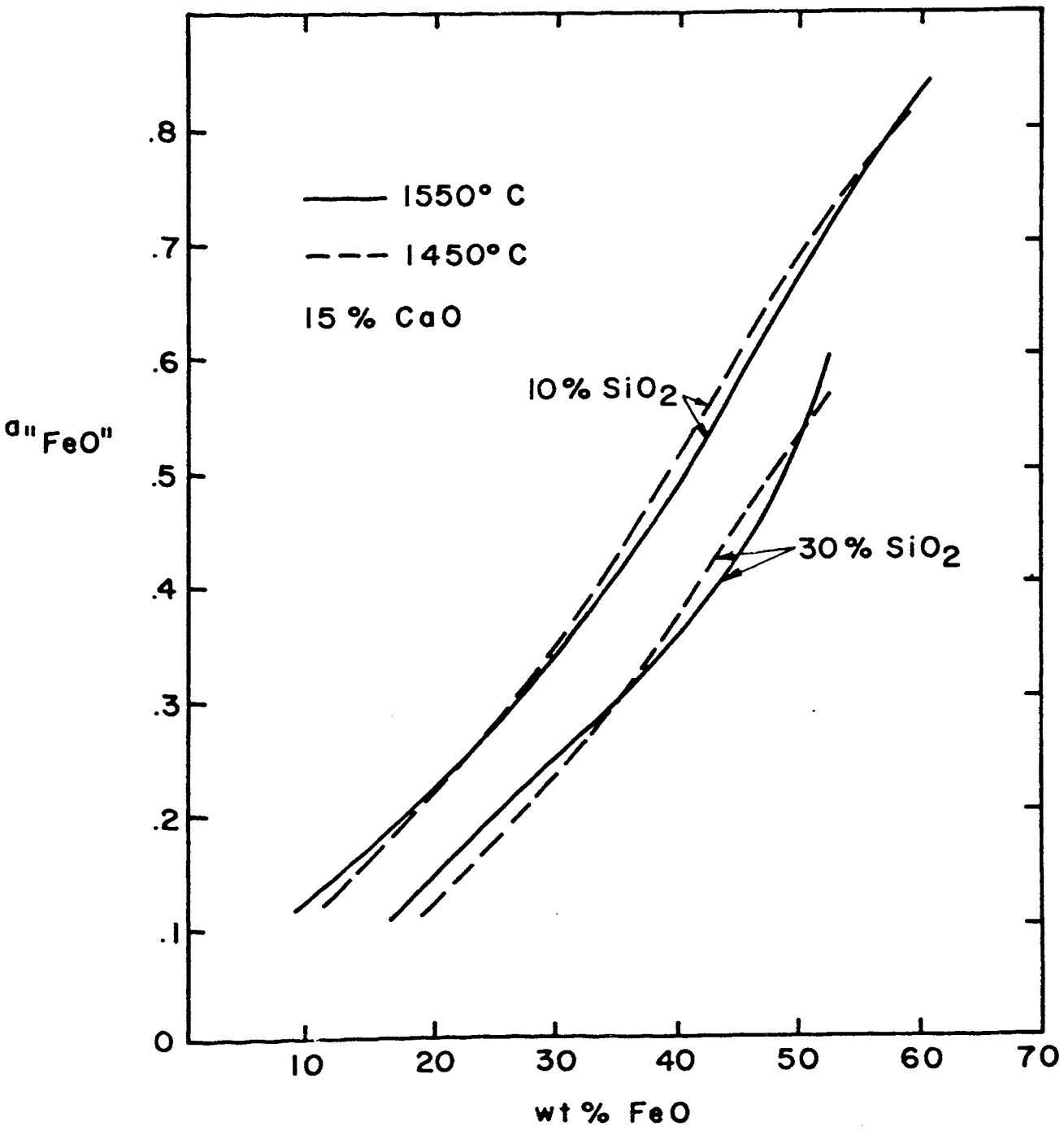

Figure 46. Effect of Temperature on "FeO" Activities of $CaO-FeO-Fe_2O_3-SiO_2$ Melts Containing 15% CaO.

However, as will be noted from Tables XVI and XVII of Appendix IV silica activities seem to be quite reliable. For the sake of convenience some of the values around the silica saturation field are summarized in Table XVIII.

TABLE XVIII

SILICA ACTIVITIES AROUND SILICA SATURATION

Temperature	$\%SiO_2$	Fe/CaO	$\log a_O$	a_{SiO_2}	Location
1450°C	20	6.010	0.0	.93	Close to the Liq. + Mag. + SiO_2 field.
1450°C	30	6.010	0.0	1.04	SiO_2-saturation field.
1450°C	30	6.010	-1.448	.98	On the SiO_2 saturation curve.
1450°C	30	2.710	-1.448	1.01	SiO_2-saturation field.
1550°C	30	13.90	1.000	.95	Close to the SiO_2-saturation.
1550°C	30	4.0	0.000	1.02	Silica saturation field

The silica activities in the low-SiO_2 part of the CaO-FeO-SiO_2 system, particularly those on the C_2S saturation curve sticking out to the tricalcium silicate saturation, could not be calculated. An attempt was made to determine the silica activity at the C_2S-C_3S double saturation point Q by considering the following reaction,

$$3CaO(s) + SiO_2(s) = 3CaO \cdot SiO_2 \qquad (37)$$

at Q: $$\log K_{37} = -3\log a_{CaO} - \log a_{SiO_2}$$

$\log K_{37}$ values were obtained from literature[9] as 4.06 at 1450 °C and 3.91 at 1550 °C. Simultaneous solution of equations (33) and (38) resulted in lime activities greater than one. It, therefore, appears that because of less reliable data logK values of C_3S are in error. Silica and lime activities in Figures 37 and 41, (i.e. 5% SiO_2 sections) were tentatively drawn on the basis of estimations from Figures 8(a) and 8(b), and approximate CaO activities of Figures 35 and 36.

The "FeO" activities in the 5% SiO_2 sections could not be calculated in the composition range where CaO contents were higher than 15%. It is necessary to obtain experimental data to draw additional isothermal phase diagrams at several other constant silica sections between 0 to 10% SiO_2 in order to get sufficient number of points to construct iso-oxygen activity lines in n_{CaO}/n_{SiO_2} planes corresponding to CaO contents higher than 15%. The known parts of iso-"FeO" activity curves in that section were connected to the known "FeO" activities along the iron + liquid oxide phase boundary in a manner similar to the shape of "FeO" activity curves in the ternary $CaO-FeO-Fe_2O_3$ system.

The accuracy of iron activities, therefore those of "FeO", could be checked by again considering reaction (16). The standard free energy of fromation of magnetite from iron

and oxygen was given as -138.2 (±1.2) kcal/mole. From the integrated Fe activities and experimentally determined Po_2 values the following Table could be prepared at 1450°C:

TABLE XIX

FREE ENERGY OF FORMATION OF MAGNETITE

Po_2	$\log a_{Fe}$ (from eqn. 27)	$\Delta F°_{Fe_3O_4}$	$\%SiO_2$
$10°$	-5.477	130.0	5
$10^{-2.9}$	-3.757	136.0	5
$10^{-3.7}$	-3.236	135.5	5
$10°$	-5.800	137.0	10
$10^{-2.9}$	-3.850	136.6	10
$10^{-3.7}$	-3.290	136.0	10
$10°$	-5.900	139.0	20
$10^{-2.9}$	-3.904	138.3	20

With the exception of the 130.0 kcal/mole value at 5% SiO_2, the other free energies can be considered to be in good agreement with the literature value, considering that magnetite dissolves excess oxygen at high Po_2.

The "FeO" activities at 1550°C are in very good agreement with those calculated by Larson and Chipman[24] up to about 10% SiO_2. Their activities are slightly higher at higher SiO_2 contents probably because they have taken the 1600°C reference activities along the iron-saturation boundary. CaO and SiO_2 activities could not be compared with previous literature since they were not calculated before.

CHAPTER VI

SUMMARY AND CONCLUSIONS

The objective of this work was to determine the phase equilibria and activity-composition relations in the $CaO-FeO-Fe_2O_3-SiO_2$ system at 1450°C and 1550°C for silica contents ranging from zero to thirty weight percent. The experimental procedure involved equilibrating the selected oxide, ferrite, and silicate mixtures with a gas phase of known oxygen partial pressure obtained by mixing O_2, N_2, CO, and CO_2 gases in controlled proportions. After equilibration, the samples were quenched to room temperature.

Based on the experimental data obtained from chemical analyses, and microscopic and x-ray examinations of these samples isothermal phase diagrams were constructed for the ternary $CaO-FeO-Fe_2O_3$ system, and for 5, 10, 20, and 30 weight percent silica sections of the quaternary system.

The phase diagrams were conclusive in showing that increased temperature, or increased SiO_2 additions at a given temperature, increase the relative stability of the divalent iron cations in the liquid oxides, while CaO additions have the reverse effect. It was thereby concluded that the ability of the slag to transfer oxygen via the ferric ion decreases with increased temperature and SiO_2 additions.

Phase diagrams also showed that the stability of magnetite decreases rather rapidly with silica additions at a constant temperature. Elevated temperature has the same

effect on magnetite stability. At 1450°C in the 20% SiO_2 section silica has appeared as a stable solid phase in low-lime high-Po_2 regions of the diagram. The stability of silica increases with increasing SiO_2 addition at the expense of magnetite stability. In the CaO-FeO-Fe_2O_3 ternary and in 5% SiO_2 sections of the quaternary system the lime-saturated liquids were in equilibrium with CaO containing a small amount of FeO in solid solution, except that at 1450°C tricalcium silicate was stable at oxygen pressures below 10^{-6} atm. At higher silica contents the lime-saturated liquids were all in equilibrium with dicalcium silicate.

The activities of the oxide components FeO, CaO, and SiO_2 were calculated by using the Schuhmann and Darken methods of ternary and quaternary Gibbs-Duhem integrations, where data has permitted such calculations.

In the course of evaluating the activities it was noticed that the standard free energies of formation of tricalcium silicate compound were inconsistent with those of the dicalcium silicate. Therefore, in order to refine and complete the activity-composition relations given in this work the free energies of formation of tricalcium silicate should be determined by an independent method. Considering the following reaction, above 1300°C:

$$Si(s) + 2MgO(s) + 3CaO(s) \quad > 2Mg(g) + 3CaO\cdot SiO_2 \ .$$

A determination of equilibrium magnesium vapor pressure over a mixture of metallic silicon, MgO, CaO, and $3CaO \cdot SiO_2$ can provide the necessary ΔF° data for tricalcium silicate.

For the improvement of the CaO activities in the ternary $CaO-FeO-Fe_2O_3$ system the exact solubility limits of wustite in lime should be determined as a function of oxygen pressure of the gas phase. The higher silica part of the quaternary system needs more experimental work to aid in the improvement of activities.

The free energies of formation of compounds like dicalcium ferrite and magnetite as determined in the present study showed, in general, good agreement with other independently determined values.

The phase diagrams and activity-composition relations derived therefrom provide a valuable guide in judging the oxidizing power of metallurgical slags, particularly those which are involved in BOF steelmaking processes. It has long been recognized that the elimination of phosphorus is favored by low temperatures and with slags of high CaO/SiO_2 ratio having high "FeO" activities. Sulphur removal, on the other hand, demands low "FeO" activities although the other factors remain the same. Lack of activity knowledge, however, did not permit a quantitative approach to the basic understanding of these reactions. Although the present work deals with a relatively simple slag system the relations presented provide a chance for a new look at these reactions.

Additional work at higher temperatures and with other slag components will certainly broaden the present knowledge.

Taking the present work as a basis some interesting topics of investigation might be:

(a) Solubility of sulphur in slags at various temperatures and oxygen potentials, as would be determined by studies involving equilibration of present slags with gases containing various sulphur bearing species,

(b) Rate of solution of lime in slags of known CaO activity,

(c) Rate of oxygen dissolution in or evolution out from a slag of known surface area.

APPENDIX I

METHODS OF CHEMICAL ANALYSIS

Compositions of the samples were determined by establishing the amounts of ferrous iron, total iron, and calcium oxide through well known dichromate and permanganate titration methods[41]. Silica was always determined by difference. The following solutions were prepared from Fisher Certified analytical grade reagents for iron analysis:

0.1 N Potassium Dichromate solution: Prepared by dissolving 4.903 grams of dry $K_2Cl_2O_7$ (99.98% min. purity) in distilled water and diluted exactly to one liter. After filtering the solution, the exact normality was determined by standardizing it against either Fe_3O_4 or ferrous ammonium sulfate. The dichromate solutions remained stable over long periods of time.

Mercuric Chloride: A solution containing 50 gms of $HgCl_2$ per 1000 ml of water was prepared.

Stannous Chloride: 15 grams of $SnCl_2 \cdot 2H_2O$ was dissolved in 100 ml of 1:2 HCl solution. This solution had to be prepared fresh, every day, for analysis.

Diphenylamine indicator: Prepared by dissolving 200 mg of barium diphenylamine sulfonate in 100 ml of water.

Hydrochloric acid: Approximately 12 N stock solution.

Phosphoric acid: 85% H_3PO_4 stock solution.

Sulphuric acid: 1:5 stock solution.

For every analysis slag samples were first ground to approximately -60 mesh and dried at 110°C for 1 hour.

Determination of Ferrous Iron

A representative portion of the sample weighing about 200 mg was wetted with 2 ml of water in a teflon crucible. 20 ml of HCl was added, the crucible was covered and gently heated. Almost all the samples dissolved in HCl; however for some high SiO_2 samples it was necessary to add a few drops of HF which was subsequently evaporated by boiling the solution for ten minutes. After complete dissolution the crucible was cooled quickly to room temperature and the solution was diluted to 150 ml in a 300 ml capacity tall pyrex titration-beaker. The normality of the final solution was always kept within $1<N<2$ limits in order to be able to titrate the solution with dichromate. 10 ml of 1:5 H_2SO_4 and 5 ml of H_3PO_4 were added, and the solution was titrated with 0.1 N (or for low Fe^{2+} samples with 0.05 N) dichromate by using 6 or 7 drops of diphenylamine sulfonate as the indicator.

Determination of Total Iron

Total iron was determined by following the same procedure as ferrous iron determination except that after complete

dissolution, all ferric ions were reduced to ferrous state by adding stannous chloride solution dropwise while stirring the hot sample solution until the yellow color disappeared. Following an excess of one or two more drops of stannous chloride addition, the crucible was quickly cooled to room temperature. The reducing agent had to be introduced in proper amounts, for insufficient $SnCl_2 \cdot 2H_2O$ would mean incomplete reduction as indicated by the potassium thiocyanate test in which a drop of sample solution would change the white color of thiocyanate crystals into red. Excess stannous chloride was removed by 10 ml of mercuric chloride addition. A white, silky precipitate was desirable, a gray-black precipitate would indicate too much $SnCl_2 \cdot 2H_2O$ in the solution. Both faulty solutions, having too much or too little stannous chloride, had to be discarded.

Determination of Calcium Oxide

Although the volumetric determination of CaO involved as many steps as its gravimetric determination, the former method was found to be more reliable. Volumetric analysis of CaO using an indirect oxidation-reduction method has been described in detail in chemistry books dealing with quantitative analysis (see for example Fischer[41]). The method essentially consists of dissolving the sample in HCl, precipitating the calcium ion as calcium oxalate, and filtering the precipitate in a gooch crucible by using an aqueous suspension of asbestos fibers. The precipitate was then

redissolved in 1:19 H_2SO_4 by heating nearly to boiling. The liberated oxalic acid was immediately titrated with 0.1 N standard permanganate solution. Although CaO did not enter into the final titration, it was stoichiometrically related to the amount of oxalic acid titrated. 0.1 N permanganate solution was frequently standardized against sodium oxalate. Prior to dissolution of the original sample it was heated at 700°C for 3 hours in order to oxidize most of the Fe^{2+} present, so that there would be a minimum of ferrous oxalate interference, if it co-precipitated at all.

APPENDIX II

SUMMARY OF RESULTS OBTAINED IN QUENCHING EXPERIMENTS

The results of microscopic examinations, chemical and x-ray diffraction analyses of quenched samples in the $CaO-FeO-Fe_2O_3$ system at 1450°C and 1550°C are presented in Tables II and III respectively. Tables IV to XI contain similar data for the $CaO-FeO-Fe_2O_3-SiO_2$ system.

The following abbreviations apply to all tables:

Liq. = Liquid oxide

Mag. = Magnetite (solid)

CaO (ss) = CaO-rich CaO-"FeO" solid solutions

C_2S = Dicalcium silicate

C_3S = Tricalcium silicate

T = Tridymite (1450°C stable modification of SiO_2)

C = Cristobalite (1550°C stable modification of SiO_2)

(s) = Solid

(l) = Liquid

(m) = Samples indexed by (m) mean that minor amount (1%) of the indicated solid phase was present, so that Po_2 and composition of that sample was assumed to represent the particular boundary.

n.a. = Not analyzed for

TABLE II

Summary of Results Obtained in Quenching Experiments in the System $CaO-FeO-Fe_2O_3$ at 1450°C

Sample No.	Gas Mixture	Po_2 (atm.)	Composition of Samples After Equilibration (wt%) CaO	FeO	Fe_2O_3	Stable Condensed Phase(s)
A-1	Pure O_2	10°	0.0	25.0	75.0	Liq.+Mag.
A-2		"	5.0	16.5	78.5	Liq.+Mag.
A-3		"	10.0	8.0	82.0	Liq.+Mag.
A-4		"	20.0	3.6	76.4	Liq.
A-5		"	35.0	0.6	64.4	Liq.
A-6		"	40.0	∿0	60.0	Liq.
A-7		"	44.0	0.0	56.0	Liq.+CaO (ss)
A-8	$\frac{O_2}{N_2} = \frac{5}{95}$	$10^{-1.301}$	11.5	12.7	75.8	Liq.
A-9		"	14.9	10.4	74.7	Liq.
A-10		"	20.0	7.5	72.5	Liq.
A-11		"	26.0	4.4	69.6	Liq.
A-12		"	35.0	∿1.0	64.0	Liq.
A-13	Pure CO_2	$10^{-2.896}$	0.0	30.0	70.0	Liq.+Mag.
A-14		"	6.7	23.8	69.5	Liq.+Mag.
A-15		"	12.5	18.7	68.8	Liq.
A-16		"	20.2	12.2	67.6	Liq.
A-17		"	30.0	7.0	63.0	Liq.
A-18		"	35.0	4.7	60.3	Liq.
A-19		"	40.0	2.4	57.6	Liq.
A-20	$\frac{CO_2}{CO} = 156$	$10^{-3.700}$	0.0	30.3	69.7	Liq.+Mag.

(Table II continued, $CaO-FeO-Fe_2O_3$, 1450°C)

Sample No.	Gas Mixture	Po_2 (atm.)	Composition of Samples After Equilibration (wt%) CaO	FeO	Fe_2O_3	Stable Condensed Phase(s)
A-21		"	5.4	32.8	61.8	Liq.+Mag.
A-22		"	10.9	32.2	56.9	Liq.
A-23	$\frac{CO_2}{CO} = 156$	$10^{-3.70}$	33.2	11.5	55.3	Liq.
A-24		"	39.1	7.6	53.3	Liq.
A-25		"	44.0	5.5	50.5	Liq.+CaO (ss)
A-26	$\frac{CO_2}{CO} = 34.9$	$10^{-5.00}$	0.0	31.0	69.0	Liq.+Mag.
A-27		"	6.1	48.3	44.6	Liq.
A-28		"	15.2	36.6	48.2	Liq.
A-29		"	28.4	24.8	46.8	Liq.
A-30		"	40.6	12.4	47.0	Liq.
A-31		"	43.0	12.0	45.0	Liq.+CaO (ss)
A-32	$\frac{CO_2}{CO} = 3.49$	$10^{-7.00}$	0.0	73.5	26.5	Liq.
A-33		"	9.0	58.0	33.0	Liq.
A-34		"	16.3	50.0	33.7	Liq.
A-35		"	26.0	39.0	35.0	Liq.
A-36		"	27.5	37.0	35.5	Liq.
A-37		"	39.2	25.0	35.8	Liq.
A-38		"	43.1	20.5	36.4	Liq.+CaO (ss)
A-39	$\frac{CO_2}{CO} = .35$	$10^{-9.00}$	0.0	90.0	10.0	Liq.
A-40		"	11.0	72.0	17.0	Liq.
A-41		"	17.0	64.0	19.0	Liq.
A-42		"	22.8	55.5	21.7	Liq.

(Table II continued, CaO-FeO-Fe_2O_3, 1450°C)

Sample No.	Gas Mixture	Po_2 (atm.)	Composition of Samples After Equilibration (wt%) CaO	FeO	Fe_2O_3	Stable Condensed Phase(s)
A-43		"	29.0	48.0	23.0	Liq.
A-44		"	43.1	34.3	22.6	Liq.+CaO (ss)
A-45	$\frac{CO_2}{CO} = .23$	$10^{-9.30}$	0	94	6	Liq.+Fe(s) (m)
A-46		"	11.5	74.8	13.7	Liq.
A-47		"	21.3	61.7	17.0	Liq.
A-48		"	25	57	18.0	Liq.
A-49		"	46	37	17.0	Liq.+CaO (ss)
A-50	$\frac{CO_2}{CO} = .191$	$10^{-9.360}$	10	80	10	Liq.+Fe(s) (m)
A-51		"	40	n.a.	n.a.	Liq.+CaO (ss)
A-52	$\frac{CO_2}{CO} = .142$	$10^{-9.780}$	36	n.a.	n.a.	Liq.+Fe(s) (m)

TABLE III

Summary of Results Obtained in Quenching Experiments in the System $CaO-FeO-Fe_2O_3$ at 1550°C

Sample No.	Gas Mixture	P_{O_2} (atm.)	Composition of Samples After Equilibration (wt%) CaO	FeO	Fe_2O_3	Stable Condensed Phase(s)
B-1	Pure O_2	10^0	0.0	28.5	71.5	Liq.+Mag.
B-2		"	5.0	18.0	77.0	Liq.
B-3		"	15.2	9.5	75.3	Liq.
B-4		"	26.0	3.6	70.4	Liq.
B-5		"	35.0	1.5	63.5	Liq.
B-6		"	41.3	0.7	58.0	Liq.
B-7		"	45.0	0.5	54.5	Liq.+CaO (ss)
B-8	$\frac{O_2}{N_2} = \frac{1}{99}$	10^{-2}	0.0	31.0	69.0	Liq.+Mag.
B-9		"	2.1	33.1	64.8	Liq.+Mag.
B-10		"	5.2	32.2	62.6	Liq.
B-11		"	15.3	21.0	63.7	Liq.
B-12		"	26.4	13.8	59.8	Liq.
B-13		"	41.4	3.6	55.0	Liq.
B-14		"	45.0	3.1	51.9	Liq.+CaO (ss)
B-15	Pure CO_2	$10^{-2.58}$	0.0	31.0	69.0	Liq.+Mag.
B-16		"	2.1	41.0	59.9	Liq.
B-17		"	5.2	37.7	57.1	Liq.
B-18		"	15.4	25.0	59.6	Liq.
B-19		"	26.4	15.3	58.3	Liq.
B-20		"	41.4	4.2	54.4	Liq.

(Table III continued, CaO-FeO-Fe_2O_3, 1550°C)

Sample No.	Gas Mixture	Po_2 (atm.)	Composition of Samples After Equilibration (wt%) CaO	FeO	Fe_2O_3	Stable Condensed Phase(s)
B-21	$\frac{CO_2}{CO}$ = 74.5	$10^{-3.4}$	0.0	47.1	52.9	Liq.
B-22		"	12.0	34.4	53.6	Liq.
B-23		"	26.0	19.9	54.1	Liq.
B-24		"	35.6	12.0	52.4	Liq.
B-25		"	42.8	6.7	50.5	Liq.
B-26		"	44.3	7.4	48.3	Liq.
B-27	$\frac{CO_2}{CO}$ = 20.5	$10^{-4.520}$	0.0	59.0	41.0	Liq.
B-28		"	6.3	52.2	41.5	Liq.
B-29		"	8.0	48.6	43.4	Liq.
B-30		"	14.5	41.0	44.5	Liq.
B-31		"	23.5	31.5	45.0	Liq.
B-32		"	40.0	16.7	43.3	Liq.
B-33	$\frac{CO_2}{CO}$ = 4.0	$10^{-5.94}$	0.0	73.0	27.0	Liq.
B-34		"	10.0	58.0	32.0	Liq.
B-35		"	20.0	45.0	35.0	Liq.
B-36		"	32.0	33.0	35.0	Liq.
B-37		"	37.0	28.5	34.5	Liq.
B-38		"	41.8	25.2	33.0	Liq.+CaO (ss)
B-39	$\frac{CO_2}{CO}$ = .298	$10^{-8.194}$	0.0	92.0	8.0	Liq.
B-40		"	3.0	85.5	11.5	Liq.
B-41		"	13.4	68.4	18.2	Liq.
B-42		"	20.0	57.0	23.0	Liq.

(Table III continued, $CaO-FeO-Fe_2O_3$, 1550°C)

Sample No.	Gas Mixture	Po_2 (atm.)	Composition of Samples After Equilibration (wt%) CaO	FeO	Fe_2O_3	Stable Condensed Phase(s)
B-43		"	31.0	43.0	26.0	Liq.
B-44		"	41.0	35.0	24.0	Liq.+CaO (ss)
B-45	$\frac{CO_2}{CO} = .118$	$10^{-9.0}$	46.0	35.0	19.0	Liq.+CaO (ss)

TABLE IV

Summary of Results Obtained in Quenching Experiments in the 5% Silica Section of the System $CaO-FeO-Fe_2O_3-SiO_2$ at 1450°C

Sample No.	Gas Mixture	Po_2 (atm.)	Composition of Samples After Equilibration (wt%) CaO	FeO	Fe_2O_3	Stable Condensed Phase(s)
C-1	Pure O_2	10^0	10.0	10.0	75.0	Liq.+Mag. (m)
C-2		"	14.0	6.7	74.3	Liq.
C-3		"	20.2	3.5	71.3	Liq.
C-4		"	31.2	1.1	62.7	Liq.
C-5		"	39.0	0.3	55.7	Liq.
C-6		"	43.0	0.2	51.8	Liq.
C-7		"	47.0	∿0	48.0	Liq.
C-8	$\frac{O_2}{N_2} = \frac{5}{95}$	$10^{-1.301}$	14.0	12.0	69.0	Liq.
C-9		"	20.0	7.0	68.0	Liq.
C-10		"	31.2	1.8	62.0	Liq.
C-11		"	39.0	0.9	55.1	Liq.
C-12		"	43.0	0.2	51.8	Liq.
C-13		"	47.0	0	48.0	Liq.
C-14		"	52.0	∿0.5	42.5	Liq.+CaO (ss)
C-15	Pure CO_2	$10^{-2.896}$	0.0	29.5	65.5	Liq.+Mag.
C-16		"	8.0	21.5	65.5	Liq.+Mag.
C-17		"	10.2	19.5	65.3	Liq.
C-18		"	14.0	15.4	65.6	Liq.
C-19		"	21.0	10.5	63.5	Liq.

(Table IV continued, 5% SiO_2, 1450°C)

Sample No.	Gas Mixture	Po_2 (atm.)	Composition of Samples After Equilibration (wt%) CaO	FeO	Fe_2O_3	Stable Condensed Phase(s)
C-20		$10^{-2.896}$	31.2	5.5	58.3	Liq.
C-21		"	39.0	3.0	53.0	Liq.
C-22		"	43.0	2.0	50.0	Liq.
C-23		"	52.0	0.9	42.1	Liq.+CaO (ss)
C-24	$\frac{CO_2}{CO}$ = 156	$10^{-3.70}$	0.0	31.0	64.0	Liq.+Mag.
C-25		"	4.0	32.0	59.0	Liq.+Mag.
C-26		"	9.0	29.8	56.2	Liq.
C-27		"	20.2	18.8	56.0	Liq.
C-28		"	31.2	11.0	52.8	Liq.
C-29		"	41.0	6.0	48.0	Liq.
C-30		"	52.0	2.4	40.6	Liq.+CaO (ss)
C-31	$\frac{CO_2}{CO}$ = 34.9	$10^{-5.0}$	0.0	57.2	37.8	Liq.
C-32		"	8.0	45.0	42.0	Liq.
C-33		"	14.0	37.0	44.0	Liq.
C-34		"	20.5	29.5	45.0	Liq.
C-35		"	39.4	11.3	44.3	Liq.
C-36		"	43.5	8.0	43.5	Liq.
C-37	$\frac{CO_2}{CO}$ = 3.49	$10^{-7.0}$	0.0	73.0	22.0	Liq.
C-38		"	10.5	56.5	28.0	Liq.
C-39		"	20.8	40.2	44.0	Liq.
C-40		"	32.0	27.0	36.0	Liq.
C-41		"	39.8	19.3	35.9	Liq.

(Table IV continued, 5% SiO_2, 1450°C)

Sample No.	Gas Mixture	Po_2 (atm.)	Composition of Samples After Equilibration (wt%) CaO	FeO	Fe_2O_3	Stable Condensed Phase(s)
C-42		$10^{-7.0}$	43.8	17.0	34.2	Liq.
C-43		"	47.8	16.0	31.2	Liq.+C_3S
C-44	$\frac{CO_2}{CO}$ = .35	$10^{-9.0}$	0.0	89.5	5.5	Liq.
C-45		"	10.7	66.3	18.0	Liq.
C-46		"	20.8	50.0	24.2	Liq.
C-47		"	35.0	32.5	27.5	Liq.
C-48		"	40.0	28.3	26.7	Liq.
C-49		"	44.2	24.1	26.7	Liq.+C_3S
C-50	$\frac{CO_2}{CO}$ = .241	$10^{-9.32}$	0.0	∿91.0	4.0	Liq.+Fe(s)(m)
C-51	$\frac{CO_2}{CO}$ = .225	$10^{-9.38}$	10.0	76.0	9	Liq.+Fe(s)(m)
C-52	$\frac{CO_2}{CO}$ = .183	$10^{-9.56}$	25.0	54.4	15.6	Liq.+Fe(s)(m)
C-53		"	40.0	n.a.	n.a.	Liq.
C-54	$\frac{CO_2}{CO}$ = .111	10^{-10}	38.5	n.a.	n.a.	Liq.+Fe(s)(m)
C-55	$\frac{CO_2}{CO}$ = .092	$10^{-10.16}$	38.0	n.a.	n.a.	Liq.+Fe(s)

TABLE V

Summary of Results Obtained in Quenching Experiments in the 10% Silica Section of the System $CaO-FeO-Fe_2O_3-SiO_2$ at 1450°C

Sample No.	Gas Mixture	Po_2 (atm.)	Composition of Samples After Equilibration (wt%) CaO	FeO	Fe_2O_3	Stable Condensed Phase(s)
D-1	Pure O_2	10°	0.0	25.0	65.0	Liq.+Mag.
D-2		"	5.0	16.0	69.0	Liq.+Mag.
D-3		"	13.5	5.0	71.5	Liq.
D-4		"	21.0	3.3	65.7	Liq.
D-5		"	28.5	1.4	60.1	Liq.
D-6		"	36.5	0.8	52.7	Liq.
D-7		"	40.0	n.a.	n.a.	Liq.+C_2S
D-8	$\frac{O_2}{N_2} = \frac{5}{95}$	$10^{-1.301}$	13.5	10.5	66.0	Liq.
D-9		"	21.0	8.0	61.0	Liq.
D-10		"	28.5	4.0	57.5	Liq.
D-11		"	36.4	2.2	51.4	Liq.
D-12	Pure CO_2	$10^{-2.896}$	0.0	29.0	61.0	Liq.+Mag.
D-13		"	5.0	25.3	59.7	Liq.+Mag.
D-14		"	13.5	19.0	57.5	Liq.
D-15		"	21.3	11.6	57.1	Liq.
D-16		"	28.5	7.3	53.2	Liq.
D-17		"	36.7	4.5	48.2	Liq.
D-18		"	40.0	3.2	47.8	Liq.+C_2S

(Table V continued, 10% SiO_2, 1450°C)

Sample No.	Gas Mixture	Po_2 (atm.)	Composition of Samples After Equilibration (wt%) CaO	FeO	Fe_2O_3	Stable Condensed Phase(s)
D-19	$\frac{CO_2}{CO}$ = 156	$10^{-3.70}$	0.0	31.0	59.0	Liq.+Mag.
D-20		"	6.0	36.0	48.0	Liq.+Mag. (m)
D-21		"	13.3	30.0	46.7	Liq.
D-22		"	21.0	21.0	48.0	Liq.
D-23		"	28.5	15.5	46.0	Liq.
D-24		"	36.5	10.5	43.0	Liq.
D-25	$\frac{CO_2}{CO}$ = 34.9	$10^{-5.0}$	0.0	57.0	33.0	Liq.
D-26		"	6.3	48.0	35.7	Liq.
D-27		"	13.9	37.1	39.0	Liq.
D-28		"	21.3	28.7	35.0	Liq.
D-29		"	29.2	20.7	35.1	Liq.
D-30		"	37.1	15.3	37.6	Liq.+C_2S (m)
D-31		"	40.0	n.a.	n.a.	Liq.+C_2S
D-32	$\frac{CO_2}{CO}$ 3.49	$10^{-7.0}$	0.0	69.0	21.0	Liq.
D-33		"	6.0	59.8	24.2	Liq.
D-34		"	13.3	50.0	26.7	Liq.
D-35		"	21.0	39.2	29.8	Liq.
D-36		"	28.5	31.5	30.0	Liq.
D-37		"	36.5	25.0	28.5	Liq.+C_2S
D-38	$\frac{CO_2}{CO}$ = .35	$10^{-9.0}$	0.0	85.0	5.0	Liq.
D-39		"	6.0	74.0	10.0	Liq.
D-40		"	13.3	63.0	13.7	Liq.

(Table V continued, 10% SiO_2, 1450°C)

Sample No.	Gas Mixture	Po_2 (atm.)	Composition of Samples After Equilibration (wt%) CaO	FeO	Fe_2O_3	Stable Condensed Phase(s)
D-41		$10^{-9.0}$	21.0	52.0	17.0	Liq.
D-42		"	36.5	36.0	17.5	Liq.+C_2S
D-43	$\frac{CO_2}{CO}$ = .223	$10^{-9.39}$	0.0	86.5	4.0	Liq.+Fe(s) (m)
D-44	$\frac{CO_2}{CO}$ = .213	$10^{-9.43}$	10.0	73.0	7.0	Liq.+Fe(s) (m)
D-45	$\frac{CO_2}{CO}$ = .247	$10^{-9.30}$	28.0	n.a.	n.a.	Liq.+C_2S (m)
D-46	$\frac{CO_2}{CO}$ = .156	$10^{-9.70}$	20.0	n.a.	n.a.	Liq.+Fe(s)

TABLE VI

Summary of Results Obtained in Quenching Experiments in the 20% Silica Section of the System $CaO-FeO-Fe_2O_3-SiO_2$ at 1450°C

Sample No.	Gas Mixture	Po_2 (atm.)	Composition of Samples After Equilibration (wt%) CaO	FeO	Fe_2O_3	Stable Condensed Phase(s)
E-1	Pure O_2	10^0	5.0	10.1	64.9	Liq.+Mag.
E-2		"	12.0	8.3	59.7	Liq.
E-3		"	21.0	4.8	54.2	Liq.
E-4		"	27.5	2.3	51.2	Liq.
E-5		"	34.3	1.6	44.1	Liq.
E-6		"	37.0	0.6	42.4	Liq.+C_2S (m)
E-7	$\frac{O_2}{N_2} = \frac{5}{95}$	$10^{-1.301}$	12.0	14.5	53.5	Liq.
E-8		"	21.0	9.2	49.8	Liq.
E-9		"	27.5	6.7	45.8	Liq.
E-10		"	34.3	4.0	41.7	Liq.
E-11		"	36.0	n.a.	n.a.	Liq.
E-12	Pure CO_2	$10^{-2.896}$	0.0	34.0	46.0	Liq.+Mag. (m)
E-13		"	2.0	31.3	46.7	Liq.+Mag. (m)
E-14		"	5.1	27.4	47.5	Liq.
E-15		"	12.0	21.1	46.9	Liq.
E-16		"	21.0	14.0	45.0	Liq.
E-17		"	27.5	10.8	41.7	Liq.
E-18		"	34.5	7.0	38.5	Liq.
E-19		"	37.0	n.a.	n.a.	Liq.+C_2S

(Table VI continued, 20% SiO_2, 1450°C)

Sample No.	Gas Mixture	Po_2 (atm.)	Composition of Samples After Equilibration (wt%) CaO	FeO	Fe_2O_3	Stable Condensed Phase(s)
E-20	$\frac{CO_2}{CO}$ = 156	$10^{-3.70}$	0.0	45.0	35.0	Liq.
E-21		"	5.2	40.0	34.8	Liq.
E-22		"	12.0	31.6	36.4	Liq.
E-23		"	21.0	23.0	36.0	Liq.
E-24		"	27.8	17.1	35.1	Liq.
E-25		"	34.3	13.0	32.7	Liq.
E-26		"	37.2	11.3	31.5	Liq.+C_2S
E-27	$\frac{CO_2}{CO}$ = 34.9	$10^{-5.0}$	0.0	55.0	25.0	Liq.
E-28		"	5.3	47.7	27.0	Liq.
E-29		"	12.2	39.4	28.4	Liq.
E-30		"	21.6	30.1	28.3	Liq.
E-31		"	27.5	24.5	28.0	Liq.
E-32		"	34.5	18.7	26.8	Liq.
E-33	$\frac{CO_2}{CO}$ = 3.49	$10^{-7.0}$	0.0	67.0	13.0	Liq.
E-34		"	5.3	59.0	15.7	Liq.
E-35		"	12.2	49.5	18.3	Liq.
E-36		"	22.1	38.7	19.2	Liq.
E-37		"	28.0	33.0	19.0	Liq.
E-38		"	37.2	26.5	16.3	Liq.+C_2S
E-39	$\frac{CO_2}{CO}$ = .35	$10^{-9.0}$	0.0	77.5	2.5	Liq.
E-40		"	5.0	69.5	5.5	Liq.
E-41		"	12.8	57.4	9.8	Liq.

(Table VI continued, 20% SiO_2, 1450°C)

Sample No.	Gas Mixture	Po_2 (atm.)	Composition of Samples After Equilibration (wt%) CaO	FeO	Fe_2O_3	Stable Condensed Phase(s)
E-42		$10^{-9.0}$	22.0	47.0	11.0	Liq.
E-43		"	28.0	41.0	11.0	Liq.
E-44		"	34.2	36.0	9.8	Liq.+C_2S
E-45	$\frac{CO_2}{CO}$ = .19	$10^{-9.53}$	0.0	∿78.5	1.5	Liq.+Fe(s)(m)
E-46	$\frac{CO_2}{CO}$ = .175	$10^{-9.60}$	15.0	59.0	6.0	Liq.+Fe(s)(m)
E-47	$\frac{CO_2}{CO}$ = .147	$10^{-9.75}$	30.0	n.a.	n.a.	Liq.+Fe(s)(m)

TABLE VII

Summary of Results Obtained in Quenching Experiments in the 30% Silica Section of the System $CaO-FeO-Fe_2O_3-SiO_2$ at 1450°C

Sample No.	Gas Mixture	Po_2 (atm.)	Composition of Samples After Equilibration (wt%) CaO	FeO	Fe_2O_3	Stable Condensed Phase(s)
F-1	Pure O_2	10°	5.0	13.7	51.3	Liq.+SiO_2 (t)
F-2		"	18.0	5.5	46.5	Liq.
F-3		"	29.0	2.3	38.7	Liq.
F-4		"	38.7	1.8	29.5	Liq.
F-5		"	42.5	1.5	26.0	Liq.
F-6		"	45.0	1.5	23.5	Liq.+C_2S
F-7	$\frac{O_2}{N_2} = \frac{5}{95}$	$10^{-1.301}$	10.5	15.0	44.5	Liq.+SiO_2 (t)
F-8		"	18.0	11.0	41.0	Liq.
F-9		"	28.7	7.3	34.0	Liq.
F-10		"	38.7	4.1	27.2	Liq.
F-11		"	42.5	3.0	24.5	Liq.
F-12	Pure CO_2	$10^{-2.896}$	0.0	33.0	37.0	Liq.+SiO_2 (t)
F-13		"	5.2	27.3	37.5	Liq.+SiO_2 (t)
F-14		"	10.4	23.0	36.6	Liq.
F-15		"	18.0	17.5	34.5	Liq.
F-16		"	29.0	11.0	30.0	Liq.
F-17		"	39.1	6.0	24.9	Liq.
F-18		"	42.7	4.8	22.5	Liq.

(Table VII continued, 30% SiO_2, 1450°C)

Sample No.	Gas Mixture	Po_2 (atm.)	Composition of Samples After Equilibration (wt%) CaO	FeO	Fe_2O_3	Stable Condensed Phase(s)
F-19	$\frac{CO_2}{CO}$ = 156	$10^{-3.70}$	0.0	43.4	26.6	Liq.
F-20		"	10.2	33.8	26.0	Liq.
F-21		"	18.0	27.6	24.4	Liq.
F-22		"	28.7	17.5	23.8	Liq.
F-23		"	38.7	11.4	19.9	Liq.
F-24		"	45.0	9.0	16.0	Liq.+C_2S
F-25	$\frac{CO_2}{CO}$ = 34.9	$10^{-5.0}$	0.0	51.0	19.0	Liq.
F-26		"	5.0	46.0	19.0	Liq.
F-27		"	10.6	38.4	21.0	Liq.
F-28		"	18.0	32.7	19.3	Liq.
F-29		"	28.7	23.2	18.0	Liq.
F-30		"	38.7	15.4	15.9	Liq.
F-31	$\frac{CO_2}{CO}$ = 3.49	$10^{-7.0}$	0.0	60.5	9.5	Liq.
F-32		"	10.6	48.7	11.7	Liq.
F-33		"	18.0	40.0	12.0	Liq.
F-34		"	28.7	30.0	11.3	Liq.
F-35		"	38.7	20.0	11.3	Liq.
F-36		"	42.5	n.a.	n.a.	Liq.+C_2S
F-37	$\frac{CO_2}{CO}$ = .35	$10^{-9.0}$	0.0	68.0	2.0	Liq.
F-38		"	10.6	54.0	5.4	Liq.
F-39		"	18.0	46.5	5.5	Liq.
F-40		"	28.7	36.0	5.3	Liq.

(Table VII continued, 30% SiO_2, 1450°C)

Sample No.	Gas Mixture	Po_2 (atm.)	Composition of Samples After Equilibration (wt%) CaO	FeO	Fe_2O_3	Stable Condensed Phase(s)
F-41		$10^{-9.0}$	38.7	25.6	5.7	Liq.
F-42		"	42.5	23.5	5.0	Liq.+C_2S
F-43	$\frac{CO_2}{CO}$ = .147	$10^{-9.75}$	0.0	69.0	∿1.0	Liq.+Fe(s)(m)
F-44	$\frac{CO_2}{CO}$ = .135	$10^{-9.825}$	16.0	52.0	2.0	Liq.+Fe(s)(m)
F-45	$\frac{CO_2}{CO}$ = .127	$10^{-9.878}$	30	37.5	2.5	Liq.+Fe(s)(m)
F-46	$\frac{CO_2}{CO}$ = .111	10^{-10}	36.5	30.8	2.2	Liq.+Fe(s)(m)

TABLE VIII

Summary of Results Obtained in Quenching Experiments in the 5% Silica Section of the System $CaO-FeO-Fe_2O_3-SiO_2$ at 1550°C

Sample No.	Gas Mixture	Po_2 (atm.)	Composition of Samples After Equilibration (wt%) CaO	FeO	Fe_2O_3	Stable Condensed Phase(s)
G-1	Pure O_2	10^{0}	0.0	21.7	73.3	Liq.+Mag.
G-2		"	10.3	12.7	72.0	Liq.
G-3		"	30.0	3.2	61.8	Liq.
G-4		"	43.0	1.0	51.0	Liq.
G-5		"	49.0	0.5	45.5	Liq.
G-6		"	52.0	0.6	42.4	Liq.+CaO (ss)
G-7	$\frac{O_2}{N_2} = \frac{1}{99}$	$10^{-2.0}$	0.0	34.0	61.0	Liq.+Mag.
G-8		"	10.0	23.0	62.0	Liq.
G-9		"	20.0	16.0	59.0	Liq.
G-10		"	31.2	9.3	54.5	Liq.
G-11		"	43.0	4.7	46.3	Liq.
G-12		"	49.0	1.0	45.0	Liq.+CaO (ss)
G-13	$\frac{CO_2}{CO} = 74.5$	$10^{-3.40}$	0.0	45.0	50.0	Liq.
G-14		"	4.0	41.0	50.0	Liq.
G-15		"	15.0	29.0	51.0	Liq.
G-16		"	30.0	16.0	49.0	Liq.
G-17		"	43.0	8.0	44.0	Liq.
G-18		"	47.0	6.0	42.0	Liq.

(Table VIII continued, 5% SiO_2, 1550°C)

Sample No.	Gas Mixture	Po_2 (amt.)	Composition of Samples After Equilibration (wt%) CaO	FeO	Fe_2O_3	Stable Condensed Phase(s)
G-19	$\frac{CO_2}{CO}$ = 20.5	$10^{-4.52}$	0.0	59.0	36.0	Liq.
G-20		"	4.0	54.4	36.6	Liq.
G-21		"	14.0	42.0	39.0	Liq.
G-22		"	31.2	24.2	39.6	Liq.
G-23		"	47.0	13.0	35	Liq.
G-24		"	52.0	10.2	32.8	Liq.+CaO (ss)
G-25	$\frac{CO_2}{CO}$ = 4.0	$10^{-5.94}$	0.0	73.5	21.5	Liq.
G-26		"	4.0	68.9	22.1	Liq.
G-27		"	14.0	54.6	26.4	Liq.
G-28		"	31.2	34.0	30.0	Liq.
G-29		"	43.0	22.0	30.0	Liq.
G-30		"	47.0	20.0	28.0	Liq.
G-31	$\frac{CO_2}{CO}$ = .298	$10^{-8.194}$	0.0	95.5	4.5	Liq.
G-32		"	14.0	68.0	13.0	Liq.
G-33		"	31.0	45.4	18.5	Liq.
G-34		"	43.0	34.0	18.0	Liq.

TABLE IX

Summary of Results Obtained in Quenching Experiments in the 10% Silica Section of the System $CaO-FeO-Fe_2O_3-SiO_2$ at 1550°C

Sample No.	Gas Mixture	Po_2 (atm.)	Composition of Samples After Equilibration (wt%) CaO	FeO	Fe_2O_3	Stable Condensed Phase(s)
H-1	Pure O_2	10^{0}	0.0	20.0	70.0	Liq.
H-2		"	8.0	13.9	68.1	Liq.
H-3		"	21.0	7.4	61.6	Liq.
H-4		"	28.5	4.8	56.7	Liq.
H-5		"	36.5	2.6	50.9	Liq.
H-6		"	42.5	1.4	46.1	Liq.
H-7		"	50.2	0.3	39.5	Liq.+C_2S
H-8	$\frac{O_2}{N_2} = \frac{1}{99}$	$10^{-2.0}$	0.0	34.0	56.0	Liq.
H-9		"	8.2	26.3	55.5	Liq.
H-10		"	21.0	16.3	52.7	Liq.
H-11		"	28.4	11.3	50.3	Liq.
H-12		"	36.5	6.7	46.8	Liq.
H-13		"	42.5	4.1	43.5	Liq.
H-14		"	50.0	2.0	38.0	Liq.+C_2S
H-15	$\frac{CO_2}{CO} = 74.5$	$10^{-3.40}$	0.0	48.5	41.5	Liq.
H-16		"	8.0	39.0	43.0	Liq.
H-17		"	21.0	26.3	42.7	Liq.
H-18		"	28.0	20.3	41.7	Liq.
H-19		"	36.5	13.7	39.8	Liq.

(Table IX continued, 10% SiO_2, 1550°C)

Sample No.	Gas Mixture	P_{O_2} (atm.)	Composition of Samples After Equilibration (wt%) CaO	FeO	Fe_2O_3	Stable Condensed Phase(s)
H-20		"	42.6	9.9	37.5	Liq.
H-21	$\frac{CO_2}{CO} = 20.5$	$10^{-4.52}$	0.0	60.0	30.0	Liq.
H-22		"	8.0	50.5	31.5	Liq.
H-23		"	21.0	36.0	33.0	Liq.
H-24		"	28.5	28.7	32.8	Liq.
H-25		"	36.5	21.8	31.7	Liq.
H-26		"	42.8	17.0	30.2	Liq.
H-27	$\frac{CO_2}{CO} = 4.0$	$10^{-5.94}$	0.0	72.0	18.0	Liq.
H-28		"	8.0	61.0	21.0	Liq.
H-29		"	18.0	49.2	22.8	Liq.
H-30		"	28.5	38.2	23.3	Liq.
H-31		"	36.5	30.0	23.5	Liq.
H-32		"	42.7	25.5	21.8	Liq.+C_2S
H-33	$\frac{CO_2}{CO} = .298$	$10^{-8.194}$	0.0	85.0	5.0	Liq.
H-34		"	13.5	65.0	11.5	Liq.
H-35		"	28.0	46.5	15.5	Liq.
H-36		"	36.5	37.5	16.0	Liq.

TABLE X

Summary of Results Obtained in Quenching Experiments at 20% Silica Section of the System $CaO-FeO-Fe_2O_3-SiO_2$ at 1550 °C

Sample No.	Gas Mixture	Po_2 (atm.)	Composition of Samples After Equilibration (wt%) CaO	FeO	Fe_2O_3	Stable Condensed Phase(s)
I-1	Pure O_2	10^{0}	0.0	19.1	60.9	Liq.
I-2		"	5.0	15.4	59.6	Liq.
I-3		"	12.0	11.8	56.2	Liq.
I-4		"	21.0	7.5	51.5	Liq.
I-5		"	27.5	5.3	47.2	Liq.
I-6		"	34.3	3.9	41.8	Liq.
I-7		"	39.0	2.3	38.7	Liq.
I-8	$\frac{O_2}{N_2} = \frac{1}{99}$	$10^{-2.0}$	0.0	34.1	45.9	Liq.
I-9		"	5.0	29.5	44.5	Liq.
I-10		"	12.0	24.2	43.8	Liq.
I-11		"	20.7	17.0	42.3	Liq.
I-12		"	27.5	12.7	39.8	Liq.
I-13		"	34.0	10.1	35.9	Liq.
I-14		"	39.0	7.1	33.9	Liq.+C_2S
I-15	$\frac{CO_2}{CO} = 74.5$	$10^{-3.40}$	0.0	49.2	30.6	Liq.
I-16		"	5.0	42.5	32.5	Liq.
I-17		"	12.0	33.6	34.4	Liq.
I-18		"	20.0	27.5	32.5	Liq.
I-19		"	27.5	21.0	31.5	Liq.

(Table X continued, 20% SiO_2, 1550°C)

Sample No.	Gas Mixture	Po_2 (atm.)	Composition of Samples After Equilibration (wt%) CaO	FeO	Fe_2O_3	Stable Condensed Phase(s)
I-20		$10^{-3.40}$	34.0	16.1	29.9	Liq.
I-21		"	39.0	12.0	29.0	Liq.+C_2S
I-22	$\frac{CO_2}{CO}$ = 20.5	$10^{-4.52}$	0.0	58.5	21.5	Liq.
I-23		"	12.0	44.0	24.0	Liq.
I-24		"	20.0	35.3	23.7	Liq.
I-25		"	27.5	27.6	24.9	Liq.
I-26		"	39.0	19.0	22.0	Liq.+C_2S
I-27	$\frac{CO_2}{CO}$ = 4.0	$10^{-5.94}$	0.0	70.5	9.5	Liq.
I-28		"	5.0	65.0	10.0	Liq.
I-29		"	12.0	54.0	14.0	Liq.
I-30		"	21.0	41.3	17.7	Liq.
I-31		"	27.5	35.7	16.3	Liq.
I-32		"	34.3	28.1	17.6	Liq.
I-33	$\frac{CO_2}{CO}$ = .298	$10^{-8.194}$	0.0	78.0	2.0	Liq.
I-34		"	13.3	60.5	6.2	Liq.
I-35		"	21.0	50.5	8.5	Liq.
I-36		"	27.5	42.0	10.5	Liq.

TABLE XI

Summary of Results Obtained in Quenching Experiments in the 30% Silica Section of the System $CaO-FeO-Fe_2O_3-SiO_2$ at 1550°C

Sample No.	Gas Mixture	Po_2 (atm.)	Composition of Samples After Equilibration (wt%) CaO	FeO	Fe_2O_3	Stable Condensed Phase(s)
J-1	Pure O_2	10^0	0.0	17.4	52.6	Liq.+SiO_2 (c)
J-2		"	5.0	16.9	48.1	Liq.+SiO_2 (c)
J-3		"	10.6	14.5	44.9	Liq.
J-4		"	18.0	10.8	41.2	Liq.
J-5		"	28.7	5.2	36.1	Liq.
J-6		"	38.7	3.2	28.1	Liq.
J-7		"	45.0	1.4	23.6	Liq.+C_2S (m)
J-8	$\frac{O_2}{N_2} = \frac{1}{99}$	$10^{-2.0}$	0.0	33.0	37.0	Liq.
J-9		"	10.5	24.5	35.0	Liq.
J-10		"	18.0	19.4	32.6	Liq.
J-11		"	28.7	11.5	29.8	Liq.
J-12		"	38.7	6.0	25.3	Liq.
J-13		"	45.0	4.4	20.6	Liq.+C_2S (m)
J-14	$\frac{CO_2}{CO} = 74.5$	$10^{-3.40}$	0.0	47.2	22.8	Liq.
J-15		"	10.6	37.0	22.4	Liq.
J-16		"	18.0	30.8	21.2	Liq.
J-17		"	30.0	19.6	20.4	Liq.
J-18		"	38.7	12.8	18.5	Liq.
J-19		"	45.0	8.6	16.4	Liq.

(Table XI continued, 30% SiO_2, 1550°C)

Sample No.	Gas Mixture	Po_2 (atm.)	Composition of Samples After Equilibration (wt%) CaO	FeO	Fe_2O_3	Stable Condensed Phase(s)
J-20	$\frac{CO_2}{CO}$ = 20.5	$10^{-4.52}$	0.0	56	14.0	Liq.
J-21		"	10.5	45	14.5	Liq.
J-22		"	18.0	37.5	14.5	Liq.
J-23		"	28.7	27.3	14.0	Liq.
J-24		"	38.7	18.3	13.0	Liq.
J-25		"	45.0	n.a.	n.a.	Liq.+C_2S
J-26	$\frac{CO_2}{CO}$ = 4.0	$10^{-5.94}$	0.0	64.0	6.0	Liq.
J-27		"	10.2	53.4	6.4	Liq.
J-28		"	19.0	44.0	7.0	Liq.
J-29		"	28.7	34.5	6.8	Liq.
J-30		"	38.7	24.3	7.0	Liq.
J-31		"	42.0	21.5	6.5	Liq.
J-32	$\frac{CO_2}{CO}$ = .298	$10^{-8.194}$	0.0	68.5	1.5	Liq.
J-33		"	10.0	58.0	2.0	Liq.
J-34		"	25.0	42.5	2.5	Liq.
J-35		"	35.0	32.2	2.8	Liq.
J-36		"	43.0	n.a.	n.a.	Liq.+C_2S

TABLE XII

1550°C Data Along the Liquid Iron + Liquid Oxide Boundary

A. $CaO-FeO-Fe_2O_3$ System (From Larson and Chipman)

P_{O_2} (atm.)	Composition (wt%)		
	CaO	FeO	Fe_2O_3
$10^{-8.544}$	0.0	96.0	4.0
$10^{-8.634}$	11.0	80.0	9.0
$10^{-8.75}$	20.0	67.0	13.0
$10^{-9.146}$	37.5	45.0	17.5

B. $CaO-FeO-Fe_2O_3-SiO_2$ System (From Extrapolations between this work and Taylor and Chipman)

P_{O_2} (atm.)	Composition (wt%)			
	CaO	FeO	Fe_2O_3	SiO_2
$10^{-8.56}$	0.0	97.0	3.0	5.0
$10^{-8.62}$	10.0	78.0	7.0	5.0
$10^{-8.89}$	25.0	60.0	10.0	5.0
$10^{-9.34}$	42.0	41.0	12.0	5.0
$10^{-8.616}$	0.0	87.0	3.0	10.0
$10^{-8.626}$	10.0	75.0	5.0	10.0
$10^{-8.676}$	20.0	63.0	7.0	10.0
$10^{-8.782}$	32.0	51.0	7.0	10.0

Part B (Table XII continued, 1550°C)

Po_2 (atm.)	Composition (wt%)			
	CaO	FeO	Fe_2O_3	SiO_2
$10^{-8.794}$	0.0	79.0	1.0	20
$10^{-8.796}$	25.0	50.0	5.0	20
$10^{-8.854}$	35.0	39.0	6.0	20
$10^{-8.99}$	0.0	69.5	0.5	30
$10^{-9.0}$	30.0	38.5	1.5	30
$10^{-9.11}$	41.5	27.0	1.5	30

APPENDIX III

THE RESULTS OF ACTIVITY CALCULATIONS IN THE $CaO-FeO-Fe_2O_3$ SYSTEM

The results of activity calculations in the CaO-FeO-Fe_2O_3 system at 1450°C and 1550°C are presented in Tables XIII and XIV respectively. Each table is divided into two main parts. Part A contains the $\log a_{Fe}$ values obtained from graphical integration of equation (12); and "FeO" activities calculated from equation (13). (See page 64.)

The first portion of Part B contains the $\log a^{II}_{CaO}$ values obtained from integration of equation (14). The second portion tabulates the CaO activities calculated with the aid of equation (15) along various iso-oxygen activities.

In both tables the tangent-intercept values of $\left[\frac{\partial no}{\partial n_{Fe}}\right]$ are given. a_o and %CaO values corresponding to each measured intercept are also listed. Similarly $\left[\frac{\partial no}{\partial n_{CaO}}\right]$ values obtained from tangent-intercepts along CaO-O side of CaO-Fe-O composition triangle are included in the first portions of Part B.

Abbreviation: "n.m." refers to unmeasured intercepts.

TABLE XIII

Results of Activity Calculations in the $CaO-FeO-Fe_2O_3$ System at 1450°C

Part A

$n_{Fe}:n_{CaO}$	%CaO	$-\log a_O$	$(\partial n_O/\partial n_{Fe})$	$-\log a_{Fe}$	$a_{"FeO"}$
1.29	35.2	0.000	1.465	6.223	.03
	35.4	1.448	1.380	4.143	.12
	35.6	1.850	1.310	3.608	.16
	35.9	2.500	1.230	2.787	.23
	36.3	3.500	1.175	1.595	.36
	36.8	4.500	1.124	0.448	.51
	36.9	4.653	1.075	0.276	.53
	37.0	4.898	n.m.	0.0	.57
1.70	29.2	0.000	1.460	6.129	0.34
	29.4	1.448	1.375	4.059	.14
	29.6	1.850	1.310	3.523	.19
	29.9	2.500	1.240	2.698	.29
	30.3	3.500	1.170	1.506	.44
	30.7	4.500	1.090	0.381	.59
	30.8	4.653	1.060	0.193	.65
	30.9	4.830	n.m.	0.0	.67
2.20	24.2	0.000	1.460	6.036	.04
	24.4	1.448	1.370	3.966	.17
	24.6	1.850	1.295	3.430	.24
	24.8	2.500	1.240	2.603	.35

Part A (Table XIII continued, 1450°C)

$n_{Fe}:n_{CaO}$	%CaO	$-\log a_O$	$(\partial n_O/\partial n_{Fe})$	$-\log a_{Fe}$	$a_{"FeO"}$
2.20	25.2	3.500	1.160	1.406	.56
	25.5	4.500	1.075	.294	.72
	25.6	4.653	1.050	.191	.74
	25.7	4.777	n.m.	0.0	.75
2.92	19.4	0.000	1.430	5.880	.06
	19.6	1.448	1.350	3.870	.23
	19.8	1.850	1.280	3.346	.29
	20.0	2.500	1.220	2.534	.42
	20.3	3.500	1.140	1.354	.63
	20.6	4.500	1.060	0.254	.79
	20.7	4.653	1.045	0.092	.82
	20.7	4.740	n.m.	0.0	.82
4.20	14.4	0.000	1.425	5.847	.07
	14.6	1.448	1.350	3.837	.23
	14.7	1.850	1.275	3.312	.31
	14.9	2.500	1.220	2.502	.45
	15.1	3.500	1.140	1.330	.67
	15.3	4.500	1.060	0.225	.85
	15.4	4.653	1.045	0.061	.88
	15.4	4.710	n.m.	0.0	.88

Part A (Table XIII continued, 1450°C)

$n_{Fe}:n_{CaO}$	%CaO	-log a_O	$(\partial n_O/\partial n_{Fe})$	-log a_{Fe}	$a_{"FeO"}$
6.75	9.8	1.850	1.270	3.251	.35
	9.9	2.500	1.220	2.441	.52
	10.0	3.500	1.135	1.271	.76
	10.2	4.500	1.055	0.189	.92
	10.2	4.653	1.035	0.128	.94
	10.2	4.680	n.m.	0	.94

Part B

1.) a_{CaO}^{II} values from integration of equation (14) along $n_{Fe}:n_{CaO} = 1.29$

%CaO	-log a_O	$(\partial n_O/\partial n_{CaO})$	log a_{CaO}^{II}	a_{CaO}^{II}
35.2	0.000	.040	-.5190	.3
35.4	1.448	.110	-.4150	.39
35.6	1.850	.145	-.3636	.43
35.9	2.500	.170	-.2571	.55
36.3	3.500	.116	-.1111	.77
36.8	4.500	.063	-.0231	.95
36.9	4.653	.095	-.0135	.97
37.0	4.898	n.m.	0.0	1.0

Part B (Table XIII continued, 1450°C)

2.) CaO activities from integration of equation (15) along various iso-oxygen activities

$\log a_O$	%CaO	n_{Fe}/n_{CaO}	$-\log a_{Fe}$	$-\log a_{CaO}$	a_{CaO}
0	35.2	1.29	6.223	.519	.3
	29.2	1.70	6.129	.660	.22
	24.2	2.20	6.036	.8385	.15
	19.4	2.92	5.880	1.2365	.06
	14.4	4.20	5.847	1.3355	.046
-1.448	35.4	1.29	4.143	.415	.39
	29.4	1.70	4.059	.541	.29
	24.4	2.20	3.966	.722	.19
	19.6	2.92	3.870	.966	.11
	14.6	4.20	3.837	1.326	.05
-1.850	35.6	1.29	3.608	.3636	.43
	29.6	1.70	3.523	.4866	.33
	24.6	2.20	3.430	.6606	.22
	19.8	2.92	3.346	.8866	.13
	14.7	4.20	3.312	1.0116	.1
	9.8	6.75	3.251	1.3316	.05
-2.500	35.9	1.29	2.787	.2571	.55
	29.9	1.70	2.698	.3905	.41
	24.8	2.20	2.603	.5665	.27
	20.0	2.92	2.534	.7365	.18
	14.9	4.20	2.502	.8455	.14
	9.9	6.75	2.441	1.1655	.07

Part B (Table XIII continued, 1450°C)

$\log a_O$	%CaO	n_{Fe}/n_{CaO}	$-\log a_{Fe}$	$-\log a_{CaO}$	a_{CaO}
-3.500	36.3	1.29	1.595	.1111	.77
	30.3	1.70	1.506	.2311	.59
	25.2	2.20	1.406	.4051	.39
	20.3	2.92	1.354	.5371	.29
	15.1	4.20	1.330	.6236	.24
	10.0	6.75	1.271	.9336	.12
-4.653	36.9	1.29	.275	.0135	.97
	30.8	1.70	.193	.1325	.74
	25.6	2.20	.131	.2485	.56
	20.7	2.92	.092	.3460	.45
	15.4	4.20	.061	.4545	.35
	10.2	6.75	.028	.6285	.23

TABLE XIV

Results of Activity Calculations in the $CaO-FeO-Fe_2O_3$ System at 1550°C

Part A

$n_{Fe}:n_{CaO}$	%CaO	$-\log a_O$	$(\partial n_O/\partial n_{Fe})$	$-\log a_{Fe}$	$a_{"FeO"}$
1.318	34.7	0.000	1.442	5.666	.04
	35.0	1.000	1.333	4.280	.1
	35.2	1.700	1.284	3.369	.16
	35.5	2.260	1.228	2.667	.22
	35.8	2.970	1.186	1.808	.31
	36.1	4.097	1.113	0.515	.46
	36.4	4.573	1.053	0.0	.5
1.766	28.5	0.000	1.414	5.515	.06
	28.8	1.000	1.327	4.150	.13
	29.0	1.700	1.274	3.248	.21
	29.2	2.260	1.206	2.553	.29
	29.5	2.970	1.166	1.704	.40
	29.7	4.097	1.103	0.429	.56
	30.0	4.485	1.043	0.0	.60
2.28	23.6	0.000	1.414	5.443	.07
	23.9	1.000	1.334	4.059	.16
	24.1	1.700	1.270	3.148	.27
	24.3	2.260	1.214	2.452	.36
	24.6	2.970	1.136	1.607	.50
	24.8	4.097	1.075	0.353	.66
	25.0	4.434	1.030	0	.69

Part A (Table XIV continued, 1550°)

$n_{Fe}:n_{CaO}$	%CaO	-log a_O	$(\partial n_O/\partial n_{Fe})$	-log a_{Fe}	$a_{"FeO"}$
3.05	18.8	0.000	1.415	5.3685	.08
	19.0	1.000	1.317	4.001	.19
	19.0	1.700	1.266	3.100	.30
	19.2	2.260	1.206	2.411	.40
	19.6	2.970	1.145	1.576	.53
	19.8	4.097	1.077	0.303	.74
	20.0	4.382	n.m.	0	.78
4.34	14.0	0.000	1.410	5.2865	.10
	14.3	1.000	1.318	3.914	.23
	14.4	1.700	1.280	3.009	.37
	14.5	2.260	1.205	2.320	.50
	14.7	2.970	1.139	1.499	.64
	14.9	4.097	1.057	0.257	.83
	15.0	4.344	n.m.	0.0	.85
6.915	9.4	0.000	1.386	5.218	.11
	9.5	1.000	1.311	3.859	.26
	9.6	1.700	1.258	2.964	.41
	9.7	2.260	1.196	2.281	.54
	9.8	2.970	1.128	1.457	.70
	10.0	4.097	1.052	0.225	.89
	10.0	4.315	n.m.	0.0	.90
14.65	4.6	0.000	1.363	5.185	.12
	4.7	1.000	1.304	3.836	.27
	4.8	1.700	1.252	2.944	.42
	4.9	2.970	1.134	1.434	.74

Part A (Table XIV continued, 1550°C)

$n_{Fe}:n_{CaO}$	%CaO	-log a_O	$(\partial n_O/\partial n_{Fe})$	-log a_{Fe}	$a_{"FeO"}$
14.65	5.0	4.097	1.044	0.201	.94
∞	0.0	1.700	1.250	2.904	.48
	0.0	2.260	1.190	2.219	.62
	0.0	2.970	1.124	1.396	.80
	0.0	4.097	1.036	0.178	.99
	0.0	4.272	1.018	0.0	1.00

Part B

1.) a_{CaO}^{II} values from integration of equation (14) along $n_{Fe}:n_{CaO} = 1.318$

%CaO	-log a_O	$(\partial n_O/\partial n_{CaO})$	log a_{CaO}^{II}	a_{CaO}^{II}
34.7	0.000	0.067	-.5797	.264
35.0	1.000	0.144	-.4632	.344
35.2	1.700	0.147	-.3612	.435
35.5	2.260	0.139	-.2805	.525
35.8	2.970	0.096	-.1861	.65
36.1	4.097	0.112	-.0531	0.89
36.4	4.573	0.113	0.0	1.0

Part B (Table XIV continued, 1550°C)

2.) CaO activities from integration of equation (15) along various iso-oxygen activities

$\log a_O$	%CaO	n_{Fe}/n_{CaO}	$-\log a_{Fe}$	$-\log a_{CaO}$	a_{CaO}
0	34.7	1.318	5.666	.5797	.264
	28.5	1.766	5.515	.8137	.153
	23.7	2.280	5.443	.9594	.110
	19.0	3.050	5.3685	1.1544	.070
	14.0	4.34	5.2865	1.4534	.035
	9.5	6.915	5.218	1.8344	.015
	5.0	14.65	5.185	2.1914	.007
-1.0	35.0	1.318	4.280	.4632	.344
	28.8	1.766	4.150	.6582	.22
	23.9	2.280	4.059	.8402	.15
	19.0	3.050	4.001	.9912	.10
	14.3	4.34	3.914	1.3052	.05
	9.5	6.915	3.859	1.6192	.04
	4.7	14.65	3.836	18.672	.01
-1.70	35.2	1.318	3.369	.3612	.435
	29.0	1.766	3.248	.5397	.29
	24.1	2.280	3.148	.7372	.18
	19.0	3.050	3.100	.8596	.14
	14.4	4.340	3.009	1.1966	.06
	9.6	6.915	2.964	1.4466	.04
	4.8	14.650	2.944	1.6366	.02

Part B (Table XIV continued, 1550°C)

log a_O	%CaO	n_{Fe}/n_{CaO}	-log a_{Fe}	-log a_{CaO}	a_{CaO}
-2.26	35.5	1.318	2.667	.2805	.525
	29.2	1.766	2.553	.4515	.354
	24.3	2.280	2.452	.6535	.220
	19.2	3.050	2.441	.7560	.176
	14.5	4.340	2.320	1.0560	.09
	9.7	6.915	2.281	1.263	.05
	4.8	14.650	2.261	1.465	.034
-2.97	35.8	1.318	1.808	.1861	.65
	29.5	1.766	1.704	.3422	.45
	24.6	2.280	1.607	.5407	.29
	19.6	3.050	1.576	.6228	.24
	14.7	4.340	1.499	.9038	.12
	9.8	6.915	1.457	1.2108	.06
	4.9	14.650	1.434	1.4578	.03
-4.097	36.1	1.318	.515	.0531	.89
	29.7	1.766	.429	.1778	.67
	24.8	2.280	.353	.3258	.47
	19.8	3.050	.303	.4608	.35
	14.9	4.340	.257	.6308	.23
	10.0	6.915	.225	.7988	.16
	5.0	14.650	.201	1.0408	.09

APPENDIX IV

THE RESULTS OF ACTIVITY CALCULATIONS IN THE $CaO-FeO-Fe_2O_3-SiO_2$ SYSTEM

The results of activity calculations in the $CaO-FeO-Fe_2O_3-SiO_2$ system at 1450°C and 1550°C are presented in Tables XVI and XVII respectively. Each table has three main parts, designated by 1, 2, and 3, showing, respectively the $\log a_{Fe}$ and $a_{"FeO"}$ values calculated from equations (27) and (13); the a_{SiO_2} values calculated from equation (28); and the CaO activities calculated with the aid of equation (29).

The main parts 1, 2, and 3, are divided into 4 sections, designated by A, B, C, and D, showing the results of activity calculations in 5%, 10%, 20%, and 30% silica sections of the system.

For Fe and SiO_2 activities the tangent-intercepts and the %CaO values are listed. For lime activities, the silica activities along which the integrals of equation (29) were performed are given.

Abbreviation: "n.m." refers to unmeasured intercepts.

TABLE XVI

1. Iron and Ferrous Oxide Activities in the $CaO-FeO-Fe_2O_3-SiO_2$ System at 1450°C

Part A

5% SiO_2 section

n_{CaO}/n_{SiO_2}	$-\log a_O$	$\partial n_O/\partial n_{Fe}$	$-\log a_{Fe}$	$a_{"FeO"}$	%CaO
1.072	2.500	1.20	2.435	.52	4.8
	3.500	1.12	1.269	.77	4.9
	4.500	1.055	.183	.93	5.0
	4.676	1.03	0.0	.95	5.2
2.380	1.448	1.35	3.755	.28	10.7
	1.850	1.30	3.235	.37	10.8
	2.500	1.205	2.440	.52	10.9
	3.500	1.12	1.285	.74	11.0
	4.500	1.06	.205	.89	11.2
	4.694	n.m.	0	.91	11.2
3.340	0	1.43	5.947	.05	14.6
	1.448	1.37	3.827	.24	14.7
	1.850	1.30	3.301	.32	14.7
	2.500	1.20	2.470	.48	14.8
	3.500	1.13	1.313	.69	14.9
	4.500	1.06	0.225	.85	15.0
	4.714	n.m.	0.0	.87	15.2

Part B (Table XVI continued, 1450°C)

10% SiO_2 section

n_{CaO}/n_{SiO_2}	-log a_O	$\partial n_O/\partial n_{Fe}$	-log a_{Fe}	$a_{"FeO"}$	%CaO
.578	1.850	1.275	3.290	.32	4.9
	2.500	1.190	2.432	.53	5.0
	3.500	1.125	1.278	.75	5.0
	4.500	1.040	0.201	.89	5.2
	4.694	n.m.	0.0	.91	5.3
1.072	1.448	1.350	3.817	.24	9.8
	1.850	1.260	3.287	.33	9.8
	2.500	1.210	2.477	.47	9.9
	3.500	1.140	1.307	.70	10.0
	4.500	1.055	.215	.85	10.1
	4.714	n.m.	0.0	.87	10.2
1.672	0.000	1.440	5.851	.06	14.9
	0.650	1.395	5.136	.10	15.0
	1.448	1.350	3.826	.24	15.1
	1.850	1.280	3.303	.32	15.3
	2.500	1.210	2.493	.45	15.3
	3.500	1.135	1.328	.67	15.4
	4.500	1.050	0.238	.82	15.5
	4.729	n.m.	0.0	.84	15.5

Part B (Table XVI continued, 1450°C)

n_{CaO}/n_{SiO_2}	$-\log a_O$	$\partial n_O/\partial n_{Fe}$	$-\log a_{Fe}$	$a_{"FeO"}$	%CaO
2.380	0.000	1.430	5.872	.06	21.6
	0.650	1.400	5.312	.07	21.6
	1.448	1.375	3.912	.17	21.7
	1.850	1.325	3.422	.24	21.8
	2.500	1.240	2.592	.36	21.9
	3.500	1.150	1.397	.57	22.1
	4.500	1.085	0.280	.75	22.3
	4.761	n.m.	0.0	.78	22.3
3.34	0.000	1.460	6.187	.03	28.7
	1.448	1.400	4.079	.13	29.0
	1.850	1.370	3.534	.19	29.2
	2.500	1.250	2.695	.29	29.5
	3.500	1.160	1.500	.45	29.7
	4.500	1.100	0.374	.6	30.0

Part C (Table XVI continued, 1450°C)

20% SiO_2 section

n_{CaO}/n_{SiO_2}	-log a_O	$\partial n_O/\partial n_{Fe}$	-log a_{Fe}	$a_{"FeO"}$	%CaO
.578	0.000	1.410	5.910	.06	10.1
	0.650	1.360	5.202	∿.10	10.2
	1.448	1.325	3.902	.20	10.4
	1.850	1.290	3.376	.26	10.5
	2.500	1.210	2.561	.39	10.7
	3.500	1.130	1.386	.58	10.9
	4.500	1.030	0.306	.70	11.0
	4.790	n.m.	0.0	.73	11.0
1.072	0.000	1.410	6.021	.04	19.5
	0.650	1.380	5.322	.07	19.6
	1.448	1.360	3.922	.19	19.7
	1.850	1.280	3.406	.24	19.7
	2.500	1.210	2.600	.36	19.8
	3.500	1.135	1.428	.53	19.9
	4.500	1.070	0.326	.67	20.1
	4.808	n.m.	0.0	.70	20.2
1.672	0.000	1.470	6.263	.03	30.5
	0.650	1.430	5.530	.04	30.6
	1.448	1.400	4.180	.11	30.8
	1.850	1.320	3.639	.15	30.8
	2.500	1.270	2.795	.23	30.9
	3.500	1.200	1.565	.39	31.0
	4.500	1.120	0.405	.56	31.3
	4.868	n.m.	0.0	.61	31.4

Part D (Table XVI continued, 1450°C)

30% SiO_2 section

n_{CaO}/n_{SiO_2}	$-\log a_O$	$\partial n_O/\partial n_{Fe}$	$-\log a_{Fe}$	$a_{"FeO"}$	%CaO
.578	0.000	1.410	6.087	.04	15.5
	0.650	1.390	5.367	.06	15.6
	1.448	1.350	4.057	.14	15.7
	1.850	1.280	3.535	.18	15.7
	2.500	1.220	2.725	.27	15.9
	3.500	1.140	1.548	.40	16.0
	4.500	1.075	0.438	.52	16.2
	4.913	n.m.	0.0	.55	16.4
1.072	0.000	1.470	6.258	.03	29.4
	0.650	1.450	5.542	.04	29.5
	1.448	1.410	4.202	.10	29.6
	1.850	1.340	3.660	.14	29.7
	2.500	1.270	2.811	.22	29.9
	3.500	1.185	1.599	.36	30.1
	4.500	1.105	0.477	.48	30.3
	4.937	n.m.	0.0	.52	30.6

(Table XVI continued, 1450°C)

2. Silica Activities in the System $CaO-FeO-Fe_2O_3-SiO_2$ at 1450°C

Part A

5% SiO_2 section

n_{Fe}/n_{CaO}	$-\log a_O$	$\partial n_O/\partial n_{SiO_2}$	$-\log a_{SiO_2}$	a_{SiO_2}	%CaO
6.010	0.000	∿0	2.489	.0030	10.6
	1.448	-.171	2.622	.0024	10.9
	1.850	-.179	2.689	.0020	11.0
	2.500	-.137	2.798	.0016	11.1
	3.500	+.050	2.962	.0011	11.3
	4.500	+.069	3.003	.0001	11.4
			3.000	.001	11.5
1.565	0.000	∿0	3.879	.000130	29.3
	1.448	-.022	3.901	.000125	29.6
	1.850	-.037	3.914	.000120	29.8
	2.500	-.037	3.938	.000110	30.0
	3.500	-.037	3.975	.000105	30.4
	4.500	n.m.	3.998	.00010	30.7
	4.810	n.m.	4.000	.00010	31.0

Part B (Table XVI continued, 1450°C)

10% SiO_2 section

n_{Fe}/n_{CaO}	$-\log a_O$	$\partial n_O/\partial n_{SiO_2}$	$-\log a_{SiO_2}$	a_{SiO_2}	%CaO
6.010	0.000	-.052	1.306	.050	9.5
	1.448	-.165	1.483	.033	9.7
	1.850	-.229	1.561	.028	9.8
	2.500	-.165	1.688	.020	9.9
	3.500	-.144	1.858	.014	10.1
	4.500	-.123	1.980	.01	10.2
	4.710	n.m.	2.000	.01	10.3
2.710	0.000	-.018	2.941	.00115	18.7
	1.448	-.037	3.019	.00096	18.9
	1.850	-.109	3.057	.0009	19.1
	2.500	-.102	3.115	.0008	19.3
	3.500	-.060	3.211	.0006	19.5
	4.500	-.080	3.282	.0005	19.8
	4.760	n.m.	3.206	.0006	20.0

Part C (Table XVI continued, 1450°C)

20% SiO_2 section

n_{Fe}/n_{CaO}	-log a_O	$\partial n_O/\partial n_{SiO_2}$	-log a_{SiO_2}	a_{SiO_2}	%CaO
6.010	0.000	-.109	.030	.93	8.3
	1.448	-.151	.217	.60	8.5
	1.850	-.1545	.278	.53	8.6
	2.500	-.175	.385	.41	8.7
	3.500	-.144	.645	.23	8.8
	4.500	-.102	.769	.17	9.1
	4.790	n.m.	.796	.16	9.1
2.710	0.000	+.066	.524	.30	16.7
	1.448	-.132	.681	.21	16.8
	1.850	-.179	.742	.18	16.9
	2.500	-.158	.851	.14	17.1
	3.500	-.137	1.008	∿.10	17.3
	4.500	-.088	1.120	.076	17.5
	4.808	n.m.	1.150	.07	17.8
1.565	0.000	-.091	1.4461	.036	24.9
	1.448	-.151	1.6141	.024	25.3
	1.850	-.151	1.6687	.021	25.5
	2.500	-.189	1.7830	.017	25.7
	3.500	-.198	1.9790	.001	26.0
	4.500	-.154	2.1059	.008	26.3
	4.846	n.m.	2.1550	.007	26.4

Part D (Table XVI continued, 1450°C)

30% SiO_2 section

n_{Fe}/n_{CaO}	$-\log a_O$	$\partial n_O/\partial n_{SiO_2}$	$-\log a_{SiO_2}$	a_{SiO_2}	%CaO
6.010	0.000	(Silica Saturation Field)			7.5
	1.448	-.144	.010	.98	7.7
	1.850	-.165	.064	.86	7.7
	2.500	-.179	.139	.73	7.9
	3.500	-.151	.306	.50	8.0
	4.500	-.022	.397	.40	8.0
	4.900	n.m.	.400	.40	8.0
2.710	0.000	(Silica Saturation Field)			14.4
	1.448	-.132	.004	1.01	14.6
	1.850	-.144	.045	.90	14.9
	2.500	-.174	.150	.71	15.1
	3.500	-.151	.324	.47	15.2
	4.500	-.141	.466	.34	15.4
	4.913	n.m.	.510	.31	15.6
1.565	0.000	-.066	.148	.71	21.9
	1.448	-.100	.283	.52	22.2
	1.850	-.151	.334	.46	22.5
	2.500	-.158	.427	.37	22.7
	3.500	-.137	.574	.27	23.0
	4.500	-.066	.681	.21	23.1
	4.954	n.m.	.700	.2	23.3

(Table XVI continued, 1450°C)

3. CaO Activities in the
$CaO-FeO-Fe_2O_3-SiO_2$ System at 1450°C

Part B

10% SiO_2 section

Along $a_{SiO_2} = .001$

$-\log a_O$	n_O/n_{CaO}	$-\log a_{Fe}$	n_{Fe}/n_{CaO}	a_{CaO}	%CaO
1.448	2.97	4.027	2.11	.25	22.7
1.850	2.92	3.405	2.18	.20	22.4
2.500	2.93	2.585	2.29	.16	21.8
3.500	3.00	1.404	2.49	.13	20.7
4.500	3.18	.272	2.91	.10	18.7
4.720	3.52	0.0	3.38	.08	16.7

Part C

20% SiO_2 section

Along $a_{SiO_2} = .01$

$-\log a_O$	n_O/n_{CaO}	$-\log a_{Fe}$	n_{Fe}/n_{CaO}	a_{CaO}	%CaO
0.000	1.62	6.176	1.09	.07	31.3
1.448	1.625	4.090	1.17	.06	30.4
1.850	1.65	3.481	1.24	.046	29.5
2.500	1.68	2.676	1.35	.049	28.3
3.500	1.76	1.490	1.525	.052	26.4
4.500	1.89	0.353	1.75	.052	24.3
4.822	2.01	0.0	1.91	.05	23.0

Part C (Table XVI continued, 1450°C)

2.) Along a_{SiO_2} = .1

$-\log a_O$	n_O/n_{CaO}	$-\log a_{Fe}$	n_{Fe}/n_{CaO}	a_{CaO}	%CaO
0.000	2.26	6.109	1.54		25.1
1.448	2.39	4.028	1.75		23.3
1.850	2.48	3.405	1.92		22.0
2.500	2.66	2.597	2.18	.02	20.3
3.500	2.99	1.405	2.64	.01	17.8
4.500	3.59	0.308	3.42	.006	14.7
4.796	4.12	0.0	3.98	.005	13.0

Part D

30% SiO_2 section

1.) Along a_{SiO_2} .1

$-\log a_O$	n_O/n_{CaO}	$-\log a_{Fe}$	n_{Fe}/n_{CaO}	a_{CaO}	%CaO
0.000	.704	6.653	.473	.019	41.8
1.448	.701	4.504	.511	.018	40.9
1.850	.730	3.689	.550	.013	39.8
2.500	.744	2.810	.601	.012	38.6
3.500	.752	1.634	.665	.012	37.2
4.500	.810	0.481	.770	.011	35.0
4.953	.852	0.0	.835	.010	33.7

Part D (Table XVI continued, 1450°C)

2.) Along a_{SiO_2} = .2

$-\log a_O$	n_O/n_{CaO}	$-\log a_{Fe}$	n_{Fe}/n_{CaO}	a_{CaO}	%CaO
0.000	0.98	6.477	0.67	.011	36.0
1.448	1.01	4.359	0.74	.010	34.5
1.850	1.07	3.627	0.83	.007	32.8
2.500	1.14	2.755	0.93	.006	31.0
3.500	1.25	1.585	1.12	.005	28.3
4.500	1.45	0.454	1.36	.005	25.2
4.925	1.61	0.0	1.58	.005	23.0

3.) Along a_{SiO_2} = .3

$-\log a_O$	n_O/n_{CaO}	$-\log a_{Fe}$	n_{Fe}/n_{CaO}	a_{CaO}	%CaO
0.000	1.28	6.351	.87	.0049	31.3
1.448	1.35	4.301	1.02	.0051	29.0
1.850	1.55	3.573	1.24	.0031	26.1
2.500	1.72	2.722	1.45	.0025	23.8
3.500	2.01	1.551	1.83	.0021	20.6
4.500	2.46	0.437	2.37	.0016	17.2
4.913	2.90	0.0	2.84	.0015	15.0

Part D (Table XVI continued, 1450°C)

4.) Along $a_{SiO_2} = .4$

$-\log a_O$	n_O/n_{CaO}	$-\log a_{Fe}$	n_{Fe}/n_{CaO}	a_{CaO}	%CaO
1.448	1.58	4.250	1.18	.0023	26.6
1.850	1.82	3.548	1.46	.0019	23.5
2.500	2.09	2.706	1.77	.0014	20.8
3.500	2.63	1.540	2.42	.0010	16.8
4.500	3.85	0.392	3.74	.0006	12.0
4.897	4.69	0.0	4.66	.0007	10.0

TABLE XVII

1. Iron and "FeO" Activities in the $CaO-FeO-Fe_2O_3-SiO_2$ System at 1550°C

Part A

5% SiO_2 section

n_{CaO}/n_{SiO_2}	$-\log a_O$	$\partial n_O/\partial n_{Fe}$	$-\log a_{Fe}$	$a_{"FeO"}$	%CaO
1.071	0.000	1.364	5.192	.12	4.7
	1.000	1.325	3.849	.27	4.8
	1.700	1.258	2.945	.43	4.9
	2.260	1.195	2.252	.57	4.9
	2.970	1.138	1.426	.75	4.9
	4.097	1.036	0.206	.93	5.0
	4.313	n.m.	0.0	.96	5.0
1.990	0.000	1.400	5.272	.10	9.7
	1.000	1.340	3.895	.24	9.8
	1.700	1.260	2.971	.40	9.8
	2.260	1.210	2.279	.54	9.9
	2.970	1.130	1.450	.71	10.0
	4.097	1.045	0.230	.88	10.2
	4.308	n.m.	0.0	.91	10.4

Part B (Table XVII continued, 1550°C)

n_{CaO}/n_{SiO_2}	$-\log a_O$	$\partial n_O/\partial n_{Fe}$	$-\log a_{Fe}$	$a_{"FeO"}$	%CaO
.578	0.000	1.364	5.305	.09	4.8
	1.000	1.324	3.962	.20	4.9
	1.700	1.260	2.958	.41	4.9
	2.260	1.208	2.266	.56	5.0
	2.970	1.130	1.450	.72	5.1
	4.097	1.043	0.230	.88	5.2
	4.313	n.m.	0.0	.91	5.3
1.071	0.000	1.387	5.229	.10	9.4
	1.000	1.325	3.822	.24	9.5
	1.700	1.258	2.977	.40	9.5
	2.260	1.195	2.227	.54	9.5
	2.970	1.133	1.455	.71	9.5
	4.097	1.048	0.224	.89	9.5
	4.314	n.m.	0.0	.91	10.0
1.99	0.000	1.39	5.311	.09	18.0
	1.000	1.35	3.941	.22	18.1
	1.700	1.27	3.028	.35	18.2
	2.260	1.21	2.335	.48	18.3
	2.970	1.14	1.464	.69	18.4
	4.097	1.05	0.245	.85	18.4
	4.318	n.m.	0.0	.90	18.5

Part C (Table XVII continued, 1550°C)

20% SiO_2 section

n_{CaO}/n_{SiO_2}	-log a_O	$\partial n_O/\partial n_{Fe}$	-log a_{Fe}	$a_{"FeO"}$	%CaO
.578	0.000	1.418	5.361	.08	9.6
	1.000	1.326	3.902	.23	9.7
	1.700	1.265	3.090	.30	9.8
	2.970	1.148	1.577	.53	9.9
	4.097	1.096	0.311	.73	10.0
	4.380	n.m.	0.0	.78	10.0
1.071	0.000	1.418	5.436	.07	19.0
	1.000	1.340	4.057	.17	19.3
	1.700	1.265	3.140	.27	19.4
	2.260	1.200	2.452	.36	19.6
	2.970	1.145	1.612	.49	19.8
	4.097	1.085	0.300	.75	19.9
	4.391	n.m.	0.0	.76	20.0
1.310	0.000	1.44	5.504	.06	23.9
	1.000	1.37	4.096	.15	23.9
	1.700	1.27	3.178	.25	24.0
	2.260	1.23	2.480	.34	24.1
	2.970	1.17	1.620	.48	24.2
	4.097	1.10	0.337	.69	24.3
	4.397	n.m.	0.0	.75	24.4

Part D (Table XVII continued, 1550°C)

30% SiO_2 section

n_{CaO}/n_{SiO_2}	$-\log a_O$	$\partial n_O/\partial n_{Fe}$	$-\log a_{Fe}$	$a_{"FeO"}$	%CaO
.578	0.000	1.444	5.493	.06	15.5
	1.000	1.350	4.096	.15	15.6
	1.700	1.290	3.180	.25	15.6
	2.260	1.206	2.486	.33	15.7
	2.970	1.120	1.656	.44	15.8
	4.097	1.090	0.411	.58	15.9
	4.472	n.m.	0.0	.63	16.1
1.071	0.000	1.478	5.608	.05	29.0
	1.000	1.344	4.191	.12	29.1
	1.700	1.278	3.272	.20	29.1
	2.260	1.221	2.576	.27	29.3
	2.970	1.163	1.732	.37	29.5
	4.097	1.109	.450	.53	29.7
	4.500	n.m.	0.0	.59	30.0
1.310	0.000	1.46	5.619	.045	35.9
	1.000	1.37	4.213	.11	36.0
	1.700	1.31	3.273	.20	36.0
	2.260	1.25	2.553	.29	36.1
	2.970	1.20	1.693	.40	36.3
	4.097	1.12	0.493	.48	36.5
	4.539	n.m.	0.0	.54	36.7

(Table XVII continued, 1550°C)

2. Silica Activities in the $CaO-FeO-Fe_2O_3-SiO_2$ System at 1550°C

Part A

5% SiO_2 section

n_{Fe}/n_{CaO}	$-\log a_O$	$\partial n_O/\partial n_{SiO_2}$	$-\log a_{SiO_2}$	a_{SiO_2}	%CaO
13.9	0.000	-.020	1.276	.053	4.9
	1.000	-.075	1.380	.042	5.0
	1.700	-.180	1.489	.033	5.0
	2.260	-.261	1.612	.024	5.0
	2.970	-.229	1.776	.017	5.1
	4.097	-.110	1.980	.001	5.2
	4.300	n.m.	2.000	.010	5.3
4.0	0.000	-.11	1.741	.018	14.3
	1.000	-.15	1.873	.013	14.5
	1.700	-.192	1.993	.010	14.6
	2.260	-.225	2.110	.008	14.7
	2.970	-.218	2.270	.005	15.0
	4.097	-.218	2.485	.003	15.2
	4.320	∿-.110	2.520	.003	15.4

Part B (Table XVII continued, 1550°C)

10% SiO_2 section

n_{Fe}/n_{CaO}	$-\log a_O$	$\partial n_O/\partial n_{SiO_2}$	$-\log a_{SiO_2}$	a_{SiO_2}	%CaO
13.9	0.000	-.060	0.472	.35	4.4
	1.000	-.110	0.546	.29	4.4
	1.700	-.144	0.638	.23	4.5
	2.260	-.225	0.731	.19	4.6
	2.970	-.180	0.860	.14	4.6
	4.097	-.092	1.030	.09	4.7
	4.310	n.m.	1.050	.09	4.7
4.0	0.000	-.110	1.232	.06	14.6
	1.000	-.144	1.357	.044	14.5
	1.700	-.212	1.477	.03	14.3
	2.260	-.245	1.606	.02	14.2
	2.970	-.261	1.792	.016	14.0
	4.097	-.190	2.136	.007	13.8
	4.313	n.m.	2.523	.003	13.6
2.0	0.000	-.040	2.476	.0033	23.5
	1.000	-.116	2.550	.0028	23.7
	1.700	-.192	2.672	.0021	24.0
	2.260	-.245	2.794	.0016	24.2
	2.970	-.225	2.964	.0011	24.5
	4.097	-.158	3.181	.0007	24.8
	4.358	n.m.	3.220	.0006	26.3

Part C (Table XVII continued, 1550°C)

20% SiO_2 section

n_{Fe}/n_{CaO}	$-\log a_O$	$\partial n_O/\partial n_{SiO_2}$	$-\log a_{SiO_2}$	a_{SiO_2}	%CaO
13.9	0.000	-.050	.137	.73	4.0
	1.000	-.096	.207	.62	4.1
	1.700	-.144	.291	.51	4.2
	2.260	-.144	.372	.42	4.2
	2.970	-.144	.474	.34	4.2
	4.097	-.11	.599	.25	4.3
	4.380	n.m.	.638	.23	4.3
4.0	0.000	-.10	.423	.38	12.1
	1.000	-.11	.523	.30	12.3
	1.700	-.15	.610	.25	12.5
	2.260	-.18	.700	.20	12.7
	2.970	-.18	.830	.15	12.8
	4.097	-.10	1.000	.10	13.0
	4.380	n.m.	1.050	.09	13.0
2.0	0.000	-.074	.538	.29	20.9
	1.000	-.122	.638	.23	21.2
	1.700	-.158	.736	.18	21.5
	2.260	-.158	.828	.15	21.7
	2.970	-.150	.940	.11	22.0
	4.097	.092	1.076	∿.09	22.1
	4.386	n.m.	1.100	.08	22.3

Part C (Table XVII continued, 1550°C)

n_{Fe}/n_{CaO}	$-\log a_O$	$\partial n_O/\partial n_{SiO_2}$	$-\log a_{SiO_2}$	a_{SiO_2}	%CaO
1.29	0.000	-.037	1.811	.015	28.3
	1.000	-.088	1.875	.013	28.6
	1.700	-.154	1.966	.011	28.9
	2.260	-.182	2.064	.009	29.2
	2.970	-.168	2.200	.006	29.5
	4.097	-.126	2.367	.004	29.7
	4.408	n.m.	2.400	.004	29.9

Part D

30% SiO_2 section

n_{Fe}/n_{CaO}	$-\log a_O$	$\partial n_O/\partial n_{SiO_2}$	$-\log a_{SiO_2}$	a_{SiO_2}	%CaO
13.9	0.000	(Silica Saturation Field)			
	1.000	-.116	.02	.95	3.5
	1.700	-.158	.10	.80	3.6
	2.260	-.165	.15	.70	3.6
	2.970	-.102	.23	.59	3.6
	4.097	-.040	.31	.48	3.7
	4.494	n.m.	.32	.48	3.7
4.0	0.000				10.7
	1.000	-.110	.050	.89	10.8
	1.700	-.192	.168	.68	11.0
	2.260	-.192	.264	.54	11.2
	2.970	-.158	.387	.41	11.4
	4.097	-.137	.403	.39	11.4
	4.473	n.m.	.456	.35	11.4

Part D (Table XVII continued, 1550°C)

n_{Fe}/n_{CaO}	$-\log a_O$	$\partial n_O/\partial n_{SiO_2}$	$-\log a_{SiO_2}$	a_{SiO_2}	%CaO
2.0	0.000	-.116	.042	.90	18.4
	1.000	-.158	.170	.68	18.7
	1.700	-.131	.271	.53	19.0
	2.260	-.158	.357	.44	19.2
	2.970	-.110	.478	.34	19.4
	4.097	-.110	.603	.25	19.5
	4.478	n.m.	.638	.23	19.6
1.29	0.000	-.080	.204	.63	24.8
	1.000	-.090	.292	.51	25.1
	1.700	-.151	.386	.41	25.5
	2.260	-.152	.475	.34	25.7
	2.970	-.127	.591	.26	26.0
	4.097	-.117	.749	.18	26.2
	4.486	n.m.	.796	.16	26.2

(Table XVII continued, 1450°C)

3. CaO Activities in the
$CaO-FeO-Fe_2O_3-SiO_2$ System at 1550°C

Part B

10% SiO_2 section

1.) Along $a_{SiO_2} = .0005$

$-\log a_O$	n_O/n_{CaO}	$-\log a_{Fe}$	n_{Fe}/n_{CaO}	a_{CaO}	%CaO
0.000	1.170	5.427	.783	.20	42.5
1.000	1.175	4.158	.810	.29	42.0
1.700	1.180	3.229	.860	.33	41.0
2.260	1.215	2.481	.937	.33	39.4
2.970	1.300	1.630	1.080	.39	36.7
4.097	1.500	0.352	1.320	.47	32.7
4.390	1.795	0.0	1.710	.42	27.9

2.) Along $a_{SiO_2} = .001$

$-\log a_O$	n_O/n_{CaO}	$-\log a_{Fe}$	n_{Fe}/n_{CaO}	a_{CaO}	%CaO
0.000	1.78	5.369	1.220	.033	33.0
1.000	1.89	4.042	1.345	.043	31.2
1.700	1.98	3.095	1.480	.045	29.5
2.260	2.15	2.359	1.720	.044	27.0
2.970	2.40	1.502	2.080	.050	23.9
4.097	3.10	0.253	2.850	.048	19.0
4.317	3.67	0.0	3.540	.04	16.1

Part C (Table XVII continued, 1450°C)

20% SiO_2 section

1.) Along $a_{SiO_2} = .005$

$-\log a_O$	n_O/n_{CaO}	$-\log a_{Fe}$	n_{Fe}/n_{CaO}	a_{CaO}	%CaO
0.000	1.300	5.619	.895	.12	35.3
1.000	1.300	4.126	.934	.10	34.7
1.700	1.325	3.210	1.000	.11	33.6
2.260	1.325	2.494	1.060	.11	32.8
2.970	1.360	1.639	1.1185	.12	31.1
4.097	1.400	0.448	1.267	.14	30.0
4.403	1.430	0.0	1.360	.1	28.9

2.) Along $a_{SiO_2} = .1$

$-\log a_O$	n_O/n_{CaO}	$-\log a_{Fe}$	n_{Fe}/n_{CaO}	a_{CaO}	%CaO
0.000	1.87	5.492	1.280	.02	28.4
1.000	1.92	4.068	1.395	.02	27.2
1.700	1.98	3.157	1.535	.021	25.8
2.260	2.04	2.444	1.680	.02	24.5
2.970	2.28	1.586	2.020	.02	21.8
4.097	2.47	0.333	2.300	.016	20.0
4.390	2.65	0.0	2.540	.014	18.6

Part C (Table XVII continued, 1450°C)

3.) Along a_{SiO_2} = .2

$-\log a_O$	n_O/n_{CaO}	$-\log a_{Fe}$	n_{Fe}/n_{CaO}	a_{CaO}	%CaO
0.000	2.33	5.472	1.60	.010	24.5
1.000	2.51	4.042	1.80	.010	22.5
1.700	2.74	3.141	2.15	.011	20.3
2.260	3.09	2.421	2.61	.009	17.8
2.970	3.74	1.554	3.37	.007	14.7
4.097	5.06	0.315	4.82	.005	11.0
4.380	5.53	0.0	5.42	.003	10.0

Part D

30% SiO_2 section

1.) Along a_{SiO_2} = .1

$-\log a_O$	n_O/n_{CaO}	$-\log a_{Fe}$	n_{Fe}/n_{CaO}	a_{CaO}	%CaO
0.000	.633	5.572	.445	.028	43.0
1.000	.658	4.230	.476	.030	42.1
1.700	.689	3.350	.523	.032	40.7
2.260	.711	2.581	.597	.030	38.9
2.970	.776	1.734	.718	.030	36.1
4.097	.836	0.473	.803	.027	34.3
4.518	.878	0.0	.885	.024	32.7

Part D (Table XVII continued, 1450°C)

2.) Along a_{SiO_2} = .2

$-\log a_O$	n_O/n_{CaO}	$-\log a_{Fe}$	n_{Fe}/n_{CaO}	a_{CaO}	%CaO
0.000	0.800	5.572	0.552	.016	39.3
1.000	0.831	4.192	0.610	.017	37.9
1.700	0.905	3.272	0.710	.018	35.6
2.260	1.020	2.534	0.870	.016	32.4
2.970	1.190	1.679	1.085	.014	28.9
4.097	1.310	0.439	1.270	.012	26.5
4.486	1.500	0.0	1.490	.01	24.0

3.) Along a_{SiO_2} = .4

$-\log a_O$	n_O/n_{CaO}	$-\log a_{Fe}$	n_{Fe}/n_{CaO}	a_{CaO}	%CaO
0.000	1.77	5.670	1.26	.011	25.3
1.000	1.89	4.347	1.43	.013	23.6
1.700	2.10	3.324	1.73	.005	21.0
2.260	2.46	2.584	2.17	.003	18.1
2.970	3.35	1.700	3.19	.002	13.6
4.097	4.73	0.467	4.65	.001	10.0
4.540	5.29	0.0	5.29	.001	9.0

BIBLIOGRAPHY

1. L. S. Darken and R. W. Gurry: "The System Iron-Oxygen I. The Wustite Field and Related Equilibria". J. Am. Chem. Soc., 1945, vol. 67, pp. 1398-1412.

2. L. S. Darken and R. W. Gurry: "The System Iron-Oxygen II. Equilibria and Thermodynamics of Liquid Oxide and Other Phases". J. Am. Chem. Soc., 1946, vol. 68, pp. 798-816.

3. B. Phillips and A. Muan: "Stability Relations of Iron Oxides: Phase Equilibria in the System Fe_2O_3-Fe_3O_4 at Oxygen Pressures up to 45 Atmospheres". J. Phys. Chem., 1960, vol. 64, pp. 1451-1453.

4. A. Muan and E. F. Osborn: "Phase Equilibria Among Oxides in Steelmaking". Addison-Wesley Publishing Co., Reading, Massachusetts, 1965.

5. A. L. Day, E. S. Shepherd, and F. E. Wright: "The Lime-Silica Series of Minerals". Am. J. Sci. (4th Series), 1906, vol. 22, pp. 265-302.

6. G. A. Rankin and F. E. Wright: "The Ternary System CaO-Al_2O_3-SiO_2". Am. J. Sci. (4th Series), 1915, vol. 39, pp. 1-79.

7. J. W. Greig: "Immiscibility in Silicate Melts". Am. J. Sci. (5th Series), 1927, vol. 13, pp. 1-44.

8. K. K. Kelley: "Heats and Free Energies of Formation of Anhydrous Silicates". U.S. Bureau of Mines Rept. of Investigations, No. 5901, 1962.

9. J. F. Elliott, M. Gleiser, and V. Ramakrishna: "Thermochemistry for Steelmaking. Volume II. Addison-Wesley Publishing Co., Reading, Massachusetts, 1963.

10. E. G. King: "Heats of Formation of Crystalline Calcium Orthosilicate, Tricalcium Silicate and Zinc Orthosilicate". J. Am. Chem. Soc., 1951, vol. 73, pp. 656-658.

11. J. P. Coughlin and C. J. O'Brien: "High Temperature Heat Contents of Calcium Orthosilicate". J. Phys. Chem., 1957, vol. 61, pp. 767-769.

12. S. S. Todd: "Low Temperature Heat Capacities and Entropies at 298.16 K. of Crystalline Calcium Orthosilicate, Zinc Orthosilicate and Tricalcium Silicate". J. Am. Chem. Soc., 1951, vol. 73, pp. 3277-3278.

13. R. Benz and C. Wagner: "Thermodynamics of the Solid System $CaO-SiO_2$ from Electromotive Force Data". J. Phys. Chem., 1961, vol. 65, pp. 1308-1311.

14. J. C. Fulton and J. Chipman: "Slag-Metal-Graphite Reactions and the Activity of Silica in Lime-Alumina-Silica Slags". Trans. AIME, 1954, vol. 200, pp. 1136-1146.

15. P. T. Carter and T. G. MacFarlane: "Thermodynamics of Slag Systems. Part II--The Thermodynamic Properties of $CaO-SiO_2$ Slags". J. Iron Steel Inst., 1957, vol. 185, pp. 62-66.

16. J. D. Baird and J. Taylor: "Relation Between Silica and Carbon and the Activity of Silica in Slag Systems". Trans. Farad. Soc., 1958, vol. 54, pp. 526-539.

17. D. A. R. Kay and J. Taylor: "Activities of Silica in the Lime + Alumina + Silica System". Trans. Farad. Soc., 1960, vol. 56, pp. 1372-1386.

18. B. Phillips and A. Muan: "Phase Equilibria in the System CaO-Iron Oxide in Air and at 1 Atm. O_2 Pressure". J. Am. Ceram. Soc., 1958, vol. 41, pp. 445-454.

19. B. Phillips and A. Muan: "Stability Relations of Calcium Ferrites: Phase Equilibria in the System $2CaO \cdot Fe_2O_3-FeO \cdot Fe_2O_3-Fe_2O_3$ above 1135°C". Trans. Met. Soc. AIME, 1960, vol. 218, pp. 1112-1118.

20. W. C. Allen and R. B. Snow: "The Orthosilicate-Iron Oxide Portion of the System $CaO-FeO-SiO_2$". J. Am. Ceram. Soc., 1955, vol. 38, pp. 264-280.

21. G. Trömel, W. Jäger, and E. Schürmann: "Untersuchungen in System Eisen-Eisenoxyde-Kalk". Arch. Eisenhüttenw., 1955, vol. 26, pp. 687-700.

22. W. C. Hahn, Jr.: "Studies of the Thermodynamic Properties of Oxide Solid Solutions". Ph.D. Thesis, The Pennsylvania State University, 1960.

23. H. Larson and J. Chipman: "Oxygen Activity in Iron Oxide Slags". Trans. AIME, 1953, vol. 197, pp. 1089-1096.

24. H. Larson and Chipman: "Activities of Fe, FeO, Fe_2O_3, and CaO in Simple Slags". Trans. AIME, 1954, vol. 200, pp. 759-792.

25. E. T. Turkdogan: "Activities of Oxides in CaO-FeO-Fe_2O_3 Melts". Trans. Met. Soc. AIME, 1961, vol. 221, pp. 1090-1095.

26. A. Muan: "Phase Equilibria in the System FeO-Fe_2O_3-SiO_2". Trans. AIME, 1955, vol. 203, pp. 965-976.

27. R. Schuhmann, Jr., and P. J. Ensio: "Thermodynamics of Iron Silicate Slags: Slags Saturated with Gamma Iron". Trans. AIME, 1951, vol. 191, pp. 401-411.

28. E. T. Turkdogan: "Activities of Oxides in FeO-Fe_2O_3-SiO_2 Melts". Trans. Met. Soc. AIME, 1962, vol. 224, pp. 294-298.

29. J. White: "Equilibrium at High Temperatures in Systems Containing Iron Oxides". J. Iron Steel Inst., Carnegie Schol. Mem., 1938, vol. 27, pp. 1-75.

30. E. T. Turkdogan and P. M. Bills: "A Thermodynamic Study of FeO-Fe_2O_3-SiO_2, FeO-Fe_2O_3-P_2O_5, and FeO-Fe_2O_3-SiO_2-P_2O_5 Molten Systems". J. Iron Steel Inst., 1957, vol. 186, pp. 329-339.

31. N. L. Bowen, J. F. Schairer, and E. Posnjak: "The System CaO-FeO-SiO_2". Am. J. Sci. (5th Series), 1933, vol. 26, pp. 193-284.

32. B. Phillips and A. Muan: "Phase Equilibria in the System CaO-Iron Oxide-Silica in Air". J. Am. Ceram. Soc., 1959, vol. 42, pp. 413-423.

33. M. D. Burdick: "Studies on the System Lime-Ferric Oxide-Silica". J. Res. Nat. Bur. Standards, 1940, vol. 25, pp. 475-488.

34. Phase Equilibria Diagrams of Oxide Systems: Plates 7 and 10. American Ceramic Society, Columbus-Ohio, 1960.

35. K. L. Fetters and J. Chipman: "Equilibria of Liquid Iron and Slags of the System CaO-MgO-FeO-SiO_2". Trans. AIME, 1941, vol. 140, pp. 95-111.

36. C. R. Taylor and J. Chipman: "Equilibria of Liquid Iron and Simple Basic and Acid Slags in a Rotating Induction Furnace". Trans. AIME, 1943, vol. 154, pp. 228-247.

37. E. Görl, F. Oeters, and R. Scheel: "Gleichgewichte zwischen flüssigem Eisen und gesättigten Schlacken des Systems CaO-FeO-SiO_2 unter Berücksichtigung der Schwefelverteilung". Arch. Eisenhüttenw., 1966, vol. 37, pp. 441-451.

38. C. E. Wicks and F. E. Block: "Thermodynamic Properties of 65 Elements-Their Oxides, Halides, Carbides, and Nitrides". U.S. Bureau of Mines Bulletin, No. 605, 1963.

39. R. W. Taylor and A. Muan: "Activities of Iron in Iron-Platinum Alloys at 1300°C". Trans. Met. Soc. AIME, 1962, vol. 224, pp. 500-502.

40. H. R. Larson and J. Chipman: "Activity of Iron in Iron-Platinum Solid Solutions". Acta Met., 1954, vol. 2, pp. 1-2.

41. R. B. Fischer: Quantitative Chemical Analysis. W. B. Saunders Publishing Co., Philadelphia, Pennsylvania, 1962.

42. J. Lumsden: "The Thermodynamics of Liquid Iron Silicates". Physical Chemistry of Process Metallurgy, Part I., pp. 165-205. Interscience Publishers, New York, 1959.

43. E. Steinmetz and R. Thielmann: "Anwendung der Beziehung von Gibbs-Duhem auf die chemischen Aktivitaten flussiger Eisenlegierungen und Schlacken". Arch. Eisenhuttenw., 1968, vol. 39, pp. 481-489.

44. L. S. Darken: "Application of the Gibbs-Duhem Equation to Ternary and Multicomponent Systems". J. Am. Chem. Soc., 1950, vol. 72, pp. 2909-2914.

45. C. Wagner: Thermodynamics of Alloys. Addison-Wesley Publishing Co., Reading, Massachusetts, 1952.

46. H. A. C. McKay: "Thermodynamics of Three Component Systems". Nature, 1952, vol. 169, pp. 464-465.

47. R. Schuhmann, Jr.: "Application of Gibbs-Duhem Equations in Ternary Systems". Acta Met., 1955, vol. 3, pp. 219-226.

48. N. A. Gokcen: "Application of Gibbs and Gibbs-Duhem Equations to Ternary and Multicomponent Systems". J. Phys. Chem., 1960, vol. 64, pp. 401-406.

49. J. Chipman and L. C. Chang: "The Ionic Nature of Metallurgical Slags. Simple Oxide Systems". Trans. AIME, 1949, vol. 185, pp. 191-197.

50. J. P. Coughlin: "Contributions to the Data on Theoretical Metallurgy". U.S. Bureau of Mines Bulletin, No. 542, 1952.

51. M. F. Koehler, B. Barany, and K. K. Kelley: "Heats and Free Energies of Formation of Ferrites and Aluminates of Calcium, Magnesium, Sodium, and Lithium". U.S. Bureau of Mines Rept. of Investigations, No. 5711, 1961.

VITA

Muharrem Timucin was born in Manisa, Turkey, on April 12, 1941. He received his primary, secondary and high school educations in Manisa. He studied at the Middle East Technical University, Ankara, Turkey, from 1959 to 1964 where he received the B.S. and M.S. degrees in Mechanical Engineering.

From 1964 to 1966 he served as a teaching assistant and later as an instructor in Metallurgical Engineering Department of Middle East Technical University.

He has been enrolled in the Graduate School of the University of Missouri at Rolla since September 1966 and has received the degree of M.S. in Metallurgical Engineering in 1968. During his study at the University of Missouri at Rolla he held a UNESCO Fellowship.

He has been a student member of the American Society for Metals, and the Metallurgical Society of A.I.M.E. He has been honored by election to Alpha Sigma Mu membership.